Summer 2024

Hydrologic Modeling of the Lower Chesapeake Bay Watershed Using HECC-HMS with Implications for Future Coupled Coastal Modeling

Christopher Leonard Frost
Old Dominion, cltfrost87@gmail.com

HYDROLOGIC MODELING OF THE LOWER CHESAPEAKE BAY WATERSHED USING HEC-HMS WITH IMPLICATIONS FOR FUTURE COUPLED COASTAL MODELING

by

Christopher Leonard Frost
B.S. December 2009, University of Arizona
B.S. December 2016, University of Houston

A Thesis Submitted to the Faculty of Old Dominion University on Partial Fulfillment of the Requirements for the Degree of

MASTER OF SCIENCE

CIVIL ENGINEERING

OLD DOMINION UNIVERSITY
August 2024

Approved by:
Dr. Gangfeng Ma (Director)
Dr. Navid Tahvildari (Member)
Dr. Mujde Erten-Unal (Member)

ABSTRACT

HYDROLOGIC MODELING OF THE LOWER CHESAPEAKE BAY WATERSHED USING HEC-HMS WITH IMPLICATIONS FOR FUTURE COUPLED COASTAL MODELING

Christopher Leonard Frost

Old Dominion University, 2024

Director: Dr. Gangfeng Ma

This study explores the hydrological methodology for modeling a coastal watershed basin using the US Army Corps of Engineers hydrologic software, HEC-HMS with an objective of being able to create riverine boundary conditions that could be applied to a coupled compound flood model. Compound flooding is defined as high water inundation event that occurs due to the simultaneous occurrence of multiple flooding drivers. The Atlantic Seaboard and the Gulf of Mexico regions of the United States account for most of the compound events observed in the United States with a higher occurrence caused by hurricanes from July to November. In this study three events were modeled for the Lower Chesapeake Watershed in Virginia: Tropical Storm Andrea, Michael, and Zeta. Each event was modeled using Modified Clark transform, simple canopy interception and loss, Green and Ampt or deficit & constant infiltration loss, linear base flow, and Muskingum-Cunge routing. Gridded precipitation and temperature were applied as boundary conditions for each event. Results from the models indicated large differences between event model parameters with difficulties in modeling and calibrating the coastal transition zone. Calibration statistics to observed data was generally within acceptable statistical parameters using Nash Sutcliff, R-squared, and percent bias.

Thank you to:

My defense committee for taking the time to review my work and ask hard questions. Additional thank you to Dr. Ma, my advisor, for the assistance in completing my degree and thesis, and finally to Tamara Massong for the help and advice both for school and work.

Fortuna Eruditis Favet

TABLE OF CONTENTS

LIST OF TABLES

LIST OF EQUATIONS

LIST OF FIGURES

CHAPTER

1 INTRODUCTION

1.1 Purpose

The purpose of this study was to explore the use of the US Army Corps of Engineers hydrologic software, HEC-HMS, to create a rain and riverine flow boundary conditions that could be used for compound flood modeling using gridded precipitation and temperature from three events. Model calibration would attempt to find parameters values that could be used to create a general model for forecasting and synthetic storms enabling the development of hydrographs at model outflow locations and gridded excess precipitation for application to a coupled surface model.

1.2 Background and Literature Review

Compound flooding is defined as a high water inundation event that occurs due to the simultaneous occurrence of multiple flooding drivers, multivariate event (Leonard et al. 2014). These drivers can include fluvial, pluvial, groundwater, storm surge, or tidal (Bermudez et al. 2021; Rahimi et al. 2020; Sebastian 2022; Xu et al. 2023; Zscheischler et al. 2018). Fluvial flooding, also known as riverine flooding, occurs when the capacity of a river channel is exceeded and water spills onto the floodplain or further inland from the river channel. Pluvial flooding, which can occur along with fluvial flooding, is flooding caused by extreme rainfall saturating the soil and running off in large quantities. Pluvial effects can also be caused by ponding in low lying regions with low topographic relief. Groundwater flooding, also related to fluvial and pluvial, will occur in low lying areas with a high-water table, such as coastal regions. When large quantities of water saturate the soil and then enter the nearest aquifer the groundwater table will rise leading to soil saturation, reduced infiltration, and water influencing river channels and conditions. Finally, storm surge and tidal flooding happen when wave movement is influenced by winds from storms and increases in sea level due to climate change and regular tidal events (Bermudez et al. 2021; Jalili Pirani and Najafi 2023).

Compound flooding is commonly caused by an atmospheric event, most often an extra-tropical or tropical storm system in the coastal regions of the continental United States (Couasnon et al. 2020; Hendry et al. 2019; Jalili Pirani and Najafi 2023). The Atlantic Seaboard and the Gulf of Mexico region account for most of the compound events observed in the United States. This higher occurrence is caused by hurricanes from July to November as well as by an extra tropical storm such as Nor'easters that occurs during the winter (Konrad II and Perry 2010; Wahl et al. 2015). Tropical storm events can precipitate large amount of rain inland of the coast as well as significant storm surges that push water inland from the coast. With the combination of these two flood drivers, tropical storms have the potential to cause large amounts of flooding within a region. However, not all tropical storm events result in a compound flood. The occurrence of a tropical storm driven compound event is defined by the timing of the storm surge inland, the flood wave arrival, and the presence of intense rainfall (Shields et al. 2023). When two of these flood drivers occur in a region then a compound event has occurred. The required combination of events has led to much research in statistical modeling to determine the risk and probability of events (Jane et al. 2020).

Climate change due to carbon emissions has also altered the frequency and intensity of storms leading to an increase in compound flooding events. Several studies have found compound flooding return frequencies to be increasing with increases in global air temperatures as well as sea level rise (Rahimi et al. 2020; Zscheischler et al. 2018). With a warmer atmosphere, more energy is available to tropical storm systems which leads to higher amounts of rainfall as well as increased rainfall intensity. In other words, larger more powerful storms lead to higher amounts of precipitation. In fact one can expect a threefold increase in people exposed to the 100 year flood by 2070, with much of those effects being observed in the coastal regions due to sea level rise (Shen et al. 2019, 2022; Wahl et al. 2015). Following this increase in exposure to flooding, infrastructure damage cost will also rise, giving increased need to study and plan for future scenarios with greater amounts of risk to life and property (Tahvildari et al. 2022).

Climate change also brings new uncertainties in precipitation, storm surge, tropical storm events, and other weather phenomena. In much of research and civil design, we have used past events or records to determine the level of risk that can be used to inform everything from infrastructure design to policy decisions. However, with a changing climate we can no longer rely on past records that were measured in a constant climate. For example, past records of precipitation frequency and intensity will not indicate future risk as that risk is changing. (Shields et al. 2023; Zscheischler et al. 2018). To mitigate this issue new methods will need to be used to better determine risk based on projections and we must find ways to more accurately forecast our models.

At present research has been shifting gears to focus on flooding caused by compound events and how to best to predict and model them. This creates a challenge as most of coastal, hydraulic, and hydrological modeling has been focused on singular parts of the problem, e.g. hurricane storm surge, coastal flooding, coastal groundwater, etc. (Couasnon et al. 2020). Compound flooding events require a much broader approach than traditional fluvial, pluvial, groundwater, or coastal modeling (Leonard et al. 2014; Shields et al. 2023). New approaches such as coupling individual domain models into a single unified model has led to a more interdisciplinary aspect to compound flood modeling. Several studies have used this method to model hydrology, hydraulic, and coastal storm surge as separate model and then apply them as boundary conditions to either the hydraulic or coastal model (Gori et al. 2020; Lee et al. 2020; Peña et al. 2023; Saleh et al. 2017). Using coupled models has been found to be more accurate than super-position of water surface elevation which has been used in the past (Serafin et al. 2019; Shields et al. 2023). This approach is contrasted with the more probabilistic method of using statistical models to determine flooding. However, numerical models allow for a higher resolution when determining inundation spatially.

Software options to model compound flooding are quite widespread throughout the world. For the application of surface water software related to: hydrological, inland hydraulic, and coastal is important. Groundwater models are another driver of compound flooding but are in the initial stages of application to coupled models. Several models for hydrology exist just within the United States, US Army Corps of Engineers Hydraulic Engineering Center Hydrologic Modeling System (HEC-HMS), Soil & Water Assessment Tool (SWAT), Precipitation Runoff Modeling System (PRMS), etc. These software packages utilize different methods and models within the software to model hydrological events. HEC-HMS is one of the most common software packages used and is part of the US Army Corps of Engineers Corps Water Management Model (CWMS) that is used to simulate watershed events within district boundaries (Pabst 2000). HEC-HMS is a numerical model that applies a range of available models for precipitation

transformation to runoff, soil infiltration, base flow, canopy interception, surface ponding, and routing between basins. These models rely on empirical or mathematical methods to determine precipitation runoff (Hydrologic Engineering Center 2023; Sahu et al. 2023).

Similar numbers of options exist for software developed in the United States for hydraulic simulation and modeling. By far the most common model used is the US Army Corps of Engineers Hydraulic Engineering Center's River Analysis System (HEC-RAS). HEC-RAS allows for both one-dimensional (1D) and two-dimensional (2D) modeling of a riverine system or basin. HEC-RAS 2D capabilities have allowed for the application of rain on grid as well as new infiltration methods applied to a 2D mesh. The 2D method applies the shallow water equation, depending on the equation set used, to model flow over a meshed surface similar to coastal models (Brunner 2020). Recent studies have applied both the coastal storm surge component and the rainfall excess from the hydrologic model to HEC-RAS to combine the results and determine inundation extents of compound events (Campbell et al. 2023).

Coastal compound flooding has been modeled in many studies using several different software suites (Kumbier et al. 2018; Lee et al. 2020; Loveland et al. 2021; Saleh et al. 2017; Shen et al. 2019). These include: Delft3D, Telemac-Mascaret, MIKE, and ADCIRC. These models all rely on three dimensional (3D) numerical simulations to model wave propagation, storm surge, tidal influence, and some application to inland flooding. In many compound flood models, the coastal simulation results are applied as boundary conditions to the hydraulic software (Xu et al. 2023). These models use a similar surface mesh applied to the area of interest to simulate the coastal conditions. Boundary conditions applied to the coastal model are often taken from larger ocean models, thus requiring additional knowledge of ocean modeling.

Coupled models have allowed for researchers to begin to model compound events. However, much uncertainty and error can be created with so much complexity. Many parameters defined in a model, such as manning-n values or soil loss, are deterministic in that a value assigned is decided upon by the modeler (Zhang et al. 2018). These values might be bias or subjective, which will translate to errors and uncertainty in the model. In addition, boundary condition data such as gridded precipitation, digital elevation models, bathometry, wind, etc. have some amount of measurement error as well. To account for this uncertainty and error in the models being created and the events being run, Monte Carlo and ensemble simulation methods have been created (Saleh et al. 2017). The ensemble method creates multiple runs from a variable parameter or parameters to give a series of results. These results can be used to determine a range of results that could occur from a simulation with uncertain boundary conditions. Monte Carlo simulations can be applied to deterministic parameter values to allow for an understanding of the likelihood of results based on the variability of a parameter value.

CHAPTER

2 METHODOLOGY

The hydrologic model used in this study is The United States Army Corps of Engineers (USACE) Hydrologic Modeling System (HMS) developed by the specialist center, the Hydraulic Engineering Center (HEC). This software is often referred to by its acronym HEC-HMS and will be referenced as such throughout the remainder of this paper. Hydrologic modeling with HEC-HMS requires the development of model geometry including sub-basins, reaches, junctions, computation points, and sinks using digital elevation models as starting input. After the completion of basin delineation and model elements described above additional physical parameters are defined for each basin and the application of boundary conditions, precipitation and temperature are applied. These will be described in the appropriate sub sections that follow. Table 1 summarizes the boundary conditions and applied models for the boundary conditions and physical model sections.

Table 1. Sub models and methods used in hydrologic modeling.

Component	Summary
Model Geometry	TauDEM Delineation Algorithms
Applied Boundary Conditions	Gridded Dataset of Events– Analysis of Record for Calibration Precipitation, Temperature
Canopy Model	Simple Model
Evapotranspiration	Hamon Method
Soil Infiltration Model	Layered Green & Ampt Infiltration Loss Model Deficit and Constant Infiltration Loss Model
Transform Model	ModClark Model
Base Flow Model	Linear Reservoir Model
Routing Model	Muskingum-Cunge Model

2.1 Model Geometry

The geometry for the development of the sub-basins and reaches was created using an internal delineation algorithm within HEC-HMS utilizing terrain rasters of the model region extent. Base digital elevation models (DEM) for the model were created using Quantum Geographic Information System (QGIS) to merge multiple United States Geological Survey (USGS) 3D Elevation Program DEM (3DEP) tiles covering the full extent of the Lower Chesapeake Bay Watershed. The USGS 3DEP dataset is described in more detail in the following section, Dataset Description. The basin and reach delineation process utilized both the terrain reconditioning process (AgreeDEM) developed by Ferdi Hellweger at the University of Texas (Hellweger and Maidment 1997) and TauDEM created by David Tarboton at Utah State University (Tarboton 2005).

AgreeDEM is used for correcting hydraulic connections in digital elevation models (DEM) by using line vector files to lower or raise elevation in the DEM to "burn in" stream or watershed boundaries (Hellweger and Maidment 1997; Maidment 2002). The reconditioning process is optional, however often when an elevation model is created hydraulic connections are blocked. This can happen due to the presence of bridges, culverts, high water surface elevations during LiDAR flights, etc. The stream burn process allows for modelers to correct for these missing connections and get the correct flow path through the terrain. For the model process, the National Hydraulic Dataset Plus High Resolution (NHDPlus HR) burn lines features were used for burning hydraulic connections into the merged USGS 3DEP DEM.

TauDEM is a set of a geographic information system (GIS) tools for the analysis of DEMs and delineation of sub-basins, streams, etc. Within HEC-HMS, TauDEM is used to delineate sub-basins, reaches, and junctions for the model (Hydrologic Engineering Center 2023; Tarboton 2005). TauDEM uses the following process to determine a final set of basins, streams, and junctions:

sink removal → flow accumulation and direction → stream identification → basin delineation at break points.

At the flow accumulation and direction stage, TauDEM uses eight flow directions at each raster elevation cell to determine the direction of flow from the head of a basin to the confluence and then outfall of the system. Other methods are available outside of HEC-HMS that can provide different approaches to delineation, however, the difference is often minimal when looking at the watershed scale. The steps for the development of the model geometry and terrain within HEC-HMS and QGIS are shown in Figure 2 below with descriptions that follow.

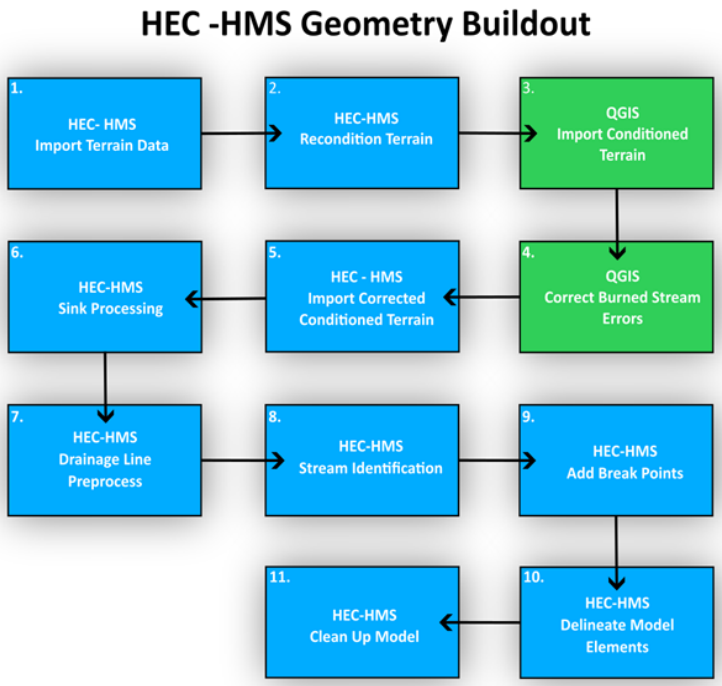

Figure 1. HEC-HMS sub-basin and reach delineation process diagram.

1. USGS 3DEP DEMs are imported into HEC-HMS where hill shade and symbology are added automatically by HEC-HMS.
    a. Output: Terrain DEM
2. NHD lines features (such as burn lines and watershed boundaries) are used to burn in stream and watershed boundary features into the terrain DEM. Stream drop depth of 20ft and watershed boundary elevation increase of 100ft is used to define the amount to change pixels intercepted by the NHD line features.
    a. Output: Conditioned DEM
3. The HEC-HMS conditioned DEM created is imported to QGIS where corrections for burn process errors or incorrect burn depth are applied.
4. Within QGIS the Serval plugin is used to make the noted corrections. The Serval plugin allows for the user to make changes to raster pixel values individually or in groups like an image editing program.
    a. Output: Conditioned DEM (corrected copy)
5. The HEC-HMS conditioned raster is replaced in the /GIS/<BASIN NAME> directory with the corrected copy from QGIS. Replacement of the HEC-HMS conditioned raster with the corrected copy from QGIS requires that the projection, coordinate system, extent, and name all match the original file. Failure to do so results in the program failing to find the file and continue to the next step.
    a. Output: Conditioned DEM replaced with “corrected copy”

6. Sink processing is applied within HEC-HMS to the Conditioned DEM terrain raster. Sink processing evaluates the terrain raster for pixels that have no outflow, otherwise known as sinks. The process will increase the identified sink pixel elevation until it is equal to the surrounding pixels. This is an iterative process that will continue until all pixels have an outflow.
    a. Output: Conditioned DEM with sinks removed
7. Drainage lines process is applied to the Conditioned DEM with sinks removed to create a flow accumulation and flow directions rasters. These rasters identify direction and amount of flow into each down slope pixel.
    a. Output: Flow direction raster, flow accumulation raster, eight direction file (d8 file)
8. Stream identification process is applied using the flow direction and accumulation rasters. Streams are identified as the connection between pixels based on the flow direction at each pixel.
    a. Output: Stream raster
9. User added breakpoints are applied at stream gauge locations, reservoirs/dams, terrain changes (e.g., changes in topological regions or ecological area), and outfall of the model.
    a. Note: Two breaks were placed downstream of Gathright Dam and Lake Anna since both dams regulate downstream flow.
    b. Output: Break point features stored in an SQLite database file
10. Sub basin delineation process is started using the flow accumulation raster, flow direction raster, and break point features. Delineation occurs at breakpoints and the maximum sub basin area parameter. The max area for this model was set at 150 sq mi, but trial and error is often needed to get a desired set of basins.
    a. Output: Sub basin, reach, junction, and computation point model elements.
11. The model is cleaned up using split or merge elements to get desired geometry for the model. Model elements are named according to the highest order river and ordered in the model from downstream to upstream.

The final extents of the hydrological model were determined at the upstream end by the Lower Chesapeake Watershed boundary defined by the NHD dataset and at the downstream end by the both the presence of stream gauges and channel slopes less than 0.001 ft/ft. Basins downstream of the boundary extent were kept in the model for testing purposes but not used in the results. Figure 2 shows the locations of the basins that were delineated for the model within the Lower Chesapeake watershed.

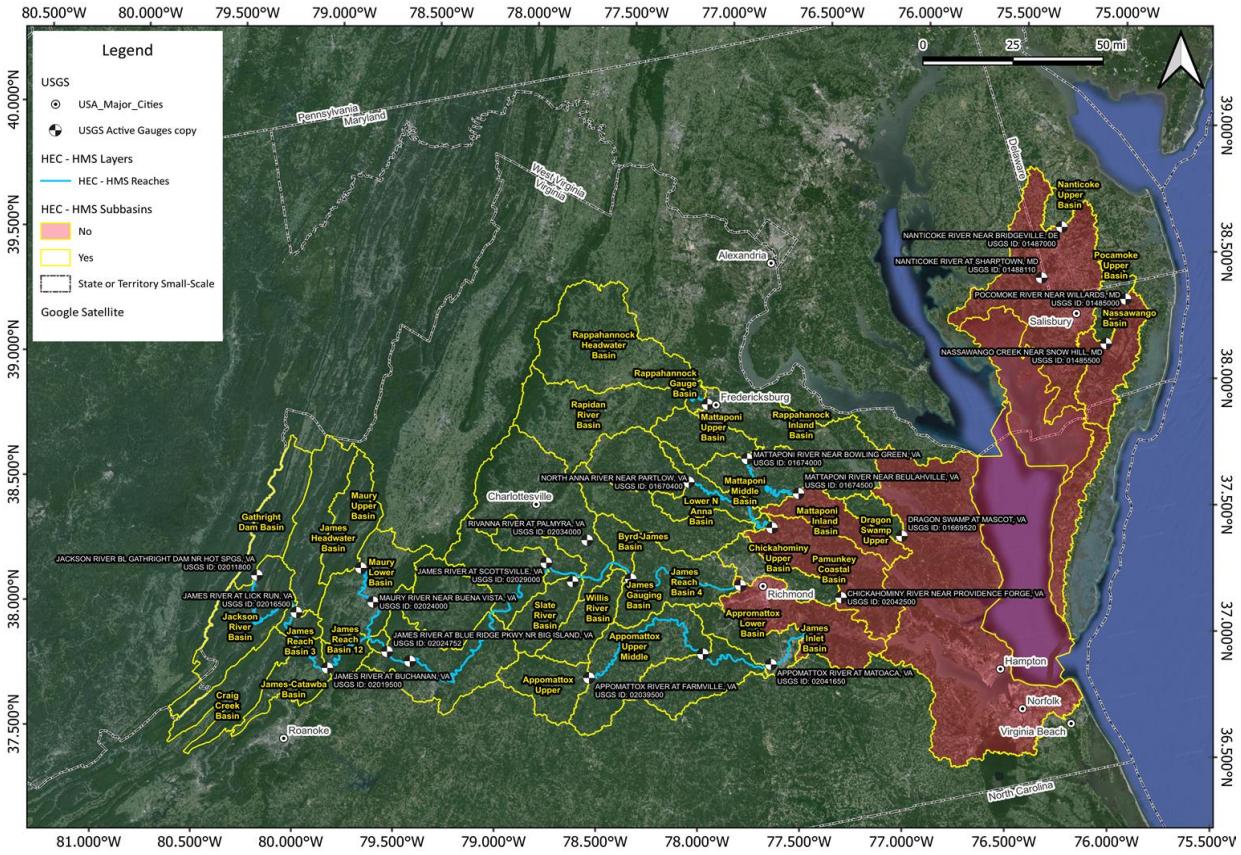

Figure 2. Basin delineation for modeling. Red indicates areas that were too shallow a slope to model in HEC-HMS

2.2 Boundary Conditions

Boundary conditions are divided into two sections: storm selection and precipitation and temperature. Storm selection will describe which events were selected to use for calibration and precipitation and temperature will describe the type of data used for each calibration event.

2.2.1 Storm Selection

Storm selection for the calibration of the Lower Chesapeake Bay model was done by selecting for tropical storm events that occurred over the region within the last 20 years. A 20-year period of record was selected to ensure that observed data (gridded precipitation, stream gauge data, tidal data) was available. In addition, model parameters are calculated from present or near present remote sensing data, making more recent events a better fit for these parameters.

A total of thirteen storms were identified to have passed within 100 miles of the Lower Chesapeake Watershed in the past 20 years. The number of storms to calibrate to was set at three storms. Storm selection was based on whether the event was observed in any of the stream gauges in the watershed, the relative size of the flow event compared to the base flow in the channel, and the presence of precipitation observed using the Community Collaborative Rain, Hail, & Snow Network

(CoCoRaHS) record, a community-based weather observation recording network present in the United States. Precipitation was noted as occurring closer to the coast or the inland portion of the watershed. Tropical storm (TS) Andrea, TS Michael, and TS Zeta were selected for modeling and calibration. A summary of reviewed events is shown in Table 2 with notes about the start and end of the rising and falling limb of the observed hydrograph, number of observed days, and the beginning and end of observed rainfall. Figure 3. maps the path of each of the storms used as well as two reference events, Hurricane Floyd and Irene.

Table 2. Tropical storm events between 2000 and 2024 within 100 miles of the Lower Chesapeake Watershed.

	Flow Gage Data Record				CoCoRaHS Data Record			
Event Name	**Start Date**	**End Date**	**Total Days**	**Notes**	**Start Date**	**End Date**	**Total Days**	**Notes**
Hurricane Isabel	-	-	-	No event	-	-	-	No event
TS Hanna	08/25/08	09/04/08	10	Small event	08/27/08	08/31/08	4	Regional rainfall
Hurricane Irene	-	-	-	No event	08/28/11	08/31/11	3	Coastal Rainfall
ET Andrea	06/06/13	06/17/13	11	Series of events	06/06/13	06/12/13	6	Coastal Rainfall
Hurricane Arthur	-	-	-	No event	07/03/14	07/06/14	3	Small Coastal Event
ET Michael	10/10/18	10/24/18	14	Large event	10/11/18	10/13/18	2	Regional Rainfall
ET Nestor	10/19/19	10/25/19	6	Small event	10/20/19	10/22/19	2	Coastal Rainfall
TS Isaias	08/02/20	08/06/20	4	Small event	08/03/20	08/10/20	7	Regional rainfall
TS Zeta	10/28/20	11/08/20	11	Small event	10/28/20	11/03/20	6	Regional rainfall
TS Claudette	-	-	-	No event	06/22/21	06/24/21	2	Coastal Rainfall
TS Elsa	-	-	-	No event	07/08/21	07/10/21	2	Coastal Rainfall

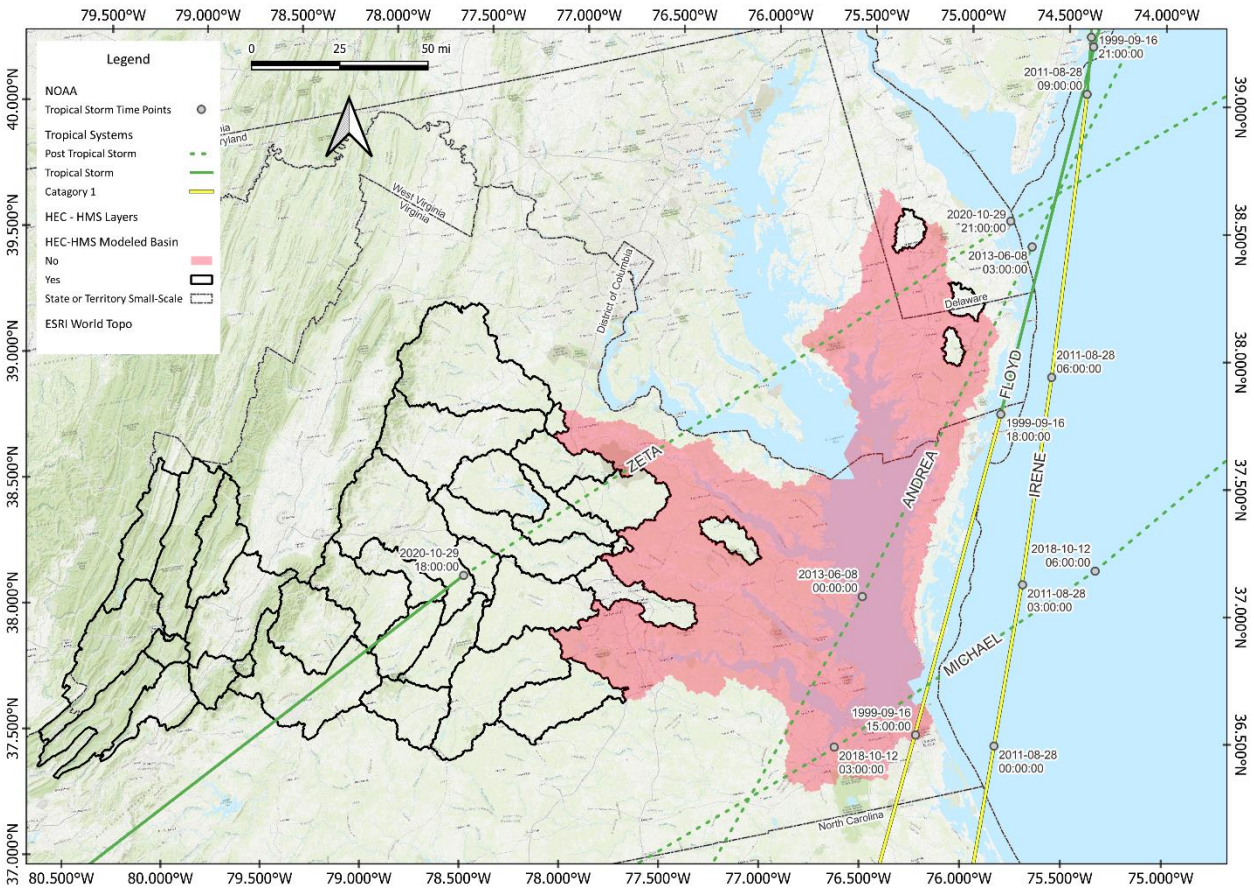

Figure 3. Storm tracks for storms selected for modeling plus two additional storms, Irene and Floyd, for reference.

2.2.2 Precipitation and Temperature

Gridded precipitation and temperature were used as model inputs to be transformed to excess runoff. Precipitation or temperature is placed into a four-dimensional dataset covering spatial x, y, time, and the measured value. From the perspective of the user, pixel values of x, y dimension are seen on the results and are cut into slices of time. Rainfall grids are defined as the instantaneous value of the rate of precipitation in units of inches per hour (in/hr) at time t and are collated in one file over a temporal range (i.e. the range of the event being modeled). Temperature grids are defined as the instantaneous temperature in units of degrees Fahrenheit at time t, and once again are collated over a temporal range. the use of gridded datasets as opposed to spatially averaged precipitation and temperature for each basin was preferred to allow for better temporal and spatial variability across each basin when used with the ModClark method, further discussed below. Gridded precipitation and temperature extents covered the entire Lower Chesapeake model. Analysis of Record for Calibration (AORC) precipitation and temperature grids were used (Fall et al. 2023) in the model. AORC datasets were preferred due to the hourly interval available and resolution of 4km. Further information on these datasets can be found in the description of datasets section.

2.3 *Physical Models - Background*

The physical model covers all the pieces of the HEC-HMS model from canopy interception, excess runoff transformation, infiltration, baseflow / interflow, evapotranspiration, ground water recharge, and routing. These processes are simulated with a physical model or models for each of the parts listed above. Figure 4 summarizes a generalized process that water moves through the hydrology model resulting in a final output of hydrographs at desired locations.

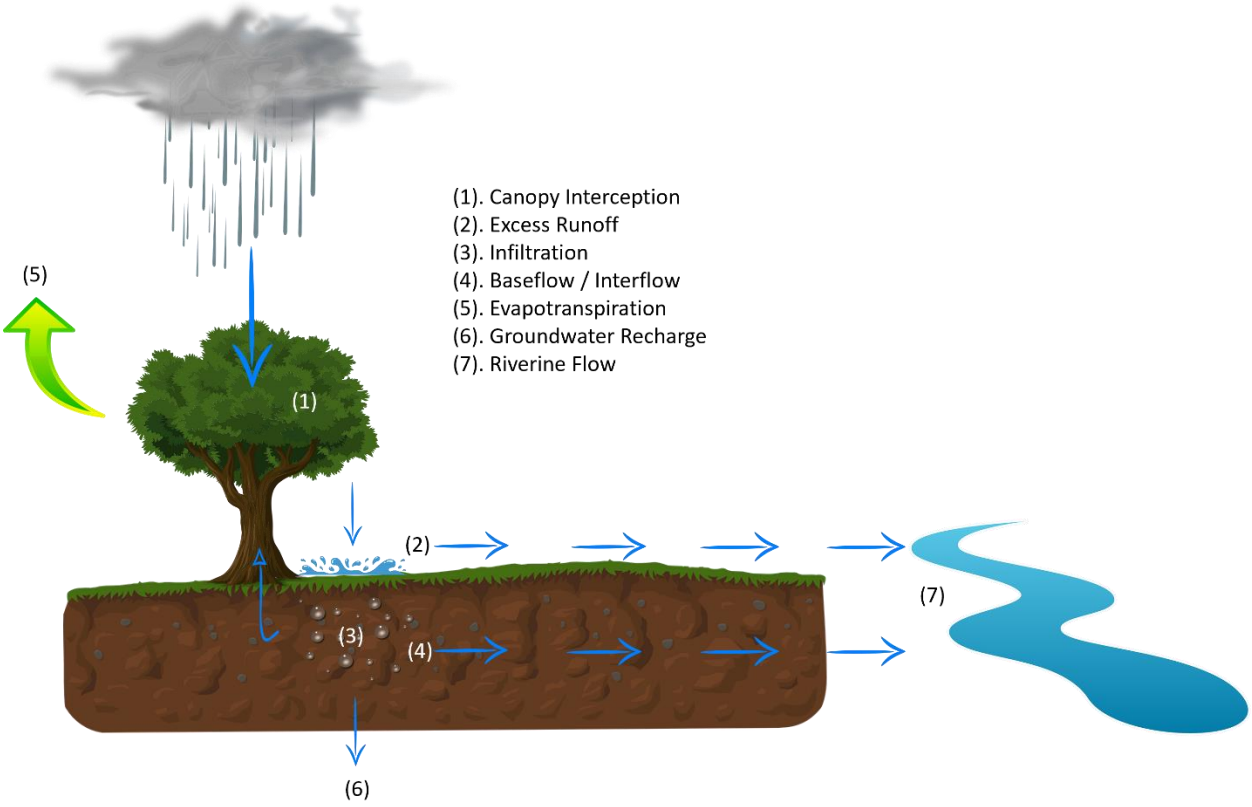

Figure 4. Diagram of physical models and parameters used in the hydrologic model.

2.3.1 *Canopy Loss Model*

The simple canopy model was selected to simulate canopy loss and evapotranspiration from the soil. The simple canopy model applies an initial and max storage value for each sub-basin to determine the amount of precipitation that is intercepted and stored by vegetation during the simulation as well as the amount of evapotranspiration that occurs from the soil during infiltration. Canopy storage works with the canopy intercepting an initial amount of available storage during the simulation (initial storage) and filling up to the maximum. Any additional amount of water past the max storage is no longer

intercepted and goes to the ground. Evapotranspiration will be discussed in the infiltration sections below. The following figure, Figure 5, shows the rules and routes for canopy interception.

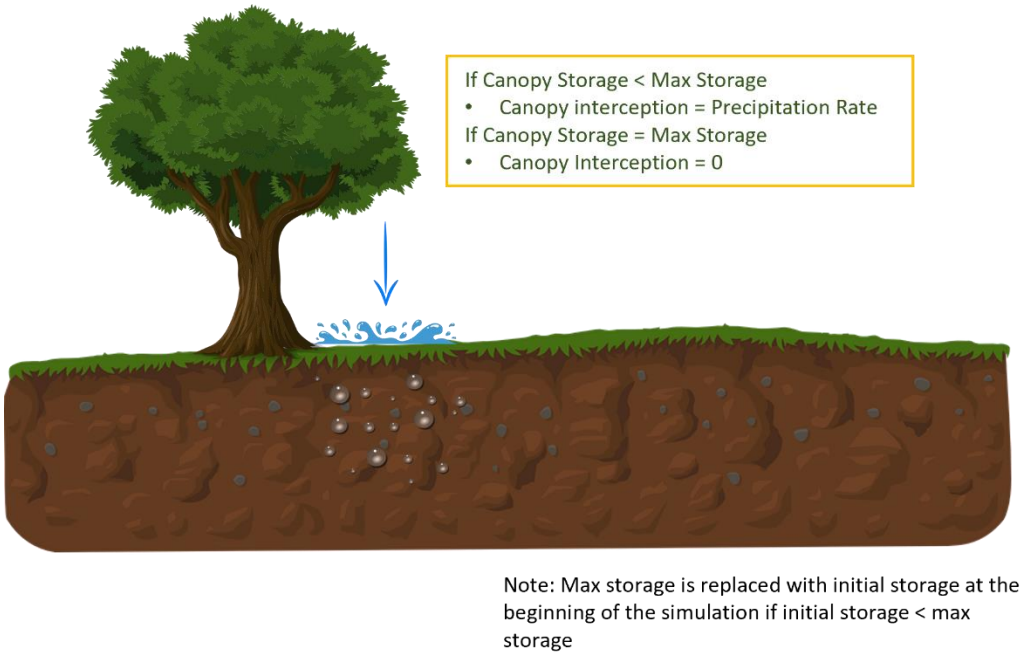

Figure 5. Diagram of canopy interception and loss model.

Canopy parameter values were calculated by spatially averaging across each sub-basin for raster storage values defined from a study by PJ Zinke in 1967 and created using land cover groups from the National Land Cover Dataset (Zinke 1967). The NLCD dataset contains twenty values describing different land cover conditions each with a unique id. The associated storage value and NLCD class applied is listed below in Table 3.

Table 3. Maximum canopy storage applied to respective NLCD class.

Canopy Description	Storage (in)	NLCD Class
General Vegetation	0.05	51, 52, 73, 74, 90, 95
Grasses and Deciduous Trees	0.08	41,43, 71, 72, 81, 82
Coniferous Trees	0.1	42

Evapotranspiration for both wet and dry periods was selected to allow for evapotranspiration to occur over the entire duration of the simulation window.

2.3.2 Evapotranspiration

Evapotranspiration in the model was calculated using the Hamon method. This method calculated the average potential evapotranspiration (ET_o) using a method developed by Hamon in 1963. The main equation uses a coefficient (c), the number of daylight hours (N), and the saturated water vapor density at the daily mean temperature (P_t).

Equation 1. Evapotranspiration

$$ET_o = c\frac{N}{12}P_t$$

Daylight hours for this equation are calculated using the following equations (Allen et al. 1998):

Equation 2. Daylight Hours from sunset angle

$$N = \frac{24}{\pi}\omega_s$$

ω_s = sunset hour angle

Equation 3. Sunset hour angle

$$\omega_s = arccos[-tan(\phi)tan(\delta)]$$

φ = latitude

δ = solar declination

Saturated vapor pressure at the daily temperature (T) is calculated using the equation (Allen et al. 1998):

Equation 4. Saturated vapor pressure at the daily temperature

$$e_s(T) = 0.6108exp\left[\frac{17.27T}{T + 273.3}\right]$$

Saturated vapor density (P_t) is calculated using the $e_s(T)$ from the previous equation and plugged into (Wiederhold 1997):

Equation 5. Saturated vapor density

$$P_t = \frac{216.7e_s(T)}{T + 273.16}$$

For Hamons coefficient 0.0065 in/g/m^3 was used (Hydrologic Engineering Center 2023). Calibration was not performed on this model as the effect was small.

2.3.3 Soil Infiltration Model

Two models were used for soil infiltration within the hydrologic model: deficit & constant loss, and layered Green and Ampt. Both infiltration models were selected to allow for multiple day events to be simulated. These two models allow for evaporation/transpiration and have a reset point where the soil returns to the wilting point storage where capillary action prevents the removal of additional water from the soil. Deficit and constant infiltration loss was used in the upstream basins where clay was the

less dominant soil type and layered Green and Ampt was used in the downstream basins where a higher concentration of clay was present in the soil substrata. The infiltration loss methods used in each basin are shown in Figure 6 below:

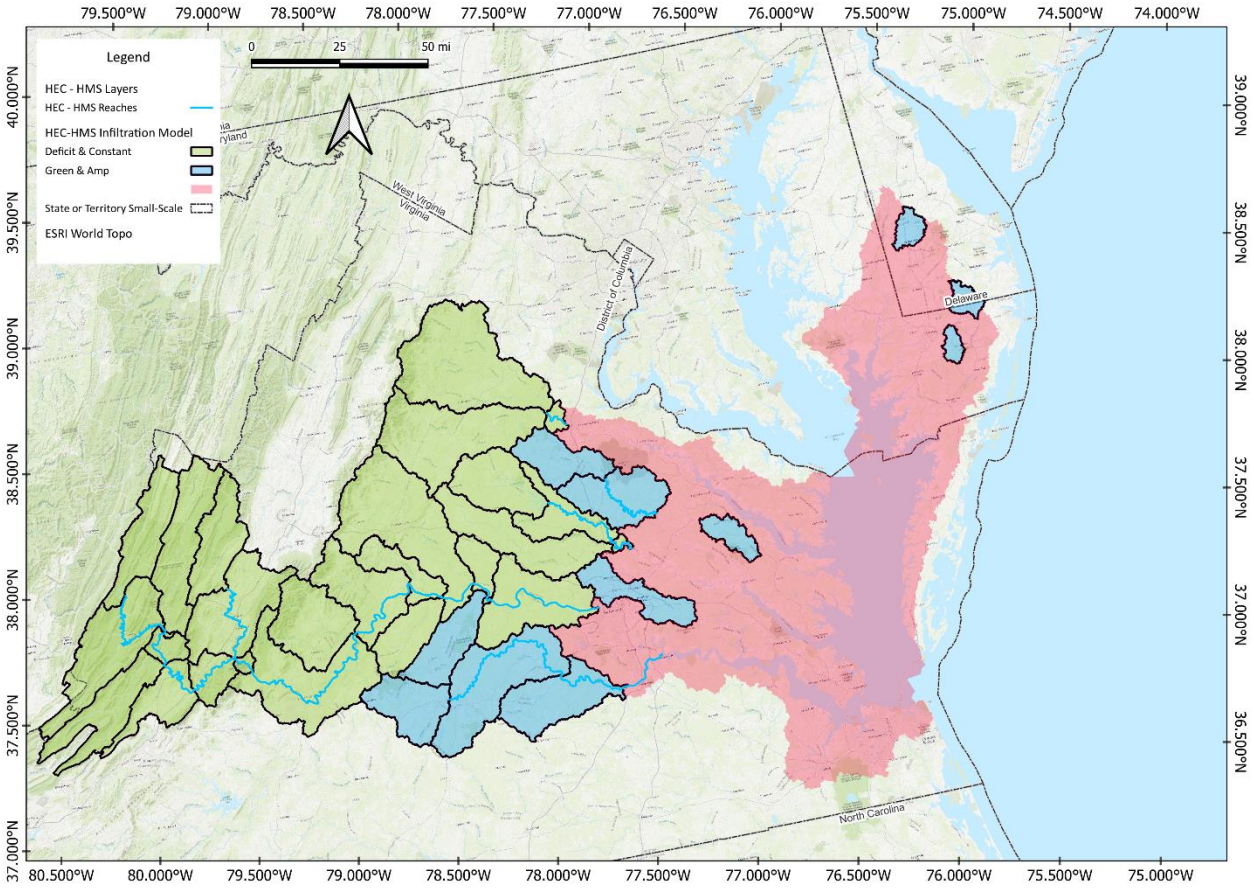

Figure 6. Infiltration model type used within the Lower Chesapeake watershed.

2.3.4 Deficit and Constant Loss Model

The deficit and constant infiltration loss model is a simple infiltration loss model that requires four parameters to be input into each sub-basin. The deficit and constant model simulate the infiltration of water through the soil by defining an initial deficit, the amount of storage available at the beginning of the simulation or reset period, a maximum deficit, the total amount of water the soil can hold at full saturation, and a constant rate, the speed at which water moves through the soil. In addition, an impervious surface cover percent is defined to account for a reduction of infiltration in regions where greater amounts of urbanization has occurred.

During the simulation surface water, post canopy interception, infiltrates into the soil at the same rate as the precipitation rate. As water enters the soil column, the soil will reach a maximum storage, defined by the difference in the maximum deficit and the initial deficit. Once at saturation, percolation occurs out from the soil column into baseflow or ground water recharge allowing for surface water to enter at the same rate. This occurs at the constant infiltration rate defined for the model. Surface water accumulated at a rate above the infiltration rate during saturation is considered as excess runoff and is then moved to the transformation part of the model. In addition, evapotranspiration takes an additional amount of water out of the soil storage based on ET demand. (Chow 1964; Hydrologic Engineering Center 2023; Maidment 1992). Figure 7 summarizes the infiltration rules for the deficit and constant loss model.

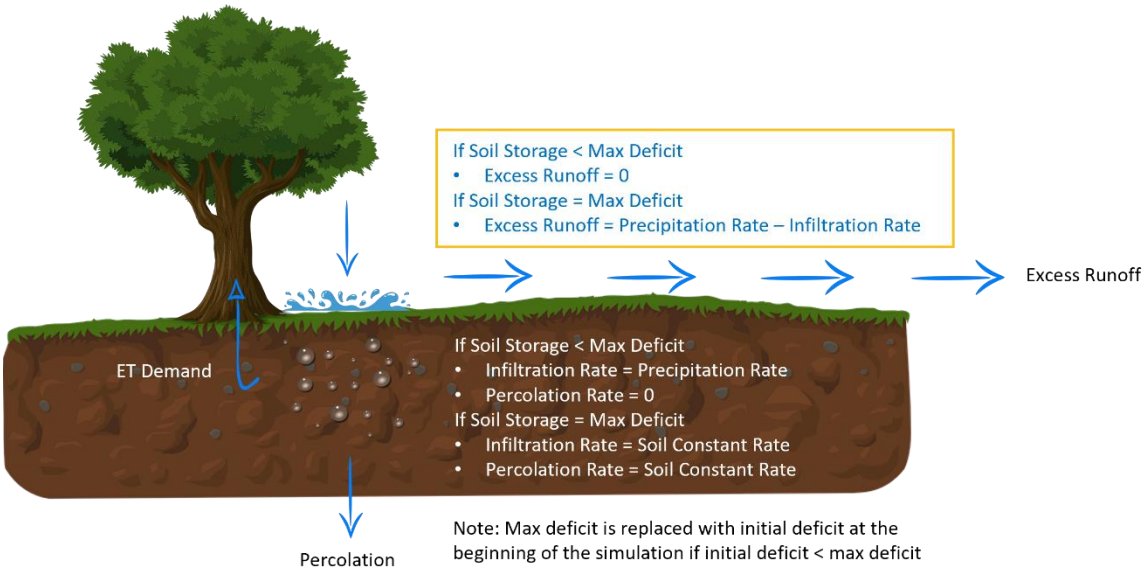

Figure 7. Diagram of deficit and constant loss model.

Impervious values were calculated from the Multi-Resolution Land Characteristics Consortium (MRLC) 2021 Urban Imperviousness raster by spatially averaging values within each sub-basin. The three layers (initial deficit, maximum deficit, and constant rate) were set with initial values using soil texture characteristics (effective porosity, wilting point, and saturated hydraulic conductivity) from the Rawls, Brakensiek, and Miller (1983) study. Soil texture characteristics are applied to raster data from the University of California Davis Soil Web-Viewer soil texture dataset before spatial averaging occurs. In addition, the initial deficit was set to the max deficit before calibration. During calibration, all values were modified to meet calibration targets.

2.3.5 Layered Green and Ampt Loss Model

Green and Ampt loss model is a more complex infiltration loss model compared to deficit and constant loss. The Green and Ampt model is an approximate method using Darcy's law to approximate water movement through the soil. In the most basic form, not considering surface ponding, the equation solved at each time step of an event is (Hydrologic Engineering Center 2023; Maidment 1992):

Equation 6. Layered Green and Ampt infiltration loss

$$f = K\left[1 + \frac{(\phi - \theta_i)S_f}{F}\right]$$

f = Infiltration rate

K = Effective hydraulic conductivity

Θ_i = Initial water content

Φ = Soil porosity

S_f = effective suction at the wetting front

Further modifications to the model can be made to account for ponding on the surface based on the rainfall rate.

The layered Green and Ampt loss model use two soil layers and evapotranspiration as opposed to the single layer model which just considers a uniform soil in which water infiltrates through. Once water infiltrates into the soil from the surface the four parameters, wetting front suction head (suction), conductivity, max seepage, and max percolation control the rate at which the water infiltrates down through the two soil columns (Maidment 1992). Suction defines the attraction of water within void spaces in the soil and influences the initial rate of downward flow. Conductivity defines the rate at which water infiltrates through the soil and is set to the saturated hydraulic conductivity of the soil. Once the first layer of soil reaches saturation, water enters the second layer with a rate being defined by the max seepage rate. Finally, after the second layer reaches field capacity the max percolation rate is applied out of the second layer into base flow. The dry duration is set to a specified time, in this case 10 – 14 hours to allow for the system to reset to initial values between storm events (Hydrologic Engineering Center 2023). This technique differs to that of Maidment 1992 in which hydraulic conductivity is changes to the harmonic mean of the two soils, once water enters the second layer:

Equation 7. Harmonic hydraulic conductivity of two soils

$$K_h = \sqrt{K_1 K_2}$$

K_h = harmonic hydraulic conductivity of layers 1 and 2

K_1 = hydraulic conductivity of layer 1

K_2 – hydraulic conductivity of layer 2

Evapotranspiration (ET) occurs differently in the layered Green and Ampt when compared to the more simplistic methods. Water available for evapotranspiration is defined as the difference between the saturated content and the wilting point. The wilting point is the water content unavailable due to capillary action in the soil. ET demand is taken from the first layer until the available water is reach and then the same is applied to the second layer. At this point ET demand is taken from both layers until one of them reached the wilting point. Upon reaching the wilting point in one layer ET is taken from the remaining reserve in the layer about the wilting point until depleted (Hydrologic Engineering Center 2023).

Initial parameters values were calculated by spatially averaging values for each sub basin using saturated capacity ratio, field capacity ratio, and wilting point ration values reported by Maidment's Handbook of Hydrology and applied to the soil texture raster from the University California Davis Soil Web-View. Table 4 lists the values used for each soil texture for calculating the Green and Ampt infiltration loss parameters. Figures 8 and 9 map the location of soil texture types at 0 – 25 cm and 25 – 50 cm depth.

Table 4. Soil water capacity parameters and respective soil textures based on University of Davis Soil Web-view data.

Soil Texture (ID)	Saturated Capacity (Ratio)	Field Capacity (Ratio)	Wilting Point (Ratio)
Sand (1)	0.417	0.091	0.033
Loamy Sand (2)	0.401	0.125	0.055
Sandy Loam (3)	0.412	0.207	0.095
Loam (4)	0.434	0.207	0.117
Silt Loam (5)	0.486	0.330	0.133
Silt (6)	0.460	0.36	0.119
Sandy Clay Loam (7)	0.330	0.255	0.148
Clay Loam (8)	0.390	0.318	0.197
Silty Clay Loam (9)	0.432	0.366	0.208
Sandy Clay (10)	0.321	0.339	0.239

Silty Clay (11)	0.423	0.387	0.250
Clay (12)	0.385	0.396	0.272

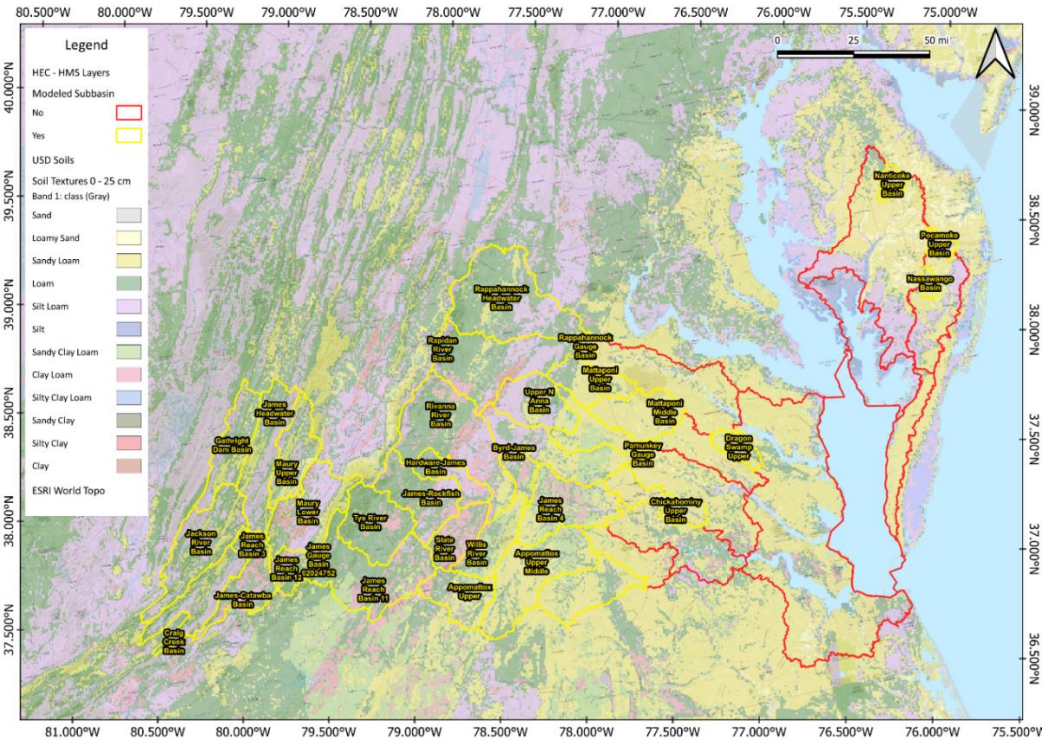

Figure 8. Soil textures from University of California Davis Soil Web-Viewer for depths 0-25cm

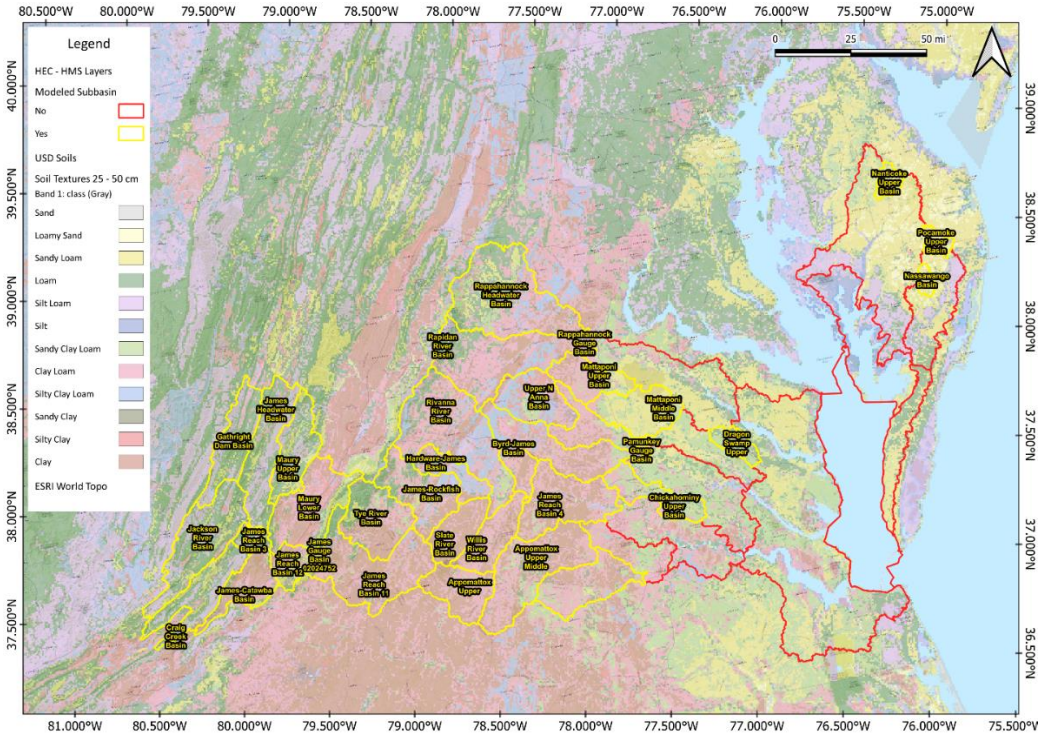

Figure 9. Soil textures from University of California Davis Soil Web-Viewer for depths 25-50cm

2.3.6 Transform Model

To use gridded precipitation data, the transform model selected to simulate the transform of precipitation to run off was the Modified Clark transform model (ModClark). This method is derived from the continuity equation and linear reservoir model (Hydrologic Engineering Center 2023):

Equation 8. Continuity equation

$$\frac{dS}{dt} = I_t - O_t$$

$\frac{dS}{dt}$ = The change in storage over time

I_t = The average inflow to storage at time t

O_t = The average outflow from storage at time t

Equation 9. Linear reservoir storage

$$S_t = RO_t$$

S_t = Storage at time t

R = Constant linear reservoir parameter

O_t = the outflow from storage at time t

Combining these two equations, applying finite difference, and calculating the coefficients of the resulting equations can be used to create the unit hydrographs for excess run off in a basin using recursive calculations between the first and last equations (Hydrologic Engineering Center 2023):

Equation 10. Combined equations for unit hydrograph calculation with defined coefficients and variables

$$O_t = C_A I_t + C_B O_{t-1}$$

C_A = Inflow coefficient

C_B = Outflow coefficient

O_t = the outflow from storage at time t

O_{t-1} = the outflow from storage at time t-1

I_t = The average inflow to storage at time t

Equation 11. Coefficient A for ModClark transformation equation

$$C_A = \frac{\Delta t}{R + 0.5\Delta t}$$

R = Constant linear reservoir parameter

Equation 12. Coefficient B for ModClark transformation equation

$$C_B = 1 - C_A$$

Equation 13. Average outflow between interval t to t-1

$$\overline{O}_t = \frac{O_{t-1} + O_t}{2}$$

In the ModClark method basins are discretized and each discretized cell has a TC and R. Time of concentration is first calculated with various available methods since many have been derived based on

different regional watersheds. In this study, eight methods were used to calculate an initial time of concentration. The trimean was then applied to these methods to get an initial TC for each basin. At the basin level the discretized cell TC is derived using the following equation (Hydrologic Engineering Center 2023):

Equation 14. Cell time of concentration

$$T_{t,cell} = T_{c,watershed} \frac{D_{cell}}{D_{Max}}$$

D_{cell} = The travel distance from a grid cell to the watershed outlet

D_{max} = the travel distance for the grid cell that is most distant from the watershed outlet

The storage coefficient for each basin is initially calculated using the following equation (Hydrologic Engineering Center 2023):

Equation 15. Storage coefficient

$$X = \frac{R}{T_C + R}$$

X = A coefficient, often set to 0.75 or using regional study information

Discretization for each basin was set to a 2000 km x 2000 km grid to match the resolution of the gridded precipitation datasets.

2.3.7 Base Flow Model

The linear reservoir model was used as the only base flow modeling method in the hydrology model. The linear reservoir uses the similar principles to the Muskingum routing method which is the basis for the routing used in this model. The Muskingum model is based on the continuity equation form (Hydrologic Engineering Center 2023; Maidment 1992):

Equation 16. Continuity equation

$$\overline{I_t} - \overline{O_t} = \frac{\Delta S_t}{\Delta t_{\square}}$$

I_t = Inflow at time t

O_t = Outflow at time t

ΔS_t = Change in storage at time t

Derivation of the model results in the basic equation (Hydrologic Engineering Center 2023; Maidment 1992):

Equation 17. Derived storage at time t for base flow

$$S_t = K[XI_t + (1 - X)O_t]$$

S_t = Storage at time t

K = Travel time

X = dimensionless weight ($0 \leq X \leq 0.5$)

HEC-HMS uses a modified form of this equation to recursively solve for storage (Hydrologic Engineering Center 2023; Maidment 1992):

Equation 18. Outflow at time t for base flow

$$O_t = \left(\frac{\Delta t - 2KX}{2K(1 - X) + \Delta t}\right) I_t + \left(\frac{\Delta t + 2KX}{2K(1 - X) + \Delta t}\right) I_{t-1} + \left(\frac{2K(1 - X) - \Delta t}{2K(1 - X) + \Delta t}\right) O_{t-1}$$

I_t = Inflow at time t

O_t = Outflow at time t

K = Travel time

X = dimensionless weight ($0 \leq X \leq 0.5$)

The Muskingum method uses K, X, and number of sub-reaches to define routing. Linear reservoir does the same method of routing using set number layered reservoirs to route the base flow, similar to Muskingum K, a coefficient of time that water is stored, similar to Muskingum X, and a number of reservoirs, similar to the number of sub reaches that water is routed through in Muskingum routing. These variables control the time in which water flows through the ground while maintaining continuity

of volume in the system. This can be modified using the groundwater fraction to calibrate what is applied as base flow and that which goes to aquifer recharge. Initial values, those not calibrated, were set as default values and were modified during calibration to meet targets.

2.3.8 Routing Model

Routing of water downstream in the hydrology model was simulated using the Muskingum-Cunge model. Muskingum-Cunge is a derivative of the Muskingum model, as described above, created by Miller and Cunge in 1975. The Muskingum-Cunge model is a conservation of volume and simplified momentum equation model with variable coefficients, those that change at every time step.

In the Muskingum-Cunge model, the parameters K and x are replaced with several additional parameters with the use of finite difference approximation to determine attenuation and travel time at multiple time steps during the simulation. With these changes the model uses applied physical parameters as opposed to the dimensionless X that must be determined through calibration. Derivations of this model are more complicated and will not be derived in this section. The parameters that are required in the Muskingum-Cunge model are initial type, reach length, reach slope, Manning's n, space-time method, index method, index flow, and a shape that defines the cross section of the reach. Most of these parameters are self-explanatory, however for my model initial type was set to discharge = inflow, space-time method was auto to force computation to stay stable, and index of flow that was set to the median discharge of the inflow hydrograph for the reach, and eight-point cross sections were created for each reach. The eight-point cross sections were selected at the most representative location along each reach as shown below in the figure.

2.4 Description of Input Datasets

Each dataset used in the model or development of the model is listed in the following sub sections. Datasets were all accessed as of 2024 but may have varying data in which they were collected or went through quality control and assurance.

2.4.1 United States Geological Survey (USGS) 3DEP Terrain Digital Elevation Model

USGS 3DEP program was created to collaborate with agency partners and industry to develop a US wide digital elevation coverage program that conforms to a set standard of accuracy, units, methods, datums, coordinate systems, etc. for elevation-based projects. Model data varies from 2004 to present if it meets the standards of the program.

2.4.2 National Weather Service (NWS) Analysis of Record for Calibration (AORC) Precipitation and Temperature Grids

AORC hourly precipitation and temperature gridded data is a high resolution, 1km mesh of hourly near surface weather. AORC data covers the continental United States ranging from 1950 to present. AORC datasets are often referenced for use in hydrologic studies.

2.4.3 California Soil Resources Lab Soil Properties Datasets

The California Soil Resource Lab soils properties datasets were created by aggregating and merging the United States Department of Agriculture National Cooperative Soil Survey datasets (USDA – NCSS). Two USDA – NCSS datasets are available that cover the continental United States, the Digital General Soil Map of the United States (STATSGO) and The Soil Survey Geographic Database (SSURGO). The California Soil Resources Datasets use STATSGO data where possible and backfill with SSURGO in missing areas. Raster datasets are set to 800m grid cells and cover multiple soil characteristics such as texture, saturated hydraulic conductivity, bulk density, drainage class, etc.

2.4.4 Multi-Resolution Land Characteristics Consortium (MRLC) Urban Impervious Dataset

The MRLC urban impervious data set is a percentage value of impervious surface coverage based on the MRLC land cover raster dataset. Machine learning is applied to the Landsat Remote Sensing data to develop a percentage of impervious cover. Raster resolution is 30 meters for the continental United States. Available dates for urban impervious range from 2001 to 2021 separated at two-to-three-year intervals.

2.4.5 Multi-Resolution Land Characteristics Consortium National Land Cover Dataset

The MRLC National Land Cover Dataset is a 30m x 30m resolution raster covering the continental United States. Land cover values are derived using multiple different techniques on Landsat imagery and various other geospatial datasets. Automated processes, such as machine learning, are used on the previous datasets to identify classifications for land cover.

2.4.6 USGS Stream Gauge Network Datasets

The USGS stream gauge network is a nationwide network maintained by the USGS. Data includes flow, stage, water quality variables, and pictures of high stage or flow events. Data is obtained on a 15 min to 1 hour interval for many of the major streams in the United States.

2.4.7 USGS National Hydraulic Plus High-Resolution Dataset (NHDPlus HR)

The USGS National Hydraulic dataset was developed by the USGS using DEMs that were hydrologically corrected and delineated. The dataset is available by watershed and contains information such as stream distances, slopes, types of streams, etc.

2.5 Calibration

Calibration is separated into a background on the statistics used to calibrate the model and the standard by which each statistic is applied in determining whether a model is calibrated. Calibration statistics include: Nash Sutcliffe Model Efficiency, percent bias error, and the coefficient of determination.

2.5.1 Statistics

The Nash-Sutcliffe model efficiency (NSE) coefficient, percent bias (P-BIAS), and Pearson's coefficient of determination (R^2) were used to determine the statistical accuracy of the predictive hydrographs of the model to the observed hydrographs. Calibration statistics are based on what is

available in the HEC-HMS and what is recommended from a study by Moriasi et al in 2007 as reliable methods in hydrological modeling.

2.5.1.1 Nash Sutcliffe Model Efficiency

The Nash-Sutcliffe model efficiency coefficient is a standard regression statistic that measures the differences in residuals between observed and simulated hydrograph points. The NSE takes the sum of the squared residuals of the observed and simulated hydrograph points and compares them to the sum of the squared residuals of the observed and observed mean to determine similarity. Values closer to 1 indicate a better fit, while values less than 1 indicate a poor fit. Values greater than 0 are generally considered adequate for a reasonably calibrated model.

Equation 19. Nash-Sutcliffe Model Efficiency

$$NSE = 1 - [\frac{\sum_{i=1}^{n}(Y_i^{\text{obs}} - Y_i^{\text{sim}})^2}{\sum_{i=1}^{n}(Y_i^{\text{obs}} - Y^{\text{mean}})^2}]$$

Y^{obs} = Observed Values

Y^{sim} = Simulated Values

Y^{mean} = Mean Values

2.5.1.2 Percent Bias Error

The percent bias (P-BIAS) is an error statistic that measures the percent difference between the observed hydrograph values and the simulated hydrograph values. The error value is calculated using the difference in observed and simulated values divided by the observed values to get a ratio. This is multiplied by 100 to get a percentage. Higher error values indicate a larger difference between the observed and the simulated hydrograph points. The optimal value for this statistic is 0.

Equation 20. Percent bias error statistic

$$PBIAS = [\frac{\sum_{i=1}^{n}(Y_i^{\text{obs}} - Y_i^{\text{sim}}) * (100)}{\sum_{i=1}^{n}(Y_i^{\text{obs}})}]$$

Y^{obs} = Observed Values

Y^{sim} = Simulated Values

2.5.1.3 The Coefficient of Determination

The coefficient of determination (R^2) is a standard regression statistic for looking at linear relationships between the observed and simulated values of the hydrographs. R^2 values closer to 1 indicate a positive linear relationship with a good fit to the observed data while values closer to 0 indicate no linear relationship, not a good fit to the observed data.

Equation 21. The coefficient of determination

$$R^2 = 1 - \frac{SS_{res}}{SS_{tot}}$$

SS_{res} = Residual Sum of Squares

SS_{tot} = Total Sum of Squares

2.5.2 Methods

Model calibration goals focused on the three statistics listed above comparing hydrographs from the simulated stream flow and observed stream flow (USGS gauge data) at computation points defined in the model, see Table 9 in the results for locations. Models were calibrated from the most upstream basins of the watershed and then proceeding downstream to the end of the model. Final USGS gauge locations are: James River near Richmond, VA (USGS 02037500), Appomattox River at Matoaca, VA (USGS 02041650), Chickahominy River near Providence Forge, VA (USGS 02042500), Pamunkey River near Hanover, VA (USGS 01673000), Mattaponi River near Beulahville, VA (USGS 01674500), and Rappahannock River near Fredericksburg, VA (USGS 0166800). Four additional Basins, Dragon Swamp, Nassawango Creek, Pocomoke River, and Nanticote River were calibrated at the basin level as no additional downstream data was available for further calibration. Statistical goals for calibration are listed below. Each basin was calibrated to optimize for Nash Sutcliffe Error, Percent Bias, and the Coefficient of Determination. The desired statistical goals are listed below in Table 5 shown below for statistical methods.

Table 5. Calibration standards based on Morasi 2007.

Performance Ratings for Evaluation Metrics for a daily and weekly time step			
Performance Rating	**R^2**	**NSE**	**PBIAS**
Very Good	0.65 < R^2 ≤ 1.00	0.65 < NSE ≤ 1.00	$PBIAS$ < ±15
Good	0.55 < R^2 ≤ 0.65	0.55 < NSE ≤ 0.65	±15 ≤ $PBIAS$ < ±20
Satisfactory	0.40 < R^2 ≤ 0.55	0.40 < NSE ≤ 0.55	±20 ≤ $PBIAS$ < ±30
Unsatisfactory	R^2 ≤ 0.40	NSE ≤ 0.40	$PBIAS$ ≥ ±30

The above performance ratings were created by Moriasi et al in 2007 and were adopted by the US Army Corps of Engineers as their standard for model calibration. In summary Moriasi stated that a NSE > 0.50, RSR < 0.70, and PBIAS ±25% for streamflow constituted a calibrated model against observed stream flows. Calibration of each basin was attempted to get as close to good or very good for performance rating. Failure to reach this performance rating would indicate either limitations with the model or methods which were employed.

Calibration of each basin and reach was completed by varying parameters, listed in the table below, from the initial calculated values in each physical model. Physical models are listed in the previous sections. Values were varied manually to ensure that changes were realistic in nature. Modifications of the parameters were done for each event modeled with a goal of obtaining similar physical parameter values between the simulated events. The model parameters that were varied are listed in Table 6 shown below.

Table 6. Varied parameters to meet calibration targets.

Sub-Model	**Varied Parameter(s)**
Infiltration (Deficit & Constant)	Initial deficit, max deficit, constant loss
Infiltration (Green & Ampt)	Initial content (layers 1 & 2), conductivity, max seepage, max percolation, suction, and dry duration.
Transform	Time of concentration (TC), storage coefficient (R)
Baseflow	Number of layers, initial base flow (layers 1 & 2), ground water recharge fraction (Layers 1 & 2), ground water coefficient (layers 1 & 2), and number or reservoirs (layers 1 & 2)

2.6. Output Data

Output data is summarized for both the model and for the frequency analysis that was performed using HEC-SSP for the model data.

2.6.1 Model Outfall Locations

For this model hydrographs at the most downstream points of the model can be used as future boundary conditions in a surface model. These points are located at USGS Gauges: James River near Richmond, VA (USGS 02037500), Appomattox River at Matoaca, VA (USGS 02041650), Chickahominy River near Providence Forge, VA (USGS 02042500), Pamunkey River near Hanover, VA (USGS 01673000), Mattaponi River near Beulahville, VA (USGS 01674500), and Rappahannock River near Fredericksburg, VA (USGS 0166800). The remaining four calibrated basins, Dragon Swamp Creek, Nassawango Creek, Pocomoke River, and Nanticoke River are to be used as representative basins that can be referenced when applying calibrated parameters to ungagged basin in future work.

2.6.2 Frequency Analysis at Outfalls

A return frequency analysis of all outfall stream gauge location was done using HEC-SSP, a statistical software for running statistical analysis on flow, stage, and precipitation data. Gauge data was downloaded from the USGS data server for each of the outflow points, James near Richmond, VA, Appomattox River at Matoaca, VA, Chickahominy River at Providence Forge, VA, Pamunkey River near Hanover, VA, Mattaponi River at Beulahville, VA, Rappahannock River near Fredericksburg, VA, Nassawango Creek near Snow Hill, VA, Dragon Swamp at Mascot, VA, and Pocomoke River near Willards, VA. A bulletin 17c analysis was done for each of the gauges to determine the return frequency of flows. The bulletin 17c analysis is an analysis created by the United States Army Corps of Engineers to calculate flow and stage return frequencies and confidence intervals using Equal Moment Analysis to define systematic or historical flow or stage records, Multiple Grubbs-Beck to remove outliers, and apply a station skew if needed. In this analysis no station skew was applied (Bartles et al. 2023).

CHAPTER

3 RESULTS

3.1 Final Model Description

The completed hydrologic model (HEC-HMS) of the Lower Chesapeake Watershed consisted of 39 modeled sub-basins, 20 reaches, 2 inflow sources, and 8 outflow sinks. 59% of the watershed was modeled using HEC-HMS, covering a total area of 12,173 mi^2. The remaining area, approximately 8,425.04 mi^2 was modeled in HEC-RAS due to the very low relief in the coastal plain. Table 7 summarizes the geospatial measures for the sub basins that were delineated in the model. Geospatial measures are taken directly from the HEC-HMS model.

Table 7. geospatial measures for delineated sub-basins in the HEC-HMS model.

Sub-Basin Name	***Area***	***Longest Flow Path***	***Longest Flow Path Slope***	***Basin Slope***	***Basin Relief***	***Relief Ratio***	***Elongation Ratio***	***Drainage Density***
Units	**(mi2)**	**(ft)**	**(ft/ft)**	**(ft/ft)**	(ft)			(mi/mi^2)
Appomattox Lower Middle	399.26	59.40	0.00147	0.061	468.88	0.0015	0.37956	0.074
Appomattox Upper	302.42	49.94	0.00257	0.098	681.07	0.0026	0.39289	0.002
Appomattox Upper Middle	640.06	86.99	0.00104	0.082	474.93	0.0010	0.32817	0.106
Appomattox Lower Basin	269.29	53.64	0.00161	0.054	462.53	0.0016	0.34522	0.065
Byrd-James Basin	127.57	32.93	0.00225	0.080	397.41	0.0023	0.38705	0.060
Chickahominy Upper Basin	251.94	53.16	0.00118	0.042	341.89	0.0012	0.33692	0.006
Craig Creek Basin	372.32	93.17	0.00686	0.280	3,448.27	0.0070	0.23370	0.121
Dragon Swamp Upper	110.23	27.23	0.00102	0.047	205.89	0.0014	0.43510	0.000
Gathright Dam Basin	344.61	54.84	0.00841	0.340	3,127.49	0.0108	0.38196	0.030
Hardware-James Basin	187.58	48.39	0.00827	0.143	2,184.27	0.0086	0.31935	0.067
Jackson River Basin	557.56	76.11	0.00721	0.323	3,042.64	0.0076	0.35007	0.081

Sub-Basin Name	*Area*	*Longest Flow Path*	*Longest Flow Path Slope*	*Basin Slope*	*Basin Relief*	*Relief Ratio*	*Elongation Ratio*	*Drainage Density*
Units	(mi2)	(ft)	(ft/ft)	(ft/ft)	(ft)			(mi/mi^2)
James Gauge Basin 02016500	4.30	4.19	0.06016	0.322	1,473.95	0.0666	0.55873	0.221
James Gauge Basin 02024752	25.45	9.55	0.03758	0.372	2,378.40	0.0472	0.59632	0.333
James Gauging Basin	3.63	3.64	0.00986	0.104	199.41	0.0104	0.59054	0.515
James Headwater Basin	463.41	94.60	0.00609	0.306	3,395.06	0.0068	0.25676	0.105
James Reach Basin 11	673.68	92.33	0.00759	0.183	3,700.63	0.0076	0.31722	0.094
James Reach Basin 12	139.07	32.61	0.01448	0.303	3,531.36	0.0205	0.40810	0.162
James Reach Basin 3	81.63	18.78	0.02527	0.288	2,708.91	0.0273	0.54295	0.182
James Reach Basin 4	497.79	56.33	0.00110	0.072	379.08	0.0013	0.44694	0.084
James-Catawba Basin	247.76	62.98	0.00521	0.221	2,798.40	0.0084	0.28200	0.093
James-Rockfish Basin	412.69	55.67	0.00767	0.198	3,691.87	0.0126	0.41175	0.077
Lower N Anna Basin	251.47	53.75	0.00150	0.064	453.01	0.0016	0.33291	0.138
Mattaponi Middle Basin	347.03	60.13	0.00112	0.065	360.37	0.0011	0.34956	0.121
Mattaponi Upper Basin	256.28	45.53	0.00186	0.059	457.13	0.0019	0.39678	0.012
Maury Lower Basin	508.51	60.88	0.00392	0.240	3,366.84	0.0105	0.41793	0.077
Maury Upper Basin	328.29	52.10	0.01112	0.277	3,356.99	0.0122	0.39245	0.016
Nanticoke Upper Basin	72.40	15.04	0.00054	0.011	50.90	0.0006	0.63830	0.000
Nassawango Basin	44.30	14.23	0.00088	0.010	73.81	0.0010	0.52790	0.000
Pamunkey Gauge Basin	17.54	14.65	0.00239	0.067	193.24	0.0025	0.32260	0.724
Pocomoke Upper Basin	64.87	16.47	0.00035	Relief	45.94	0.0005	0.55186	0.000
Rapidan River Basin	694.43	94.16	0.00709	0.130	3,917.75	0.0079	0.31579	0.059

Sub-Basin Name	*Area*	*Longest Flow Path*	*Longest Flow Path Slope*	*Basin Slope*	*Basin Relief*	*Relief Ratio*	*Elongation Ratio*	*Drainage Density*
Units	(mi2)	(ft)	(ft/ft)	(ft/ft)	(ft)			(mi/mi^2)
Rappahannock Gauge Basin	38.11	11.31	0.00511	0.102	331.66	0.0056	0.61614	0.256
Rappahannock Headwater Basin	859.09	74.52	0.00894	0.131	3,850.93	0.0098	0.44381	0.047
Rivanna River Basin	828.35	84.62	0.00376	0.152	3,404.65	0.0076	0.38380	0.074
Slate River Basin	245.15	107.31	0.00313	0.066	1,770.49	0.0031	0.22703	0.108
S. Anna River Basin	466.19	50.89	0.00331	0.095	980.23	0.0037	0.34714	0.000
Tye River Basin	417.98	48.53	0.01385	0.233	3,709.75	0.0145	0.47532	0.019
Upper N Anna Basin	342.34	38.65	0.00287	0.071	938.79	0.0046	0.54019	0.034
Willis River Basin	278.50	62.97	0.00158	0.081	526.56	0.0016	0.29903	0.041

Reaches in the model covered a total distance of 519.66 mi with the average reach distance equaling 25.98 mi. Reach slope maximum was 0.002 ft/ft and minimum was 0.001 ft/ft. The table below shows two additional topographic calculations that affect flow: the difference in minimum and maximum elevation of a basin (relief) and the amount of curvature in a river (sinuosity). Table 8 summarizes the geographic data for the reaches developed for the model.

Table 8. Reach statistics for reaches in the HEC-HMS model.

Reach	Length (MI)	Slope (FT/FT)	Relief (FT)	Sinuosity
Jackson Reach	45.20	0.00177	421.77	3.06
James Reach 15	0.96	0.00094	4.76	1.08
James Reach 14	14.87	0.00095	74.90	1.65
James Reach 13	22.93	0.00092	111.56	2.11
James Reach 12	22.53	0.00090	106.93	1.58

Reach	Length (MI)	Slope (FT/FT)	Relief (FT)	Sinuosity
Maury Reach	39.09	0.00200	413.14	1.97
James Reach 11	8.49	0.00191	85.71	1.34
James Reach 10	63.38	0.00076	253.49	2.04
James Reach 9	31.64	0.00053	89.27	1.56
James Reach 8	12.59	0.00076	50.52	1.18
James Reach 7	12.07	0.00048	30.61	1.31
James Reach 6	7.72	0.00024	9.90	1.38
James Reach 5	1.88	0.00029	2.92	1.33
James Reach 4	39.95	0.00030	62.44	1.32
Rappahannock Gauge Reach	9.76	0.00085	43.70	1.54
Appomattox Reach 3	67.77	0.00036	128.58	2.12
Appomattox Reach 2	29.47	0.00061	94.85	1.55
N Anna Reach	34.79	0.00081	148.94	1.62
Pamunkey Reach	12.71	0.00010	6.82	2.66
Mattaponi Reach	41.84	0.00030	66.70	2.42

The final HEC-HMS geometry was used across all calibration events and is shown in Figure 10 below for spatial reference.

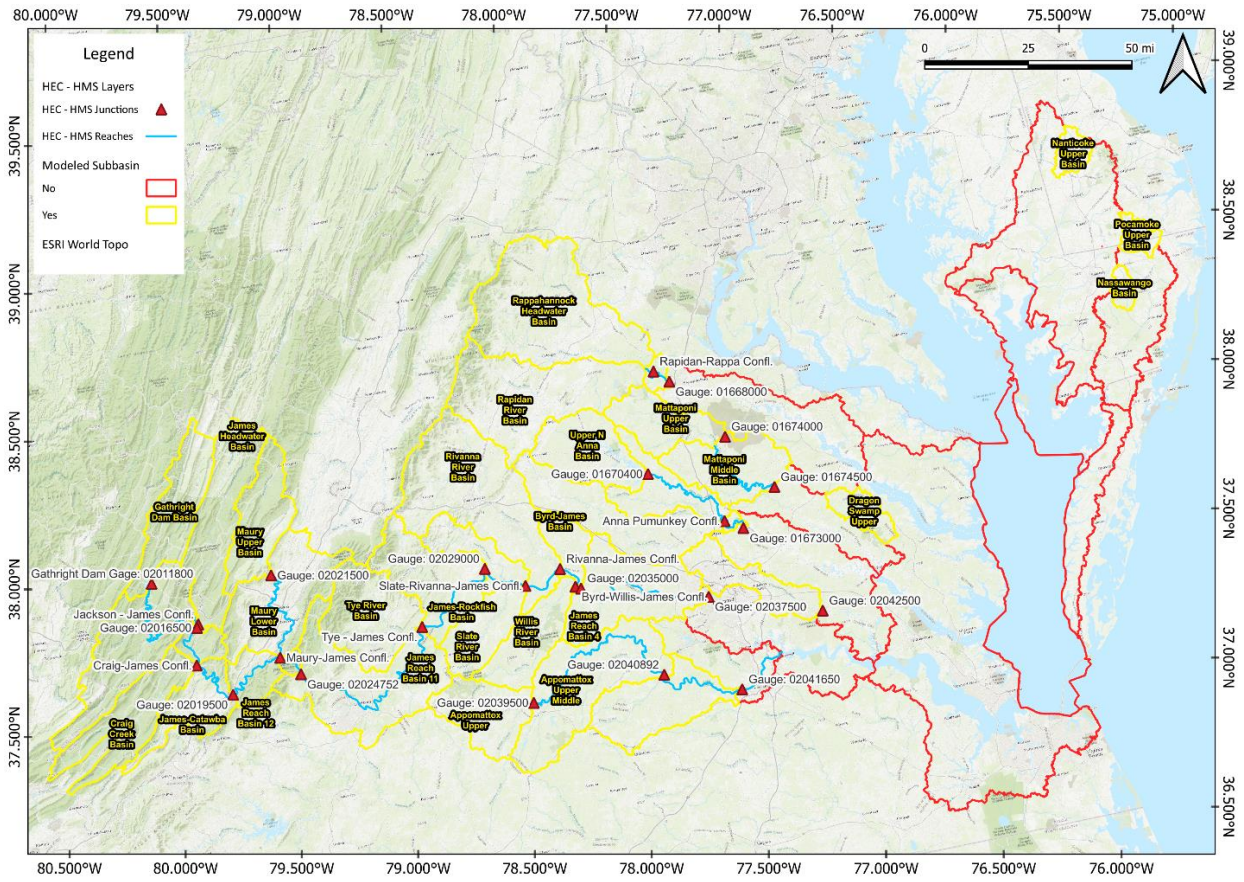

Figure 10. Final HEC-HMS model geometry.

3.2 Individual Storm Calibration

Parameter settings, canopy loss, infiltration loss, transform, etc., for the final calibrated models depended on the event. Significant differences between events were evident. Parameter settings were finalized by seeking NSE values closest to 1, bias percentage closest to 0, and R^2 values closest to 1. The calibration statistics are shown in Table 9 below for each computation point or observed basin depending on where the observed flow data was attached in the model.

Table 9. Event calibration statistics listed at each observed stream gauge or sub-basin.

	Andrea			Michael			TS Zeta		
Computation Point	**NSE**	**% Bias**	**R^2**	**NSE**	**% Bias**	**R^2**	**NSE**	**% Bias**	**R^2**
Gauge: 02016500	0.92	6.48	0.93	0.905	-15.34	0.96	0.89	-13.5	0.95

	Andrea			Michael			TS Zeta		
Computation Point	**NSE**	**% Bias**	**R^2**	**NSE**	**% Bias**	**R^2**	**NSE**	**% Bias**	**R^2**
Gauge: 02019500	0.87	7.86	0.88	0.946	-1.34	0.95	0.71	-31.06	0.88
Gauge: 02021500	0.89	9.06	0.90	0.718	-38.98	0.82	0.87	-26.33	0.96
Gauge: 02024752	0.92	7.72	0.97	0.71	25.89	0.87	0.90	-18.07	0.95
Gauge: 02029000	0.88	0.17	0.88	0.868	17.7	0.92	0.92	-12.8	0.95
Slate River Basin	0.77	5.84	0.79	0.802	18.27	0.85	0.77	-16.63	0.79
Hardware-James Basin	0.73	19.34	0.84	0.835	-6.65	0.87	0.93	3.1	0.93
Gauge: 02035000	0.87	-1.03	0.87	0.937	19.16	0.96	0.98	-9.78	0.99
Gauge: 02037500	0.80	1.44	0.81	0.908	19.45	0.95	0.90	-19.28	0.95
Gauge: 01668000	0.91	13.49	0.93	0.73	-28.68	0.85	-0.52	-18.69	0.46
Gauge: 02040892	0.82	0.27	0.84	0.981	0.57	0.98	0.21	-23.11	0.64
Gauge: 02041650	0.74	5.15	0.78	0.941	5.66	0.95	0.79	-24.36	0.93
Gauge: 01673000	0.87	2.19	0.87	0.86	4.96	0.93	0.95	0.75	0.96
Gauge: 01674000	0.78	9.48	0.81	0.841	12	0.86	0.91	4.73	0.94
Gauge: 01674500	0.96	0.45	0.96	0.858	-2.82	0.9	0.95	-4.05	0.95
Dragon Swamp Upper	0.96	-0.43	0.96	-0.127	1.96	0.25	0.84	2.11	0.92
Nanticoke Upper Basin	0.91	7.47	0.96	0.823	4.49	0.93	0.82	-4.35	0.83
Pocomoke Upper Basin	0.61	-13.18	0.69	0.124	-3.53	0.38	0.95	-0.86	0.95
Nassawango Basin	0.20	20.47	0.57	-0.623	22.37	0.21	0.96	-7.76	0.98

Statistical results at computation points for hydrograph comparisons between simulated and observed can be viewed in figures 11 – 13 for NSE, figures 14 – 16 for P-Bias, and figures 17 – 19 for R^2. Each figure is ordered by events: TS Andrea, TS Michael, and TS Zeta respectively. Color coding for each calibration statistic criteria are shown in the legend of the figures below and in the Table 10. Additional hydrographs with observed and simulated flows are added in the appendix for a more detailed look at the results.

Table 10. Legend for calibration statistics graphs.

Color Code	NSE	% Bias	R^2
Dark Green	≥ 0.8	≥ 15%	≤ 1
Light Green	≥ 0.7	≥ 10%	≤ 0.9
Yellow	≥ 0.5	≥ 5%	≤ 0.75
Red	< 0.5	< 5%	≤ 0.6

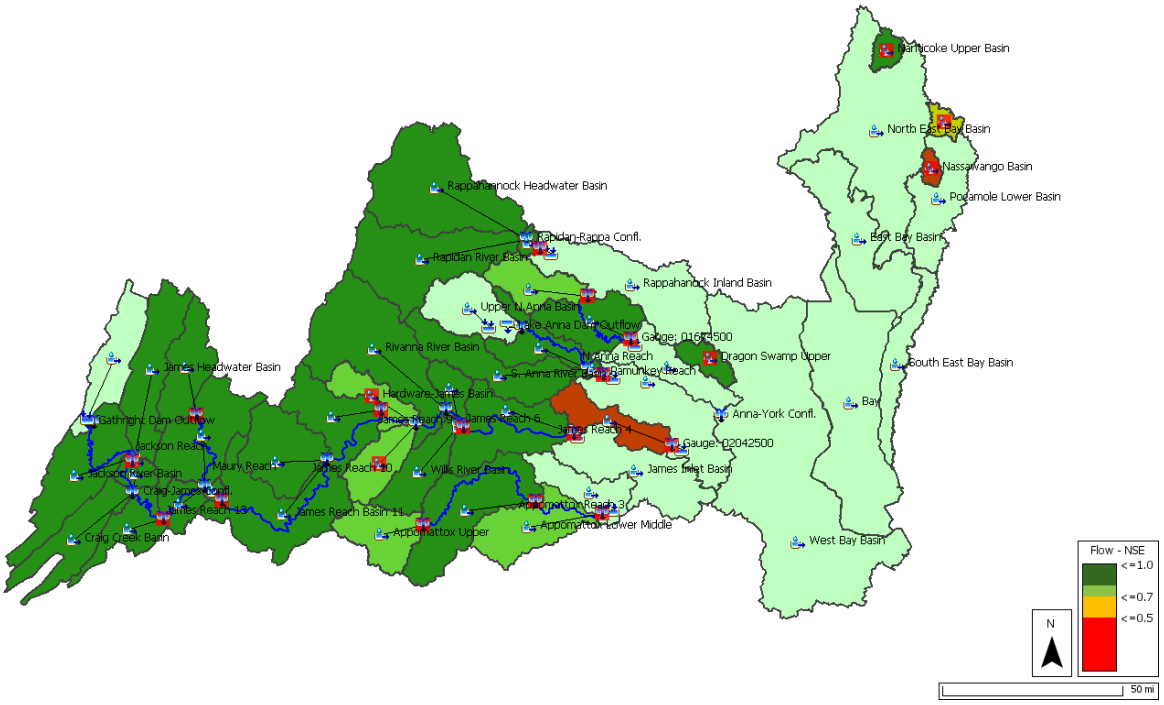

Figure 11. Tropical Storm Andrea NSE color coded calibration results

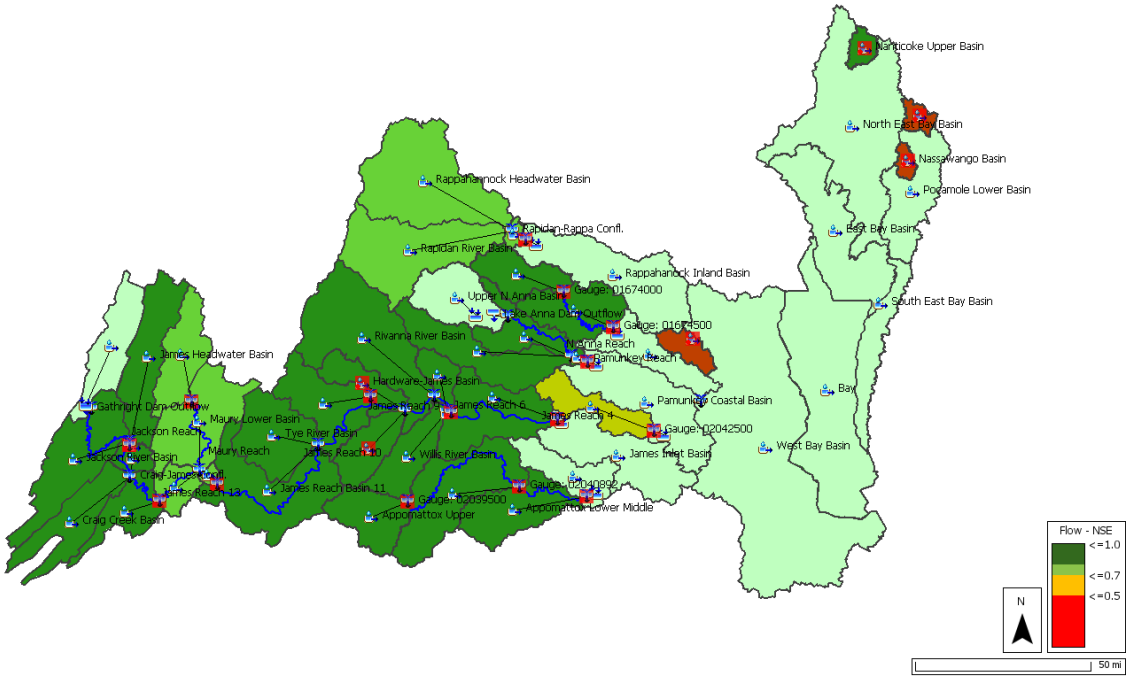

Figure 12. Tropical Storm Michael NSE color coded calibration results

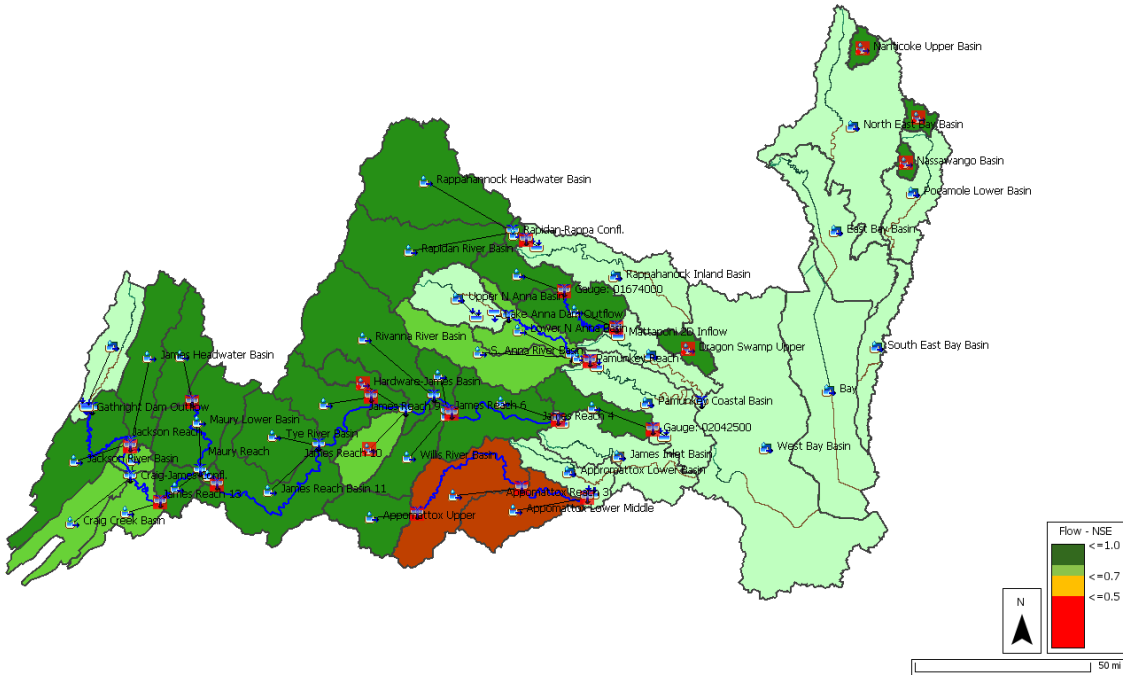

Figure 13. Tropical Storm Zeta NSE color coded calibration results

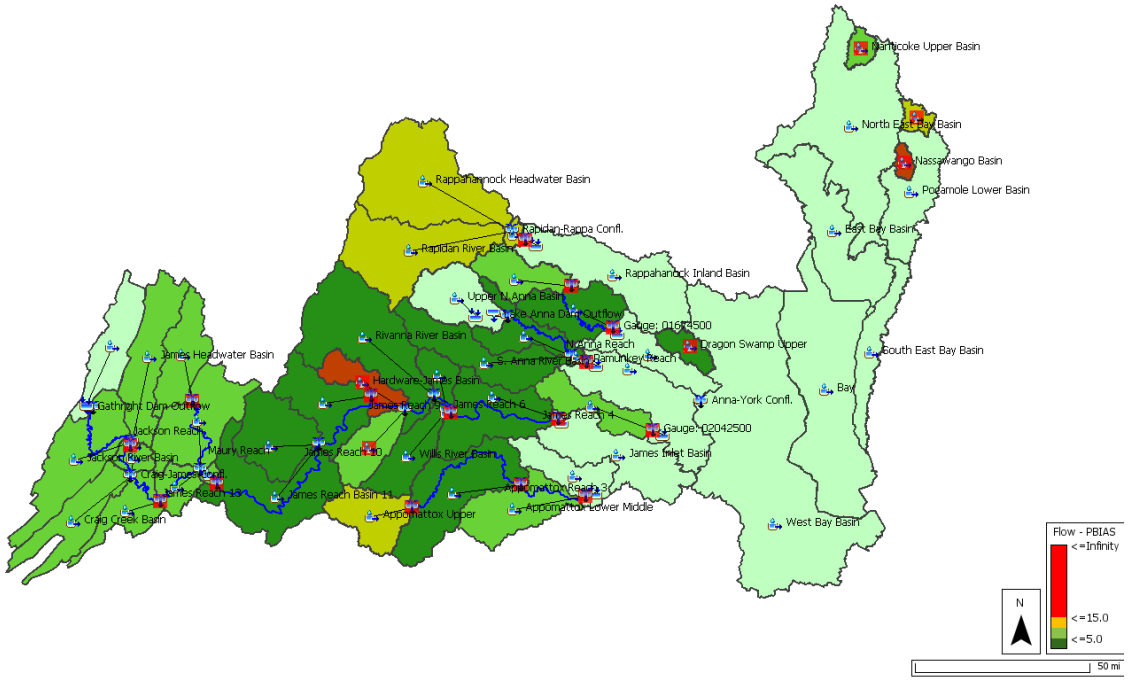

Figure 14. Tropical Storm Andrea Percent Bias color coded calibration results

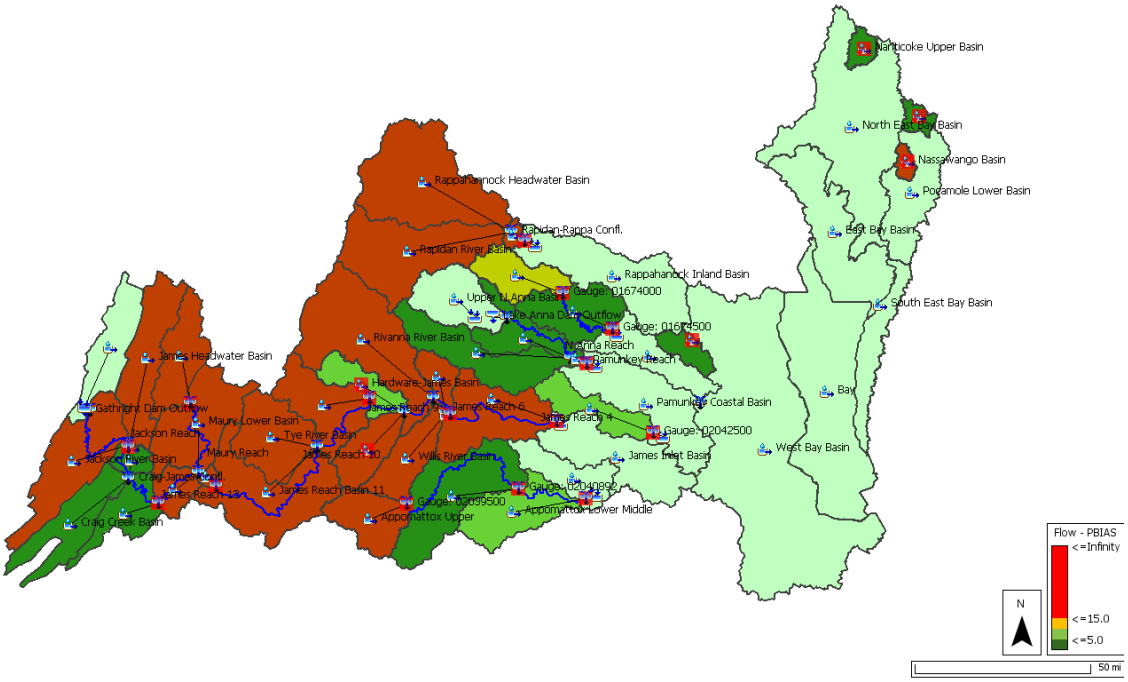

Figure 15. Tropical Storm Michael Percent Bias color coded calibration results

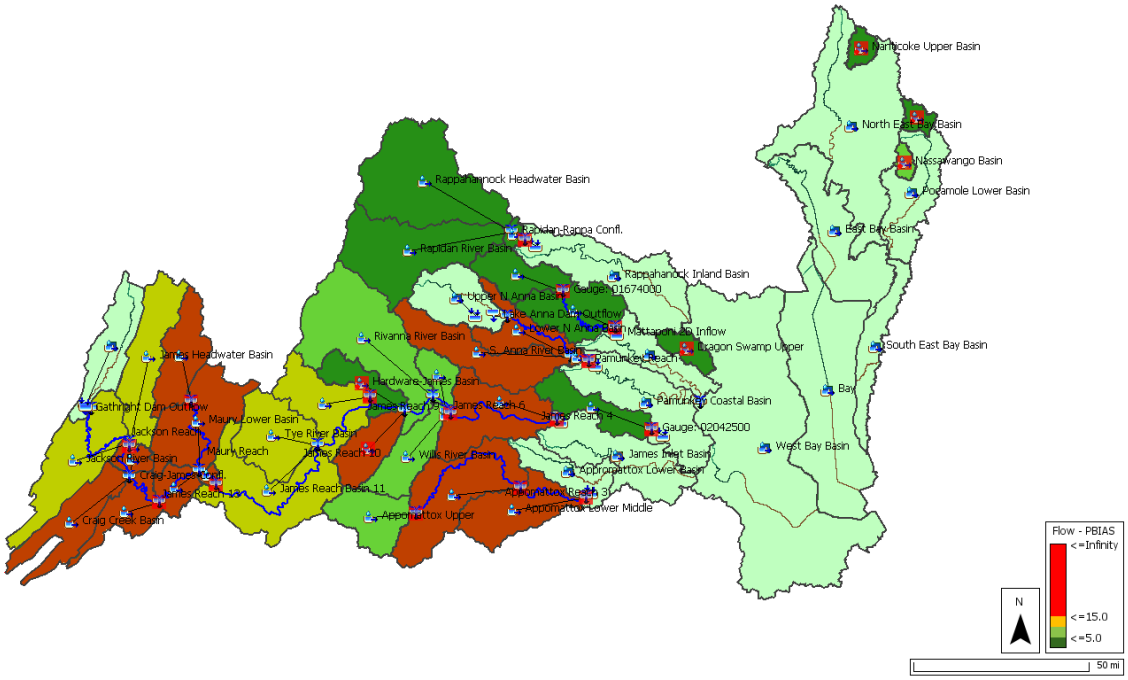

Figure 16. Tropical Storm Zeta Percent Bias color coded calibration results

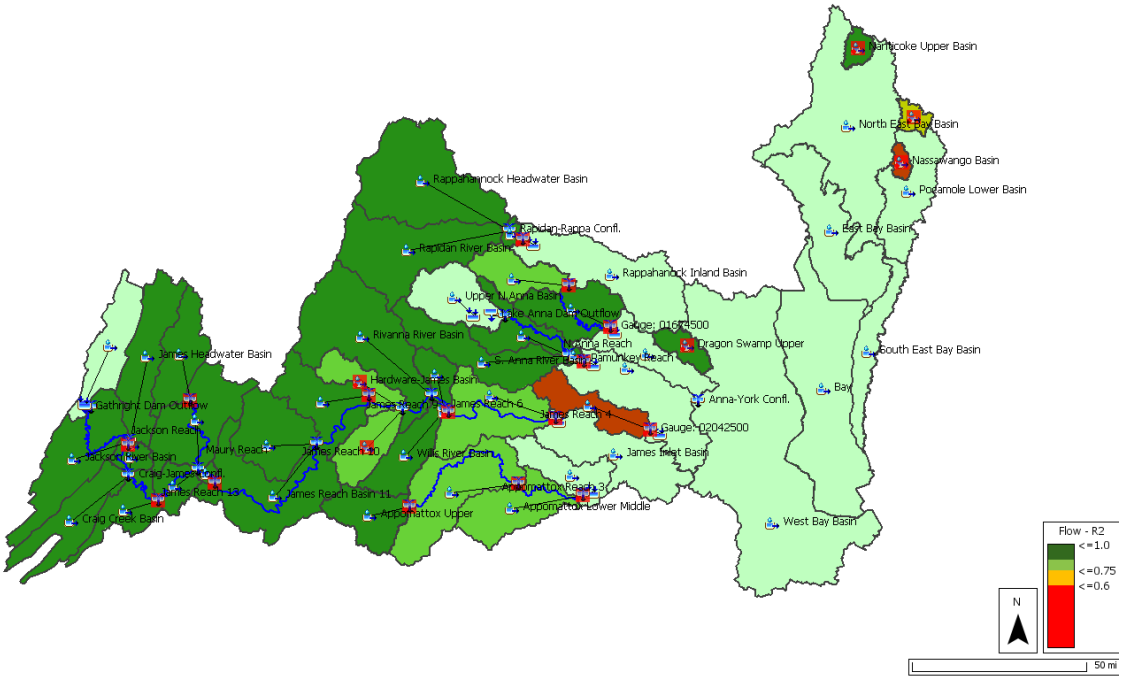

Figure 17. Tropical Storm Andrea R-squared color-coded calibration results

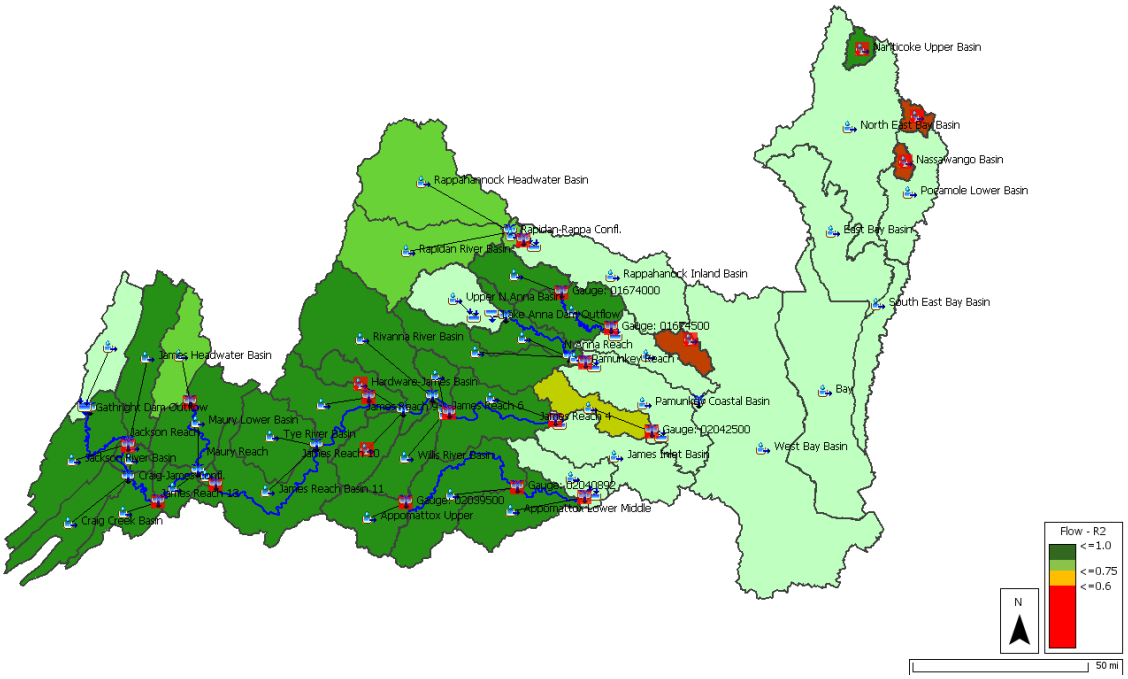

Figure 18. Tropical Storm Michael R-squared color-coded calibration results

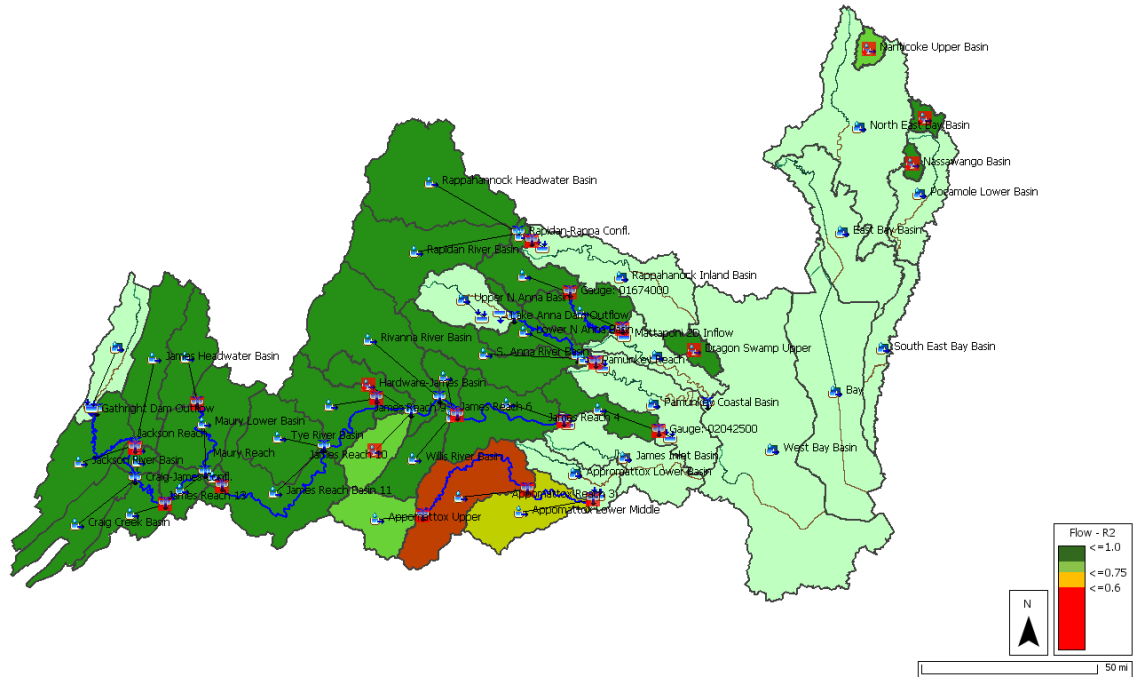

Figure 19. Tropical Storm Zeta R-squared color-coded calibration results

3.3 Precipitation, Infiltration, and Excess

Maximum incremental 15-minute precipitation calculated from the model was exported to show the areas of the most intense rainfall during the simulation. These numbers help indicate areas of high intensity that would likely receive flooding in the modeled sub basins. Maximum 15-minute incremental precipitation is summarized for each basin in Table 11.

Table 11. Maximum 15-minute incremental precipitation by sub basin

Sub Basin Name	TS Andrea	TS Michael	TS Zeta
Appomattox Lower Middle	0.359	0.332	0.330
Appomattox Upper	0.399	0.456	0.263
Appomattox Upper Middle	0.267	0.512	0.253
Byrd-James Basin	0.815	0.634	0.339
Chickahominy Upper Basin	0.395	0.356	0.285
Craig Creek Basin	0.504	0.276	0.292
Dragon Swamp Upper	0.553	0.419	0.225
Gathright Dam Basin	0.275	0.162	0.244
Hardware-James Basin	0.454	0.439	0.264
Jackson River Basin	0.281	0.185	0.256
James Gauge Basin 02016500	0.496	0.239	0.299
James Gauge Basin 02024752	0.451	0.525	0.353
James Gauging Basin	0.619	0.855	0.349
James Headwater Basin	0.420	0.191	0.224
James Reach Basin 11	0.416	0.279	0.308
James Reach Basin 12	0.602	0.351	0.313
James Reach Basin 3	0.536	0.484	0.299
James Reach Basin 4	0.510	0.697	0.315
James-Catawba Basin	0.399	0.340	0.328
James-Rockfish Basin	0.302	0.356	0.264
Lower N Anna Basin	0.403	0.416	0.314
Mattaponi Middle Basin	0.471	0.347	0.277
Mattaponi Upper Basin	0.452	0.324	0.426
Maury Lower Basin	0.405	0.247	0.308
Maury Upper Basin	0.632	0.234	0.237
Nanticoke Upper Basin	0.775	1.514	0.641
Nassawango Basin	0.596	0.603	0.579
Pamunkey Gauge Basin	0.460	0.534	0.338
Rapidan River Basin	0.397	0.266	0.383
Rappahannock Gauge Basin	0.292	0.413	0.506
Rappahannock Headwater Basin	0.343	0.210	0.252
Rivanna River Basin	0.393	0.347	0.310
S. Anna River Basin	0.345	0.391	0.322
Slate River Basin	0.452	0.363	0.419
Tye River Basin	0.398	0.353	0.322
Upper N Anna Basin	0.327	0.666	0.431
Willis River Basin	0.596	0.330	0.384

Maximum 15-minute incremental precipitation is shown in figures 20 – 22 for each calibrated event. Symbology for each category is shown in the respective legend in the figures.

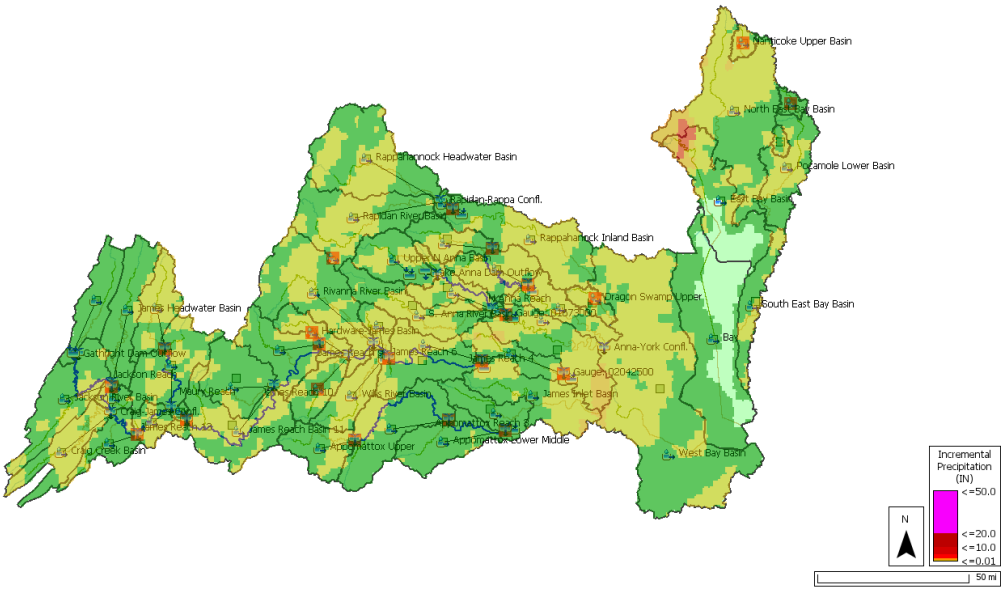

Figure 20. Maximum 15-minute incremental precipitation for tropical storm Andrea

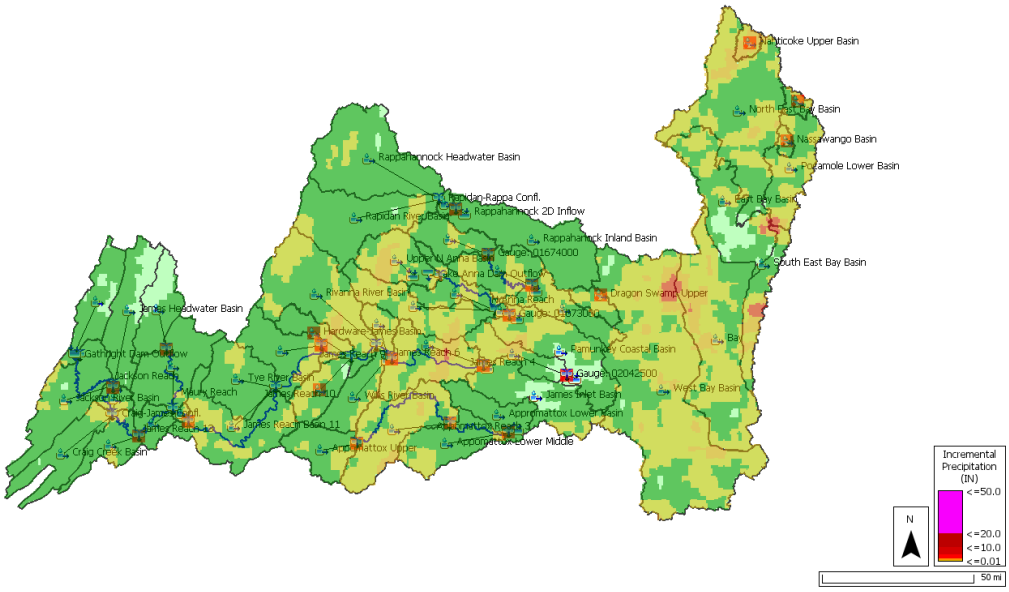

Figure 21. Maximum 15-minute incremental precipitation for tropical storm Michael

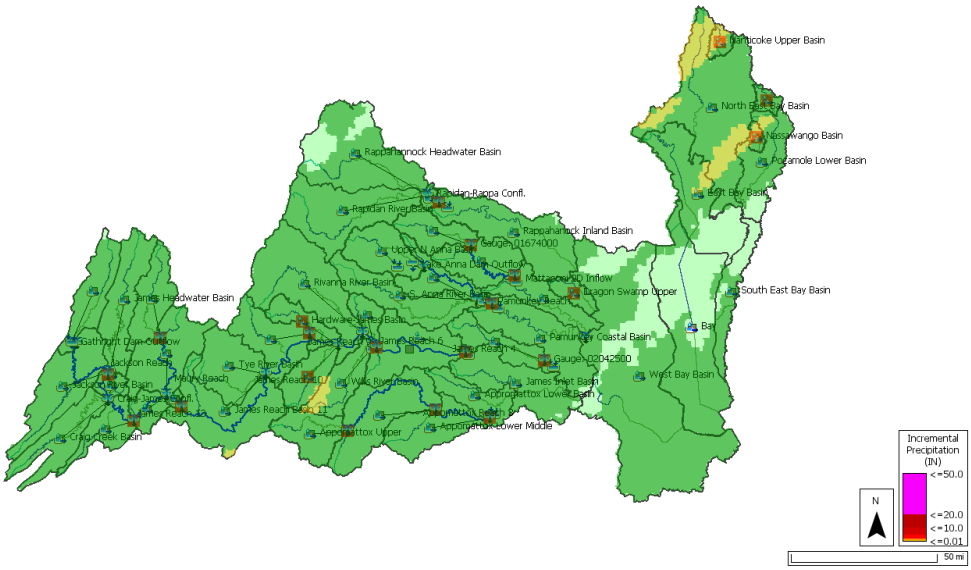

Figure 22. Maximum 15-minute incremental precipitation for tropical storm Zeta

Cumulative precipitation used for calibration was exported to show the difference in pattern rainfall between events. Cumulative precipitation for each sub-basin is listed in Table 12, seen below, for each of the calibration events and for each basin used in the model. Unused basins were excluded from the table.

Table 12. Cumulative precipitation for each event by sub basin

	Cumulative Precipitation (in)			Cumulative Excess Precipitation (in)			Cumulative Infiltration Loss (in)		
Event	**TS Andrea**	**TS Michael**	**TS Zeta**	**TS Andrea**	**TS Michael**	**TS Zeta**	**TS Andrea**	**TS Michael**	**TS Zeta**
Appomattox Lower Middle	4.149	4.510	1.888	0.180	0.619	0.018	3.969	3.892	1.870
Appomattox Upper	3.832	5.515	2.200	0.652	1.070	1.142	3.179	4.446	1.058
Appomattox Upper Middle	4.273	6.335	2.043	0.407	2.093	0.390	3.866	4.241	1.653
Byrd-James Basin	5.341	4.957	2.651	1.729	1.795	1.013	3.613	3.163	1.638
Chickahominy Upper Basin	5.325	3.631	2.186	0.757	0.563	0.613	4.568	3.068	1.573
Craig Creek Basin	7.944	4.766	2.205	1.354	0.291	0.069	6.589	4.476	2.136
Dragon Swamp Upper	6.000	3.500	1.825	0.254	0.086	0.139	5.746	3.415	1.686
Gathright Dam Basin	4.883	3.046	1.941	0.096	0.009	0.011	4.787	3.038	1.930
Hardware-James Basin	5.900	5.958	2.719	0.820	0.600	0.526	5.080	5.358	2.193
Jackson River Basin	5.991	3.457	2.121	1.831	0.628	0.419	4.160	2.829	1.702
James Gauge Basin 02016500	5.695	3.810	2.001	1.558	0.642	0.298	4.137	3.168	1.703
James Gauge Basin 02024752	5.548	7.649	2.604	0.692	2.312	0.395	4.856	5.338	2.209
James Gauging Basin	5.800	4.940	2.283	0.288	0.464	0.011	5.511	4.476	2.272

	Cumulative Precipitation (in)			Cumulative Excess Precipitation (in)			Cumulative Infiltration Loss (in)		
James Headwater Basin	5.419	3.194	1.745	0.926	0.401	0.220	4.494	2.793	1.525
James Reach Basin 11	5.554	6.208	2.742	0.911	1.417	1.207	4.642	4.791	1.534
James Reach Basin 12	7.812	6.128	2.547	2.640	1.494	0.460	5.173	4.634	2.087
James Reach Basin 3	6.341	4.562	2.126	0.559	0.208	0.027	5.782	4.355	2.100
James Reach Basin 4	5.314	5.127	2.502	0.701	1.210	0.073	4.613	3.917	2.429
James-Catawba Basin	7.310	5.221	2.347	0.765	0.556	0.158	6.546	4.665	2.189
James-Rockfish Basin	6.155	5.899	2.483	0.685	1.607	1.078	5.470	4.292	1.405
Lower N Anna Basin	4.623	3.804	2.541	1.074	0.180	1.065	3.549	3.624	1.475
Mattaponi Middle Basin	4.905	3.682	2.365	0.426	0.297	0.801	4.480	3.386	1.564
Mattaponi Upper Basin	3.961	4.051	2.924	0.509	0.325	1.213	3.452	3.726	1.711
Maury Lower Basin	6.187	5.333	2.605	1.378	2.658	0.629	4.808	2.675	1.976
Maury Upper Basin	6.261	3.429	1.680	0.798	1.064	0.262	5.464	2.365	1.418
Nanticoke Upper Basin	6.474	4.256	4.508	0.257	0.268	0.746	6.217	3.988	3.762
Nassawango Basin	5.896	3.936	3.079	0.065	0.725	1.025	5.832	3.211	2.055
Pamunkey Gauge Basin	4.660	3.849	2.631	0.018	0.802	0.443	4.642	3.047	2.188
Pocomoke Upper Basin	4.853	2.656	3.609	0.458	0.310	0.562	4.394	2.346	3.047
Rapidan River Basin	4.638	4.418	3.172	1.312	1.298	1.149	3.326	3.120	2.022

	Cumulative Precipitation (in)			Cumulative Excess Precipitation (in)			Cumulative Infiltration Loss (in)		
Rappahannock Gauge Basin	3.346	3.848	3.560	0.871	0.557	1.682	2.475	3.292	1.878
Rappahannock Headwater Basin	4.488	3.996	2.241	1.619	0.137	0.537	2.869	3.859	1.704
Rivanna River Basin	5.310	5.600	2.873	1.174	1.356	1.307	4.136	4.244	1.566
S. Anna River Basin	4.648	5.070	2.591	1.017	0.618	1.091	3.631	4.452	1.500
Slate River Basin	5.142	5.186	2.546	0.872	1.052	1.315	4.270	4.135	1.231
Tye River Basin	6.153	6.116	2.705	0.685	1.097	1.215	5.468	5.019	1.490
Upper N Anna Basin	4.472	5.280	2.939	0.150	0.707	0.065	4.322	4.573	2.875
Willis River Basin	4.930	4.113	2.631	1.168	0.765	1.218	3.763	3.348	1.413

Cumulative precipitation is shown in figures 23 – 25, cumulative excess precipitation in figures 26 - 28, and cumulative infiltration losses in figures 29 – 31, for each calibrated event. Symbology for each category is shown in the respective segments in the figures below.

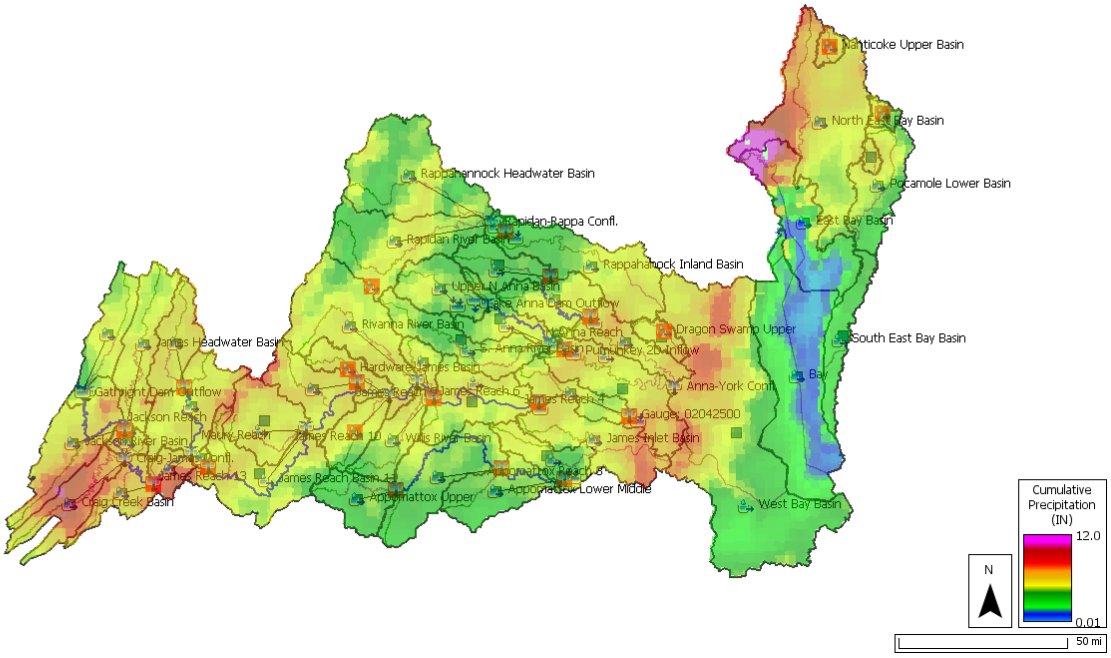

Figure 23. Tropical Storm Andrea cumulative precipitation (June 6 – 20, 2013)

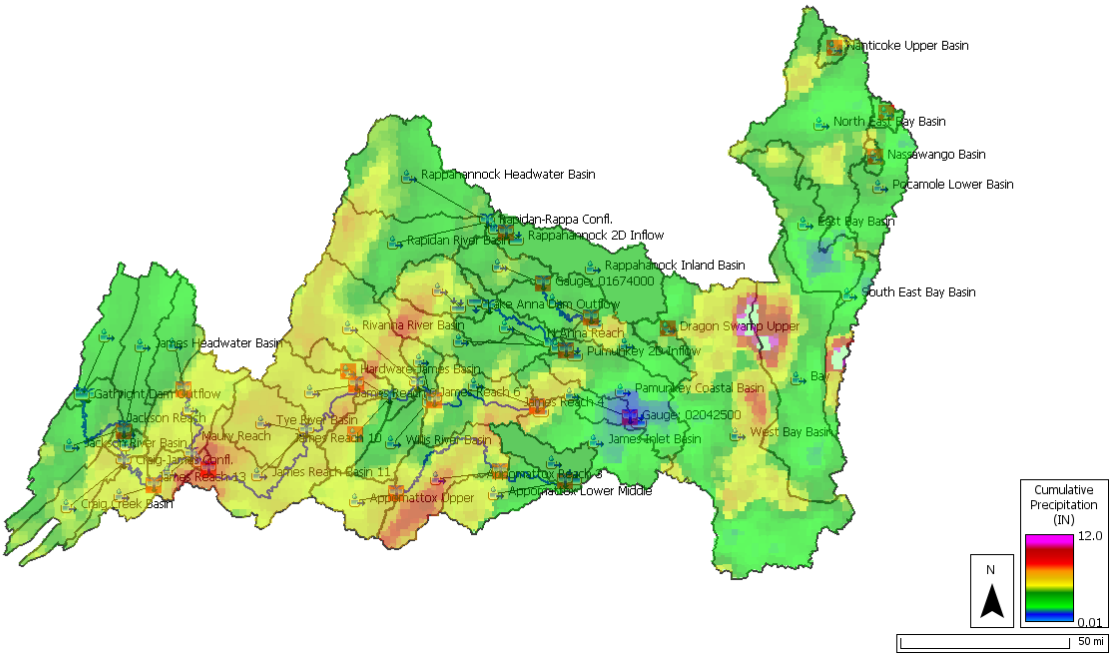

Figure 24. Tropical Storm Michael cumulative precipitation (September 8-22, 2018)

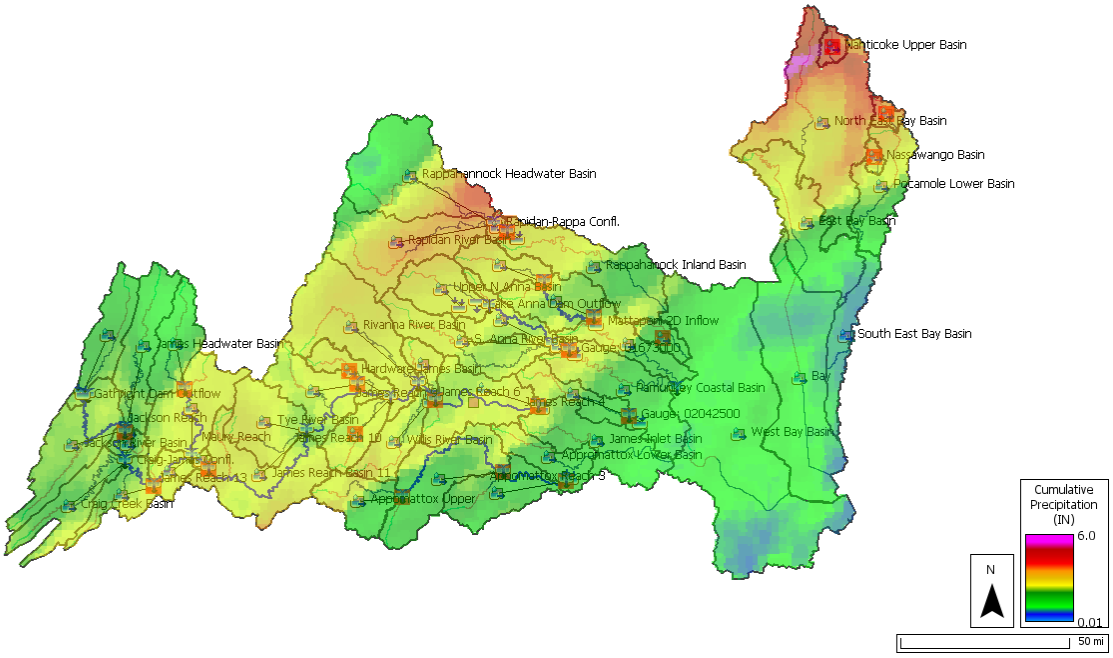

Figure 25. Tropical Storm Zeta cumulative precipitation (October 26 - November 05, 2020)

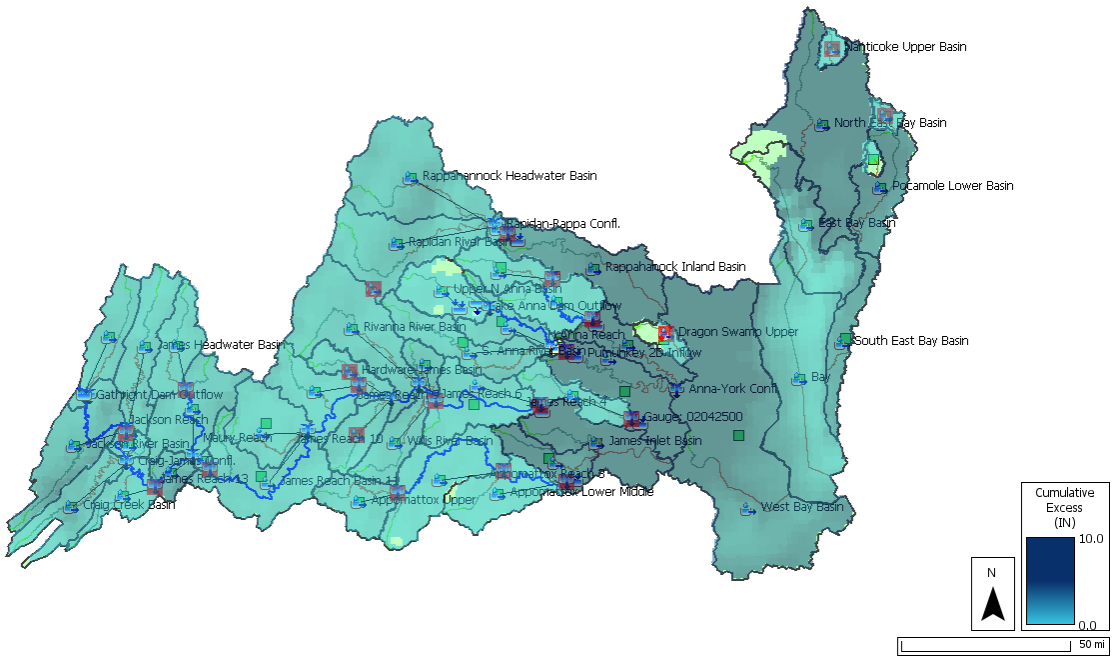

Figure 26. Tropical Storm Andrea cumulative excess (June 6 – 20, 2013)

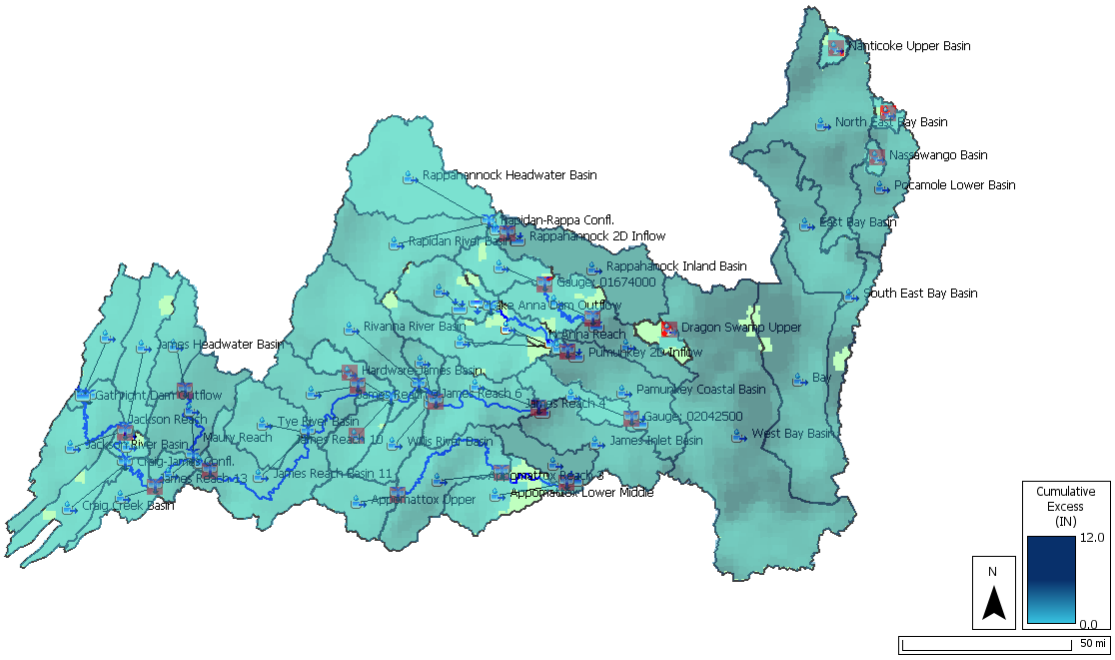

Figure 27. Tropical Storm Michael cumulative excess (September 8-22, 2018)

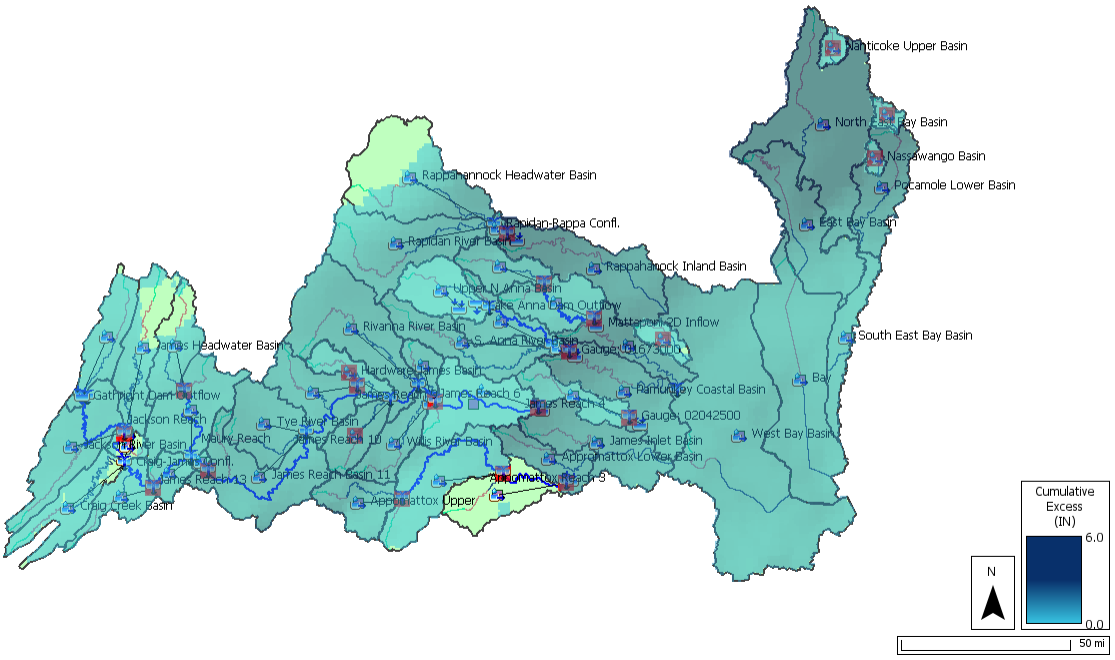

Figure 28. Tropical Storm Zeta cumulative excess (October 26 - November 05, 2020)

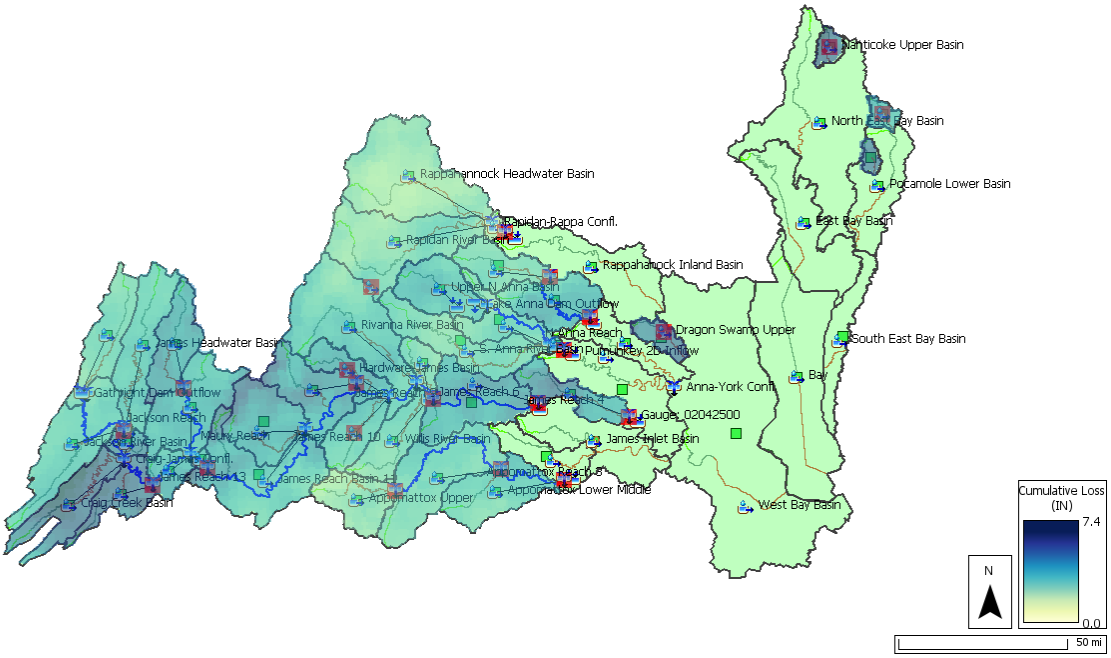

Figure 29. Tropical Storm Andrea cumulative infiltration losses (June 6 – 20, 2013)

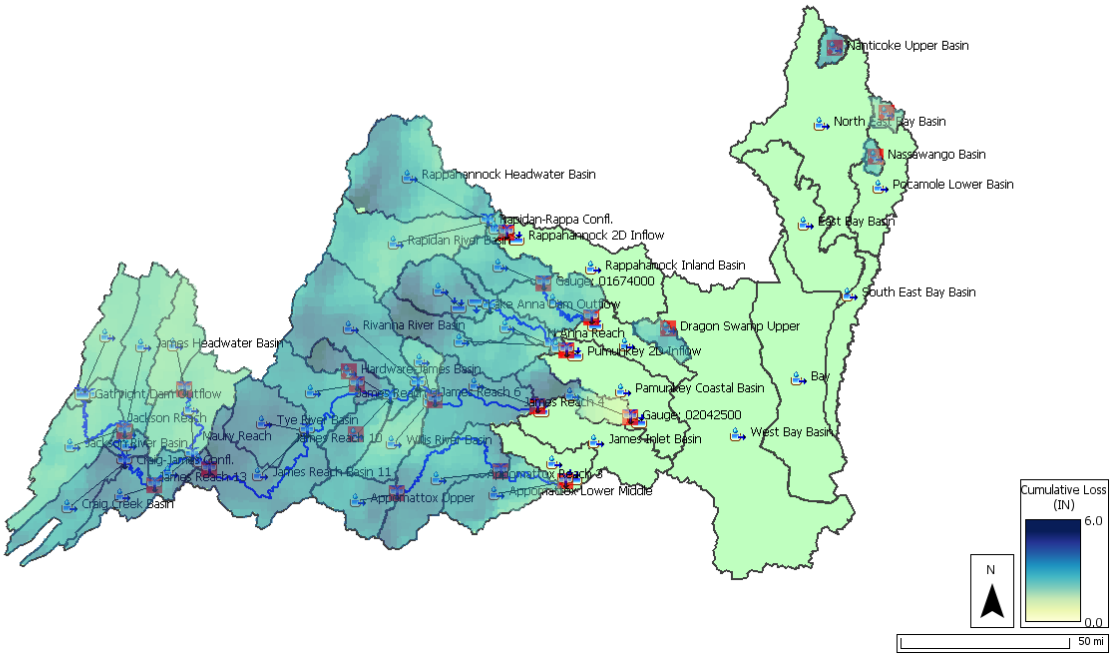

Figure 30. Tropical Storm Michael cumulative infiltration losses (September 8-22, 2018)

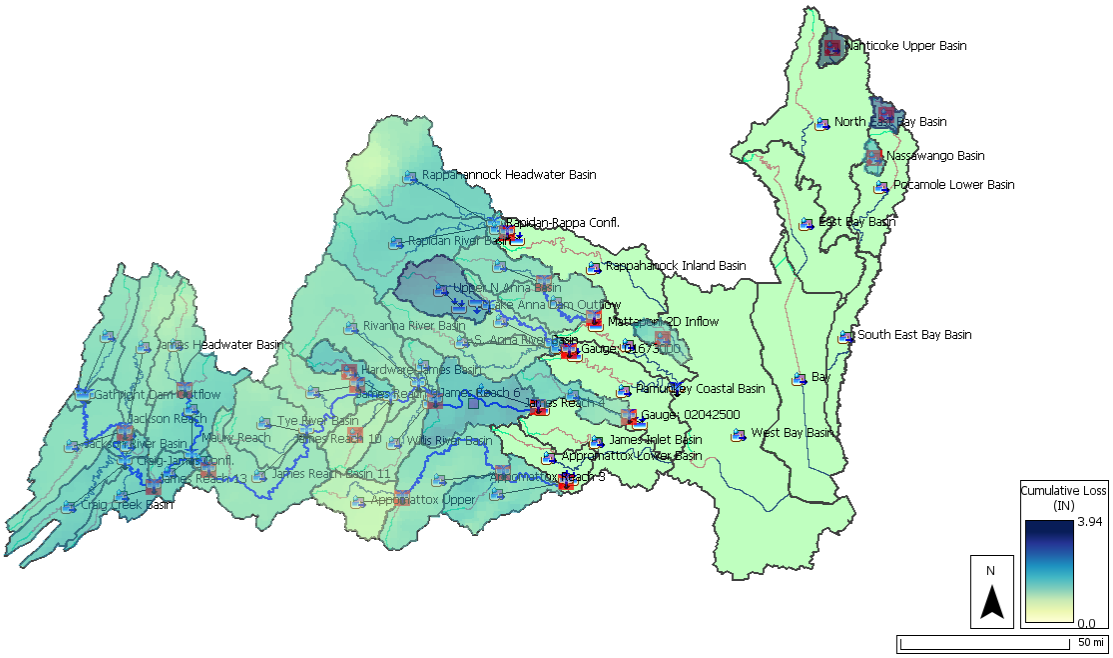

Figure 31.Tropical Storm Zeta cumulative infiltration losses (October 26 - November 05, 2020)

3.4 Physical Parameters

Final parameters for each calibrated event are viewed in the graphs below for ease of comparison. Complete tables of the final parameters for each event are summaries in the appendix. Deficit and constant infiltration loss method is described first followed by Green and Ampt infiltration loss method. Basins are grouped together by stream section, e.g., Appomattox, James, etc.

3.4.1 Deficit and Constant Infiltration Loss Parameters

Deficit and constant infiltration loss parameters were placed into charts, figures 32 and 33, with maximum minimum and average values to allow for comparison of each of the events that were modeled. This method gives a visual comparison of how the parameters differed between events and basins.

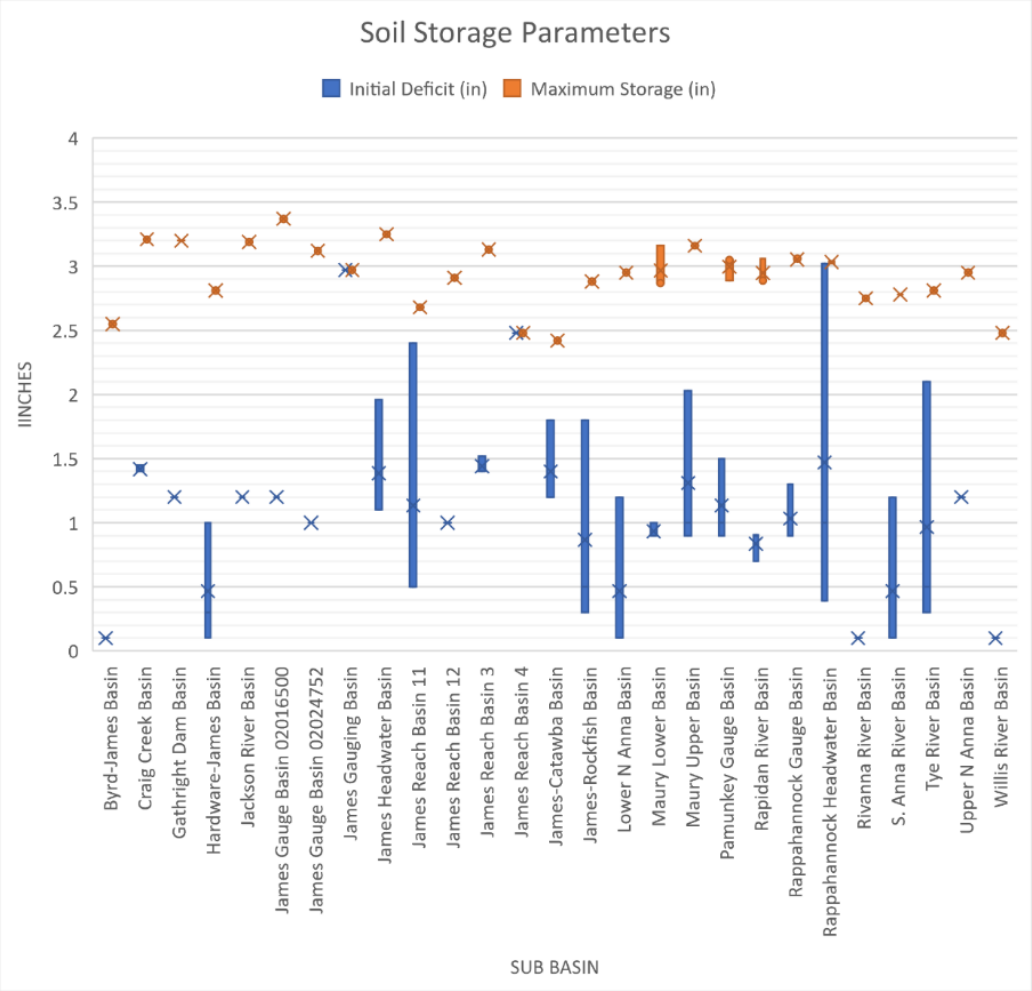

Figure 32. Soil storage parameters graphed as maximum, minimum, and average for all three events.

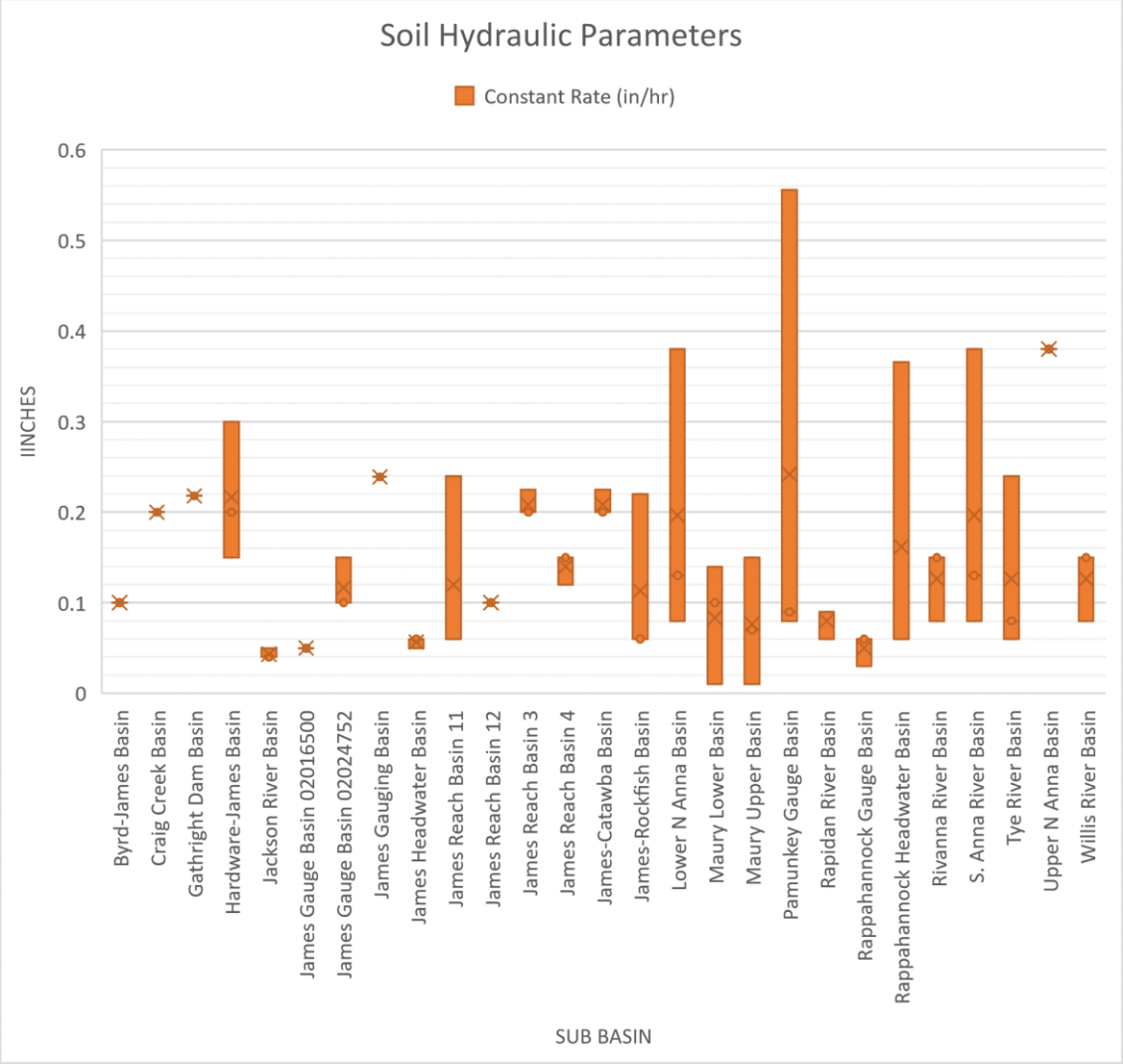

Figure 33. Soil hydraulic parameters graphed as maximum, minimum, and average for all three events.

3.4.2 Green and Ampt Infiltration Loss Parameters

Green and Ampt infiltration loss parameters were placed into charts, figures 34 - 36 with maximum minimum and average values with the same reasoning as with deficit and constant results. “X” marks indicate the middle value of the three calibrated event parameters with the other values on the top and bottom of the graph. The three graphs are divided into initial content (Figure 34), defined as the initial water content in the soil for layers 1 (L1) and 2 (L2), soil hydraulic parameters graph (Figure 35) defining water movement through the soil, and wetting suction front (Figure 36) showing the differences in the wetting front parameters for the soils.

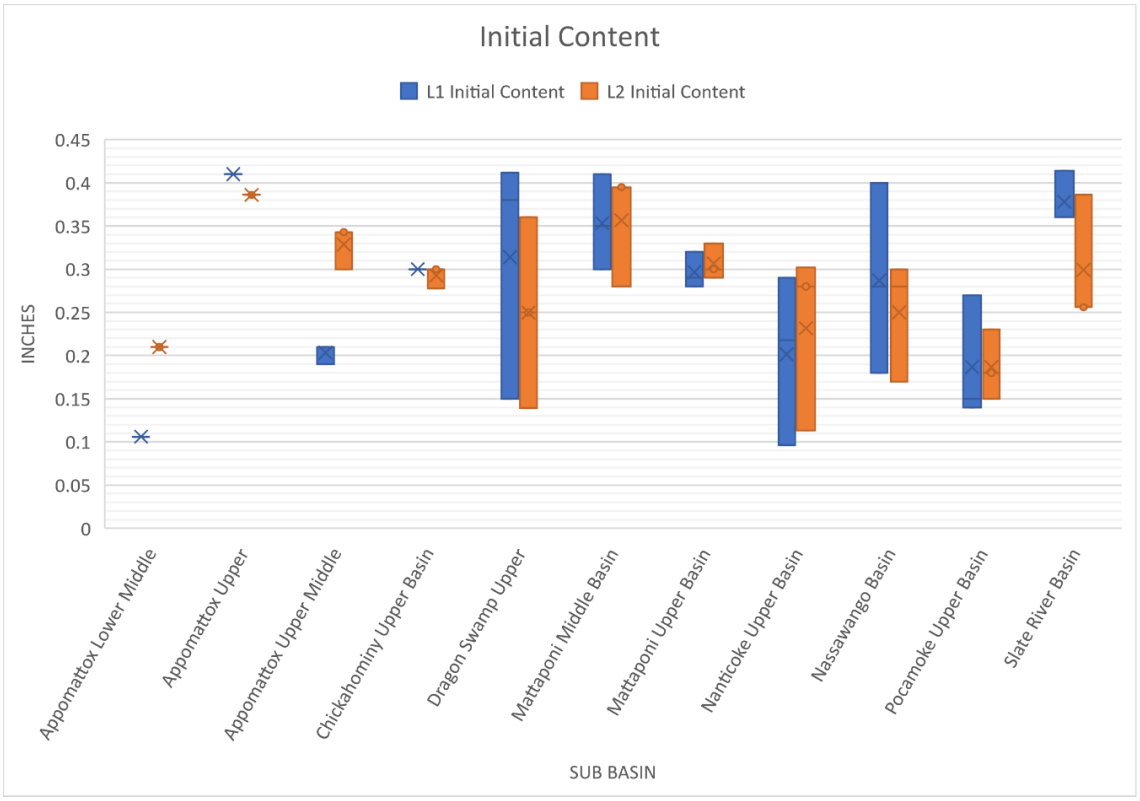

Figure 34. Initial content values graphed as maximum, minimum, and average for all three events.

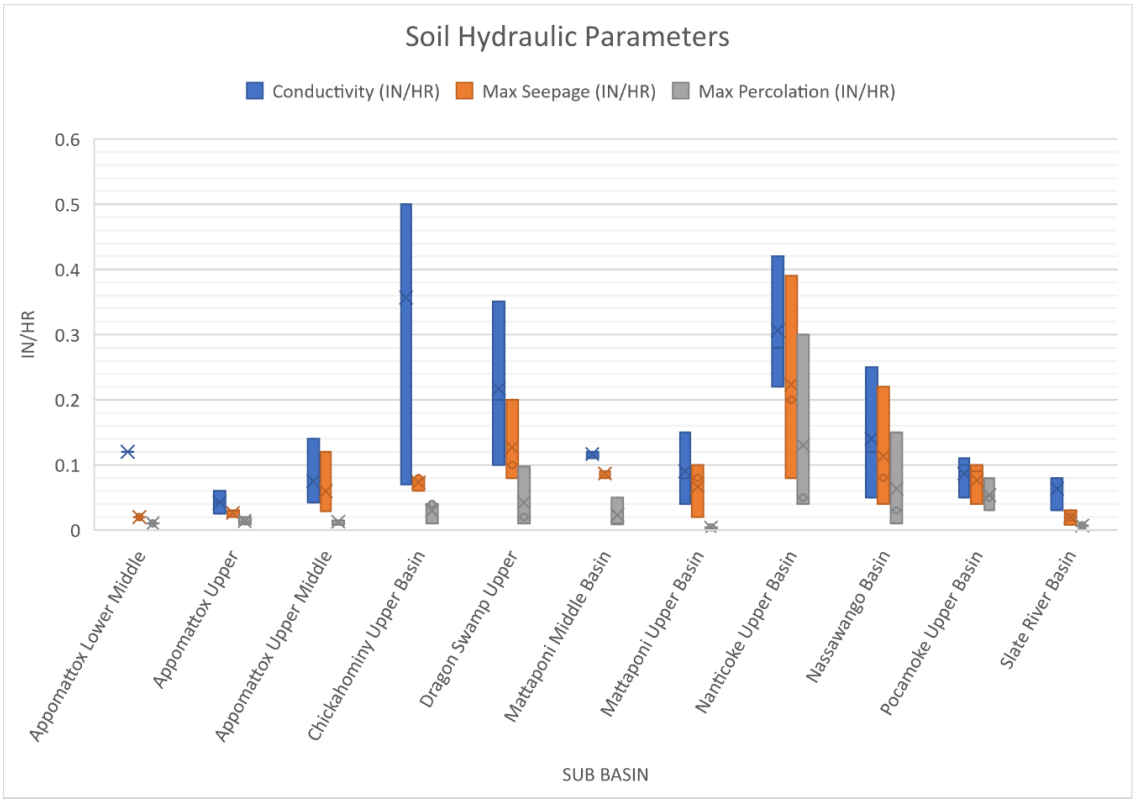

Figure 35. Soil hydraulic parameter values graphed as maximum, minimum, and average for all three events.

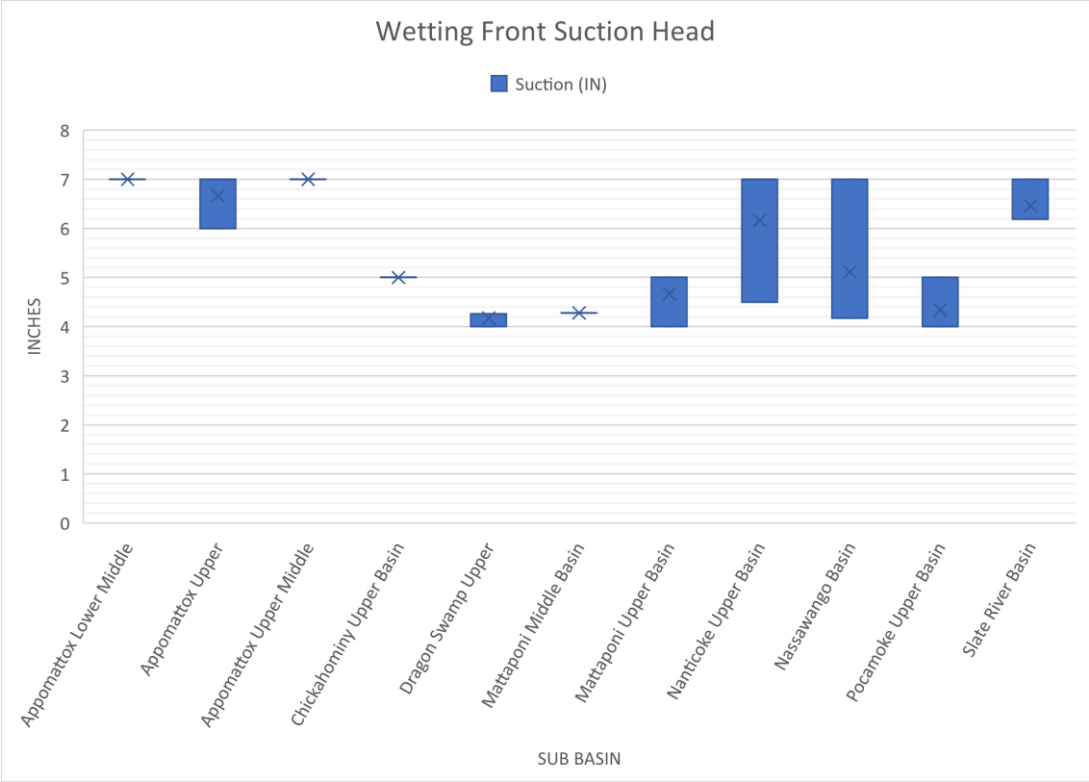

Figure 36. Wetting front suction head parameter values graphed as maximum, minimum, and average for all three events.

3.4.3 Transform Parameters

ModClark Transform parameters were placed into a graph, Figure 37, with maximum minimum and average values displayed. “X” marks indicate the average value of the three calibrated event parameters with the other values on the top and bottom of the graph. Time of concentration is abbreviated as TC and the storage coefficient as R.

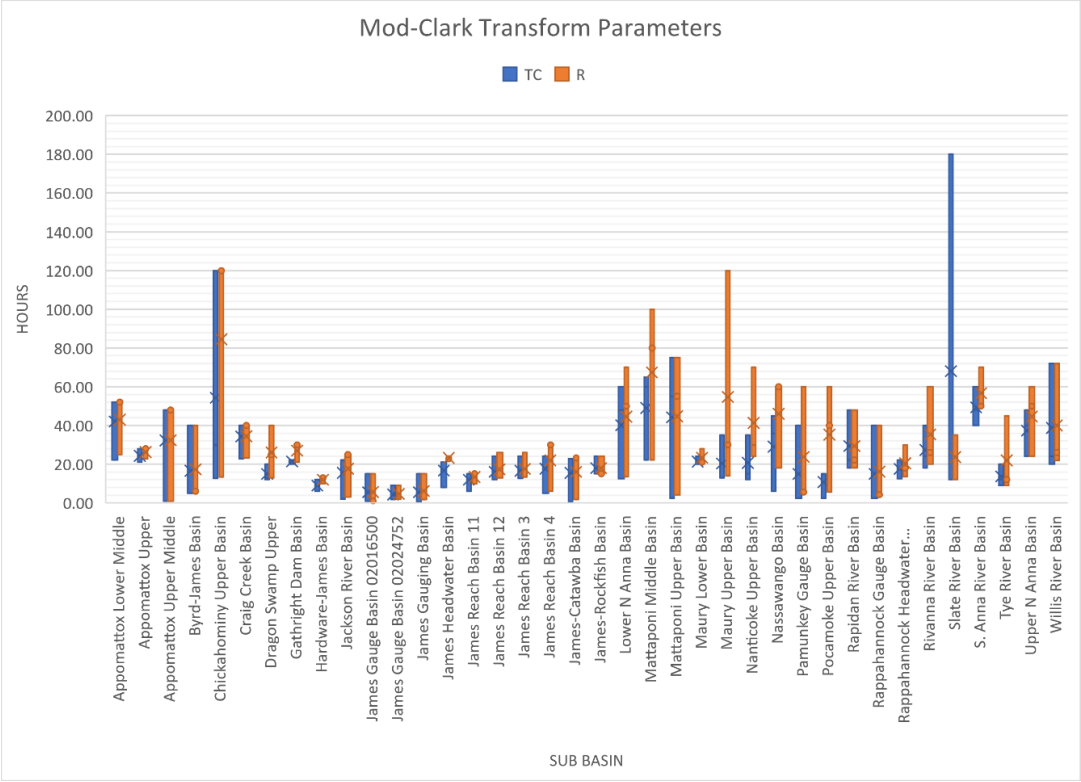

Figure 37. Mod-Clark transform parameter values graphed as maximum, minimum, and average for all three events.

3.4.4 Base Flow Parameters

Base flow parameters were placed into two graphs, Figure 37 and 38, with maximum minimum and average values displayed. “X” marks indicate the average value of the three calibrated event parameters with the other values on the top and bottom of the graph. Base flow residence time parameter graph, Figure 38, displays the range of attenuation coefficients for each layer for all events calibrated. Figure 39, the ground water recharge fraction displays the range of percents for all events calibrated that were set as ground water recharge flows.

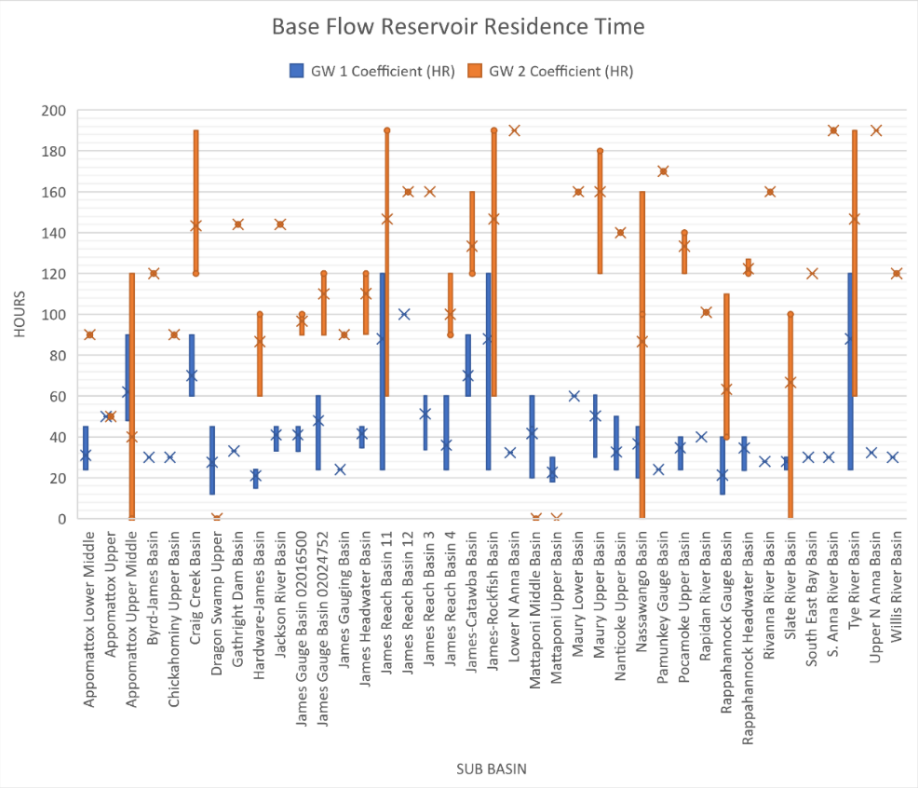

Figure 38. Base flow reservoir residence time parameter values graphed as maximum, minimum, and average for all three events.

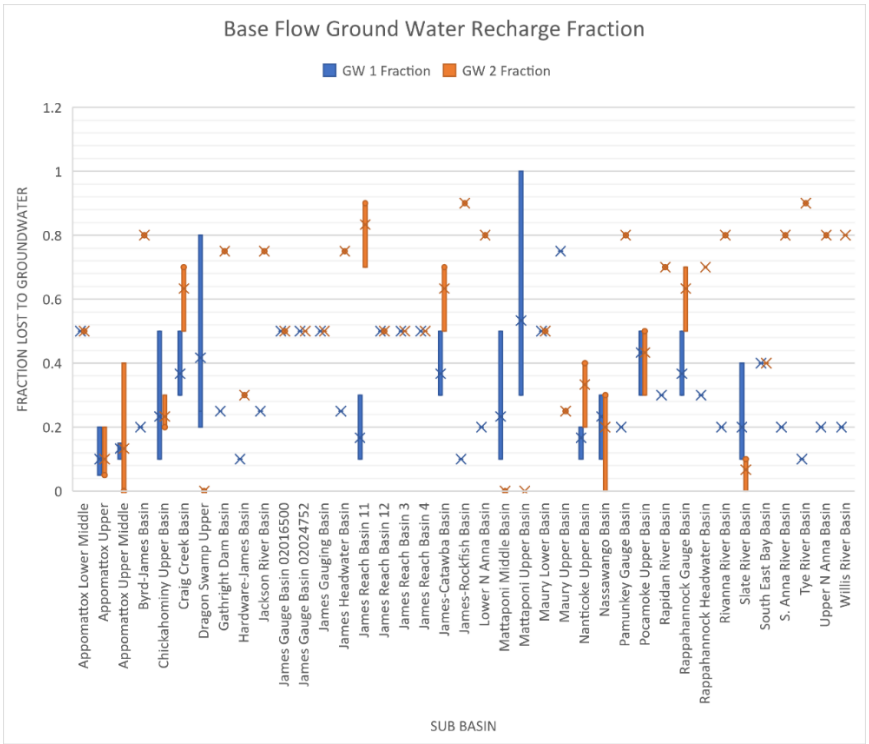

Figure 39. Ground water recharge fraction from base flow values graphed as maximum, minimum, and average for all three events.

3.5 Event Frequency Results

Event frequency results were calculated for each of the stream outfalls, Appomattox River, Chickahominy River, James River, Mattaponi River, Nassawango River, Pocomoke River, Pamunkey River, and Rappahannock River. Return frequency of flows for TS Andrea is tabulated in Table 13, TS Michael in Table 14, and TS Zeta in Table 15 with time of peak, observed flow, and frequency for each outfall. Frequency charts for each of the river outfalls is available in the appendix of this study.

Table 13. Return frequency for Tropical Storm Andrea flows at outfalls.

Gauge	Time of Peak	Observed Peak Flow (cfs)	Observed Return Frequency (%)
James River @ Richmond, VA	5/8/2013 15:00	38,300	72.71
Dragon Swamp @ Mascot, VA	6/8/2013 20:00	594	62.96
Appomattox @ Mattoax, VA	5/13/2013 19:00	2,780	65.60
Rappahannock @ Fredericksburg, VA	6/11/2013 3:00	40,100	53.32
Mattaponi @ Beulahville, VA	6/13/2013 3:00	1,490	75.84
Chickahominy@ Providence Forge, VA	6/15/2013 1:00	1,290	62.24
Pamunkey @ Hanover, VA	6/12/2013 19:00	6,750	68.45
Pocomoke @ Willards, VA	6/19/2013 13:00	261	78.68
Nassawango @ Snow Hill, VA	6/8/2013 15:00	258	67.54

Table 14. Return frequency for Tropical Storm Michael flows at outfalls.

Gauge	Time of Peak	Observed Peak Flow (cfs)	Observed Return Frequency (%)
James River @ Richmond, VA	9/19/2018 10:00	67800	63.16
Dragon Swamp @ Mascot, VA	9/15/2018 17:00	136	66.33
Appomattox @ Mattoax, VA	9/20/2018 18:00	10600	50.14
Rappahannock @ Fredericksburg, VA	9/18/2018 19:00	17600	70.78
Mattaponi @ Beulahville, VA	9/20/2018 9:00	1090	78.86
Chickahominy@ Providence Forge, VA	9/22/2018 9:00	1370	61.84

Pamunkey @ Hanover, VA	9/20/2018 11:00	4080	76.02
Pocomoke @ Willards, VA	9/12/2018 13:00	206	80.68
Nassawango @ Snow Hill, VA	9/10/2018 15:00	167	69.12

Table 15. Return frequency for Tropical Storm Zeta flows at outfalls.

Gauge	Time of Peak	Observed Peak Flow (cfs)	Observed Return Frequency (%)
James River @ Richmond, VA	10/31/2020 1:00	64500	64.22
Dragon Swamp @ Mascot, VA	11/3/2020 11:00	468	63.89
Appomattox @ Mattoax, VA	11/5/2020 7:00	4790	61.63
Rappahannock @ Fredericksburg, VA	10/30/2020 14:00	25800	64.42
Mattaponi @ Beulahville, VA	11/3/2020 20:00	3890	57.70
Chickahominy@ Providence Forge, VA	11/3/2020 17:00	1650	60.41
Pamunkey @ Hanover, VA	11/1/2020 17:00	8870	62.44
Pocomoke @ Willards, VA	11/1/2020 1:00	514	69.47
Nassawango @ Snow Hill, VA	10/31/2020 19:00	553	62.39

CHAPTER

4 DISCUSSION AND CONCLUSIONS

4.1 Overview of Output Hydrograph Results

Model calibration for all three events was mostly successful when looking at the Nash Sutcliffe error (NSE) and R-squared (R^2) statistics. Most of the basins were above 0.7 for NSE and 0.8 for R^2. This indicates that the overall shape of the hydrographs was within a statistical similarity and residuals were not too far away from expected. However, the percent bias in the results for Michael and Zeta were not acceptable for a good calibrated model. Looking at the data the peaks for both TS Michael and TS Zeta in many of these basins was above or below that of the observed flow leading to higher P-Bias values. TS Zeta hydrograph at James River shows a large difference in peaks that is likely driving the P-Bias value higher. However, NSE and R^2 values for these basins were acceptable meaning that the overall hydrograph was a good fit to the observed data. In terms of acceptance of model results in this case peak flows are important to determine flooding.

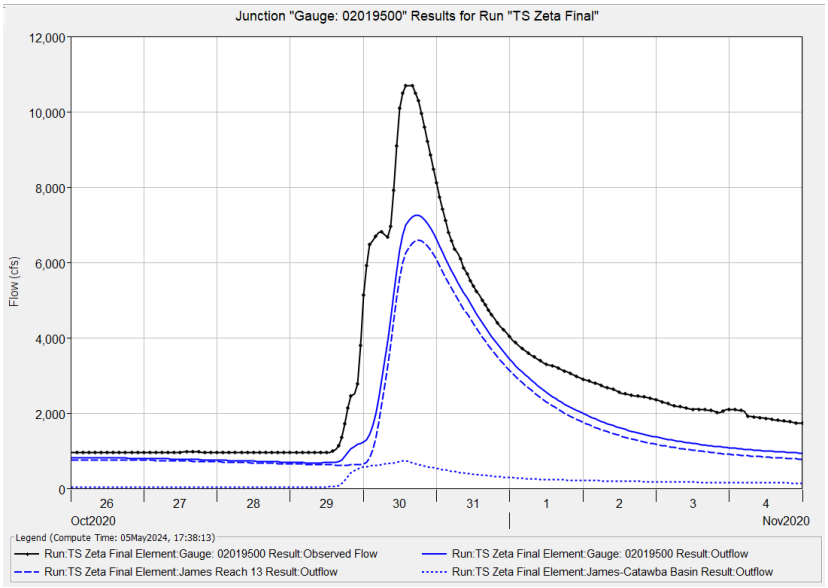

Figure 40. TS Zeta simulated vs observed flow on James River at Buchanan, VA

To understand the results for TS Michael, the temporal precipitation pattern is important. When looking at results in the upper watershed basins for both the James and Rappahannock rivers, Figures 41 and 42, two precipitation events of similar magnitude are observed. Each event is separated by a dry period in which soil dries out before the next event. Getting the correct peaks for both precipitation events in a simulated storm, while maintaining an acceptable NSE and R^2 is difficult. For the James River, compounded errors upstream create the perception that downstream basins are also incorrect. This is the wrong assumption as any deficit of flow upstream would continue downstream. Basins downstream, when looking at the other two statistics are acceptable, and it is difficult to determine if they are uncalibrated or just affected by the upstream parameters. However, this is likely different in the Rappahannock where compounding errors would not have occurred as only two basins are upstream of the final gauge. Likely this basin needs additional calibration or additional events to tease out the loss rates. It should also be noted that the results from TS Andrea also indicate difficulty in getting the Rappahannock correctly calibrated. Perhaps identifying storms with higher rainfall might be beneficial in this watershed.

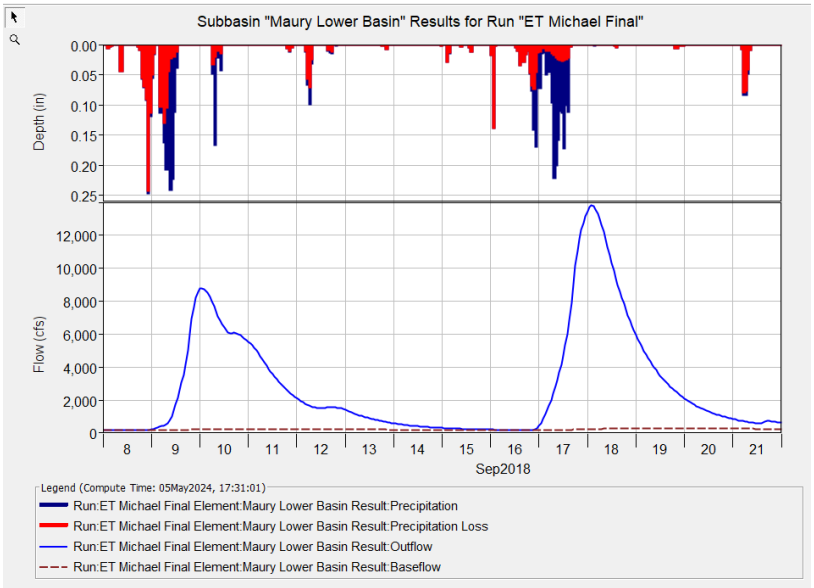

Figure 41. Upper James watershed results showing precipitation and flow for TS Micheal

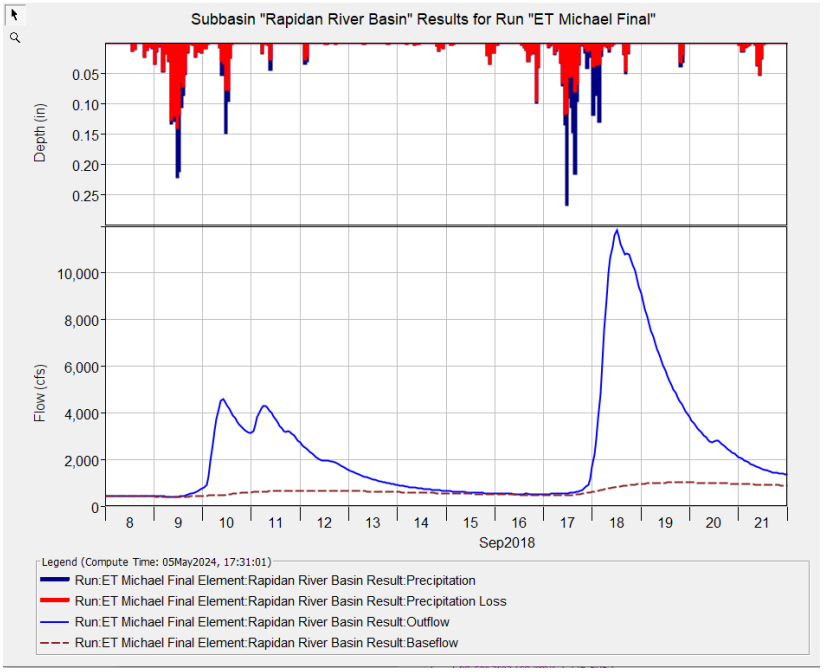

Figure 42. Upper Rappahannock watershed results showing precipitation and flow for TS Michael

The Appomattox watershed was an area of difficult calibration, as seen in the calibration results in all statistics varying between events simulated. Appomattox watershed has many dams throughout the watershed. The presence of reservoirs in this watershed was likely a major factor in poor calibration and modeling. This may also apply to the Rappahannock River, Maury River, and Rivanna River which have several large dams within their watershed. Figure 43 maps several large dams present in the watershed showing basins where effects of these dams are likely to be seen.

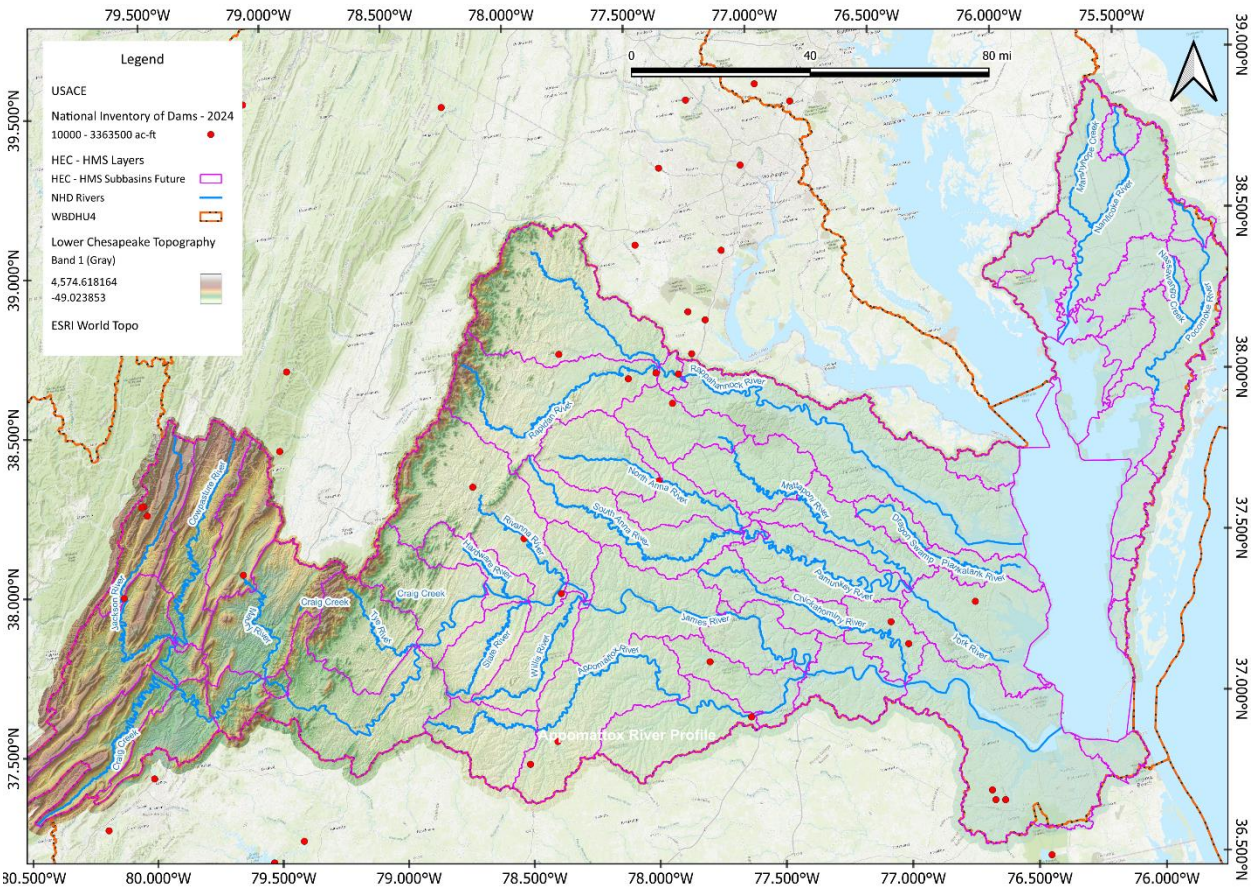

Figure 43. Dams in the Lower Chesapeake watershed greater than 10000 ac-ft

Focusing on the Appomattox, The Sandy River Reservoir and Briery Creek Lake Dam are two examples of reservoirs that likely affect the flows being modeled. These reservoirs sit higher up in the watershed of the Appomattox middle basin but are greater than 10,000 ac-ft and sit on major tributaries that feed into the Appomattox. Coupling the presence of dams with the low relief of the Appomattox watershed this would likely lead to inaccuracies in simulated flows. Future models will have to determine a methodology to model both Lake Chesdin, a water supply and storm and water treatment outfall for nearby cities, and Swift Creek Reservoir a water supply reservoir (“National Inventory of Dams” n.d.). Swift Creek is not modeled in this study; however, it will affect the final reach of the Appomattox before the confluence with the James River. In addition, these two reservoirs have no available public stream gauge data and cannot be modeled with known or observed outflows. However, when looking at the design of the reservoirs there is a main spillway that allows for water to exit the reservoir in high flow events. To better model basins with these types of reservoirs larger events need to be used that allow for flow out of the spillway.

Looking back at the P-Bias value for the Rappahannock and noting the presence of several large dams located within the Rappahannock watershed there is the possibility that reservoirs could lead to modeling errors in which flows are detained in the reservoir before being released. However further

review of the watershed indicated that the reservoirs only detain a small portion of the precipitation that falls on the watershed. Most of the areas cover by the reservoirs are small in area. This is likely also the case for the Maury River in which a small portion of the flow from the upper most basin is detained in a reservoir on a side tributary to the river.

Reservoirs in the Lower Chesapeake do affect both the James and North Anna Rivers. In these cases, the areas above the reservoirs were removed from the model and modeled with the observed outflows from the reservoirs. The James River Watershed, in line with the Jackson River, Lake Moomaw acts as a flood control reservoir operated by the US Army Corps of Engineers ("Gathright Dam Lake Moomaw" n.d.). As noted, the basin upstream of the reservoir was removed as it is managed and its operations have a large effect on the downstream James River watershed. Historical stream gauges data below the reservoir was applied during each event period as a source in the model. This same approach was used with Lake Anna along the North Anna River. Lake Anna is an operated reservoir under Dominion, and energy supply company ("National Inventory of Dams" n.d.). Unlike flood control rivers the reservoir is managed to maintain a constant outflow for power production. Flood waves are likely absorbed into the lake storage and result in higher outflows for weeks after a major storm. In more extreme events, water can enter the emergency spillway and result in significant downstream effects; however, this is a relatively uncommon occurrence since spillways are designed based on the spillway design flood, a low return frequency event.

For the creation of a forecast or model to be used with synthetic storms, how to model these basins will be an issue. This is historic data that can be used to figure out the operation of these dams; however, without a record of large flows into the reservoir some level of uncertainty will exist when making models that utilize generalized operations. How this uncertainty is determined will be difficult to quantify since operations are not always done according to strict rules of flow releases from the main conduits. This applies to all large reservoirs in the Lower Chesapeake watershed.

The low relief of many of the lower basins in the model may violate the validity of routing and transform models using the HEC-HMS due to increase effects of attenuation and backwater that is not modeled as part of the equations used. The HEC-HMS manual recommends slopes of greater than 2ft/mile or 0.00038% grade. These reaches include three reaches on the James River below the confluence with the Rivanna River to the USGS stream gauge near Richmond (0.00024 ft/ft, 0.00029 ft/ft, 0.00030 ft/ft), the most downstream reach of the Appomattox (0.00036 ft/ft) show in Figure 44, Pamunkey River reach (0.00010 ft/ft), and the Mattaponi Reach (0.00030 ft/ft). These reaches are likely unstable due to their low relief. However, due to high flows that were received by the reaches, calibration was acceptable. In the future these reaches and basins should likely be modeled using a surface model such as HEC-RAS rather than HEC-HMS. However, if these models are kept within a hydrology model a check against simulation results from a hydraulic program should be done to ensure they are correct.

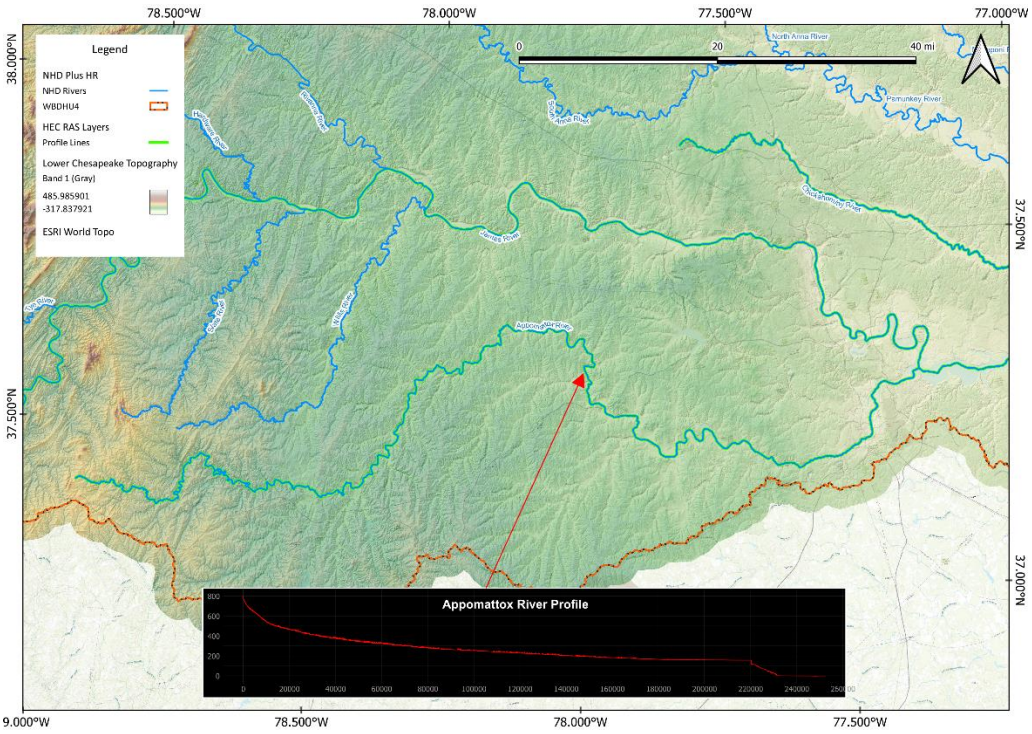

Figure 44. Appomattox watershed with a profile showing low relief area in the middle of the basin.

4.2 Review of Precipitation Distribution in the Watershed

Observation of the precipitation patterns both spatially and temporally give some understanding to the difficulty of creating a representative hydrological. Intensity of rainfall precipitation and the cumulative rainfall precipitation will change the runoff behavior of the watershed and modify downstream routing. Calibration of tropical storm models is done with the use of historical tropical events which have distinct rainfall patterns and trajectories. Spatial pattern and intensity for tropical storms (TS) rainfall varies greatly depending on environmental conditions (Atallah and Bosart 2003; Konrad II and Perry 2010). In the Atlantic Seaboard, cold troughs present in the Midwest can change the probability that a TS goes through an extra tropical transition (ET) (Atallah and Bosart 2003), a change from a symmetric warm core system to an asymmetric cold core system that takes energy from temperature and moisture gradients (Atallah and Bosart 2003; Cheung and Chu 2023; Villarini et al. 2011). Upon ET, a TS rainfall distribution changes moving outward from the core with expansion of the rain bands to 500 km from the center (Lonfat et al. 2004). Higher amounts of rainfall precipitation will be found in zones of high moisture and humidity (Villarini et al. 2011). In the Appalachian region, rainfall is often greatest on the left side of a storm track after ET. However, several studies have found that similar tracks of storms do not produce the same rainfall distribution (Matyas 2010, 2017).

In all three events, TS Andrea, TS Michael, and TS Zeta rainfall patterns were different from each other in both cumulative precipitation and max intensity. TS Andrea shows measured max cumulative rainfall going west to east, while TS Michael and TS Zeta have measured max cumulative rainfall going in

the southwest to northeast. TS Andrea and TS Michael have “left of track” rainfall as observed by their time and position while TS Zeta passed almost directly over the center of the watershed. Precipitation intensity differed little between each storm and looked more randomly uniform across all sub basins in the model. This is significant for model development as rainfall distributions are not uniform. Calibration using small flows can be difficult due to small variations in flow, and amplification of physical parameter effects on the runoff and infiltration. Some of this was observed in the events modeled in which some basins received larger amounts of precipitation. Due to this large variability in rainfall distribution developing representative parameters values for a general storm requires a larger number of events to get better calibrated parameters. In this case the use of three events was too small to calibrate parameters across the basins over multiple events. In some areas parameters could be calibrated multiple times as rainfall occurred from each event while in others, only one or two events, could lead to the ability to calibrate to an acceptable standard as defined previously in the methods section.

The concept of modeling an entire regional watershed as done in this study, as opposed to smaller river watershed, is supported by the studies indicating longer rainbands from storms post ET. Results from this study show that precipitation in the upper reaches does have a significant effect on downstream flow and could be a driver of flooding when intense rainfall occurs upstream. This is further supported by studies indicating the Appalachians as a significant source of floodwater occurring from tropical storms (O’Connor and Costa 2004). However, this is an area that could use more work to understand time of arrival and probability of simultaneous flood drivers, e.g., storm surge and fluvial flooding. Time of arrival and coincidence frequency models could shed some light on this area along with additional modeling using storms of a non-tropical nature to determine time of arrival based on precipitation spread amongst the various basins.

4.3 Availability of Events and Frequency of those Events for Modeling

The events available for calibration and simulation were limited to that of tropical storm events in the last 20 years, with a record in available USGS gauges in the Lower Chesapeake watershed. Difficulties with using older historic storms for calibration is accounting for the changes that have occurred to the landscape specifically land use. In 20 years, urbanization and terrain has changed the land leading to uncertainty in the use of parameter values when we calibrate to older storms. Furthermore, data for boundary conditions, precipitation and temperature, becomes scarcer. While additional storm for calibration would be useful in creating a better model, the uncertainty created by using those events may not add much to our model. It is possible to use uncertainty analysis to create a range of parameters and flows with an attached probability. This might be the next logical step in the evolution of modeling hydrological processes in this region.

In the dataset of available storms for calibration and modeling, lower frequency events are not selected due to the location of the rainfall or the date of the storm. Hurricane Floyd is a great example of TS based flooding, however, the event occurred in 1999 which is 25 years ago (Knapp et al. 2010; Matyas 2010; National Weather Service n.d.). The data for precipitation is available however, land cover, vegetation, urbanization, etc., has changed since that time, see paragraph above. Selecting parameters for modeling using current impervious cover, land use, and vegetation, while using older stream and precipitation data would result in a high amount of uncertainty and error. In this case, a more nuanced approach to account for this variability, perhaps using more probabilistic methods, would be more

accurate. Additional uses of ensemble or variable parameter simulations could help understand the uncertainty when looking back at older historical data (Gori and Lin 2022; Nederhoff et al. 2024; Xu et al. 2023).

TS Gaston is an additional compound flooding event that should be noted for future modeling (Knapp et al. 2010; National Weather Service n.d.). TS Gaston resulted in flooding from high intensity precipitation (pluvial) coming down in an isolated geographic area. Excess runoff was so intense during this event that the USGS stream gauge along the Chickahominy stopped functioning leaving a gap in the flow record. Unfortunately, this storm is not applicable to this model. The spatial distribution of rainfall was south and east of the boundaries of the hydrologic model. As stated earlier, the model ends at the last USGS stream gauge available for calibration. Because of the difficulty in calibrating and the assumptions of the empirical models that govern transform and routing, modeling these events in this region would need to be performed in a surface-based model such as HEC-RAS or ADCIRC. The only basin within the model for this event was the Chickahominy watershed. All other basins upstream of the Chickahominy received little to no precipitation and would likely have resulted in poor calibration due to the low amount of runoff. As stated previously, future work using a 2D surface approach with applied rainfall and infiltration would be best to capture this event.

The frequency of the events modeled in this study were relatively common, an average frequency of reoccurrence between 60-80%. However, some additional understanding of the frequency of these events could be gained using a mixed populations analysis of the events on each of the rivers. In the methods that were used in this study, populations were assumed to be the same. However, tropical storms occur during the time between July and November and could be modeled as mixed population for frequency analysis. Perhaps the frequency of the storms modeled would change if frequency analysis were done using this alternative approach.

4.4 Model Physical Parameters

As noted in the paragraphs above, tropical systems are very variable in their rainfall distribution. This creates a challenge when developing a single set of parameters for a model (Matyas 2010, 2017; Villarini et al. 2011). For example, initial conditions in the model will vary greatly based on the conditions on the ground before the beginning of the simulation. It is preferable to have conditions that are dry to avoid additional variability in the model; however, this is dependent on weather conditions before a TS passes through or near the region. For all three events the start of the simulation was chosen before the storm; however, differences in initial conditions were observed between each simulated event. As shown in the results, initial deficits using both the deficit and constant and the Green and Ampt infiltration loss models varied widely between events. High variability observed between events may have been due to the selection of the start date and time. Other storm events likely occurred before the arrival of each tropical storm event. Future application of gridded soil moisture could help account for this variability (Zheng et al. 2023) .

Using only three events for simulation and evaluation prevents any statistical analysis of parameter variability. However, when looking at the minimum and maximum for the selected parameters it is evident that there are larger variations in basin parameters as they get closer to the coastal plain. This is especially evident in the transform parameters in which larger differences in

maximum and minimum are evident as you move toward the bay. As stated earlier, one of the major challenges with this region is the transition from the Appalachians to the coastal plain. The upper watershed is a significant source of flow that slowly accumulates downstream. High flow and stage events occur with precipitation events occurring high up in the watershed and moving down slope to the tidal waters. This transition point is marked by a decrease in slope and change in ecology and geology. All these factors affect the model with slope being a major limitation to the empirical and mathematical models utilized by HEC-HMS to determine routing, transformation of precipitation to runoff, base flow, infiltration, etc. The transform parameters indicate this with high variability in attempting to accurately model the runoff effects brough by precipitation in a basin when the slope becomes too shallow for the equations. Most models for transformation of precipitation are created for areas of high relief and limited attenuation and backwater effects. When the slope decreases, these equations are no longer able to accurately simulate the excess flow. This same effect happens with routing parameters as well. With a lower slope, the models available are unable to simulate the attenuation and back water effects. It is at this point that we must move to alternate methods to simulate a reach.

4.5 Future Work

The results from this study indicate that additional modeling techniques are required to model coastal transition zones. Coastal transition zones are defined as the region joining the inland to the coastal plain. Software such as HEC-RAS can apply rainfall on a two-dimensional (2D) mesh with infiltration accounted for in each mesh cell allowing for modeling in these regions (Brunner 2020; Kalra et al. 2023). However, there is still the issue of base flow and canopy that is still missing in these models. In addition, computation power can be quite high when using HEC-RAS for this type of simulation. Mesh sizes that are smaller than those normally used in inland regions are required to get accurate results in flat regions with tidal interactions (Brunner 2020; *Episode 21* 2022). A few studies have applied this method but have done so using distributed programming to allow for more processing power. Future releases of HEC-RAS will likely be able to overcome the current limitations.

Presently, a HEC-HMS analysis on coastal transition zones can be performed by applying base flow and canopy interception to those basins in the coastal transition region. Using these basins we can account for canopy and infiltration losses and sub surface flow. The excess runoff from each basin can then be applied in gridded format to a 2D mesh in HEC-RAS to get the routing and transform over the surface. However, with the limitation noted above, this will need to be done to small regions rather than whole watersheds. In addition, this methodology still has the issues of missing data for calibration in the tidal regions. Several sources of stage data for specific regions, such as Norfolk, Virginia Beach, Hampton, etc. are available and could be used to calibrate the downstream portion of a model for the lower reaches of the Lower Chesapeake Bay and for the peninsula east of the bay. Calibration of an event would be limited to the regions in which the gauges are present. To fully create a calibrated forecast model, more gauging data is needed on a wider geographic scale. Flow gauges might not be the solution due to tidal influence, but stage gauges and tidal current gauges might be able to fill in the gaps when applied to a wider area.

Based on the previous conclusions the creation of a model that can be used with synthetic storms or as a forecast model can be done, but there are still limitations to getting a well calibrated model on a large scale. The calibration of initial conditions is very important and the most difficult part in

creating an accurate model. Quantification of uncertainty in this case will be important to ensure the model starts off at the right point and uncertainty and errors do not accumulate from the start. HEC-HMS has built in uncertainty simulation options as well as ensemble runs that allow for iteration of uncertainty using the variability of the parameters. This is often referred to as a sensitivity analysis. For forecasting storms or using synthetic storm this should be considered as a method to give a range of outcomes that cover the uncertainty in the model.

Finally, the consideration of the ecological components of the model should get additional attention. Canopy and ground cover can play an important role in absorption of precipitation and may play a more important role in low relief and heavily forested areas. An area of interest for future modeling is being done using the leaf area index (LAI) to determine rainfall interception from plants (Andersen et al. 2002; Bulcock and Jewitt 2010; Rajib et al. 2020). In my study, canopy was included but was determined to have little effect on runoff. However, data suggest that there is a significant component of precipitation loss that is driven by canopy interception. This becomes more important to TS simulation due to seasonality of the hurricane season, July through November. Canopy cover changes during this time may play a bigger role in runoff as it changes throughout the season.

REFERENCES

Allen, R. G., L. S. Pereira, D. Raes, and M. Smith. 1998. "Crop evapotranspiration-Guidelines for computing crop water requirements-FAO Irrigation and drainage paper 56." *Fao Rome*, 300 (9): D05109.

Andersen, J., G. Dybkjaer, K. H. Jensen, J. C. Refsgaard, and K. Rasmussen. 2002. "Use of remotely sensed precipitation and leaf area index in a distributed hydrological model." *J. Hydrol.*, 264 (1): 34–50. https://doi.org/10.1016/S0022-1694(02)00046-X.

Atallah, E. H., and L. F. Bosart. 2003. "The Extratropical Transition and Precipitation Distribution of Hurricane Floyd (1999)." *Mon. Weather Rev.*, 131 (6): 1063–1081. American Meteorological Society. https://doi.org/10.1175/1520-0493(2003)131<1063:TETAPD>2.0.CO;2.

Bartles, M., B. Faber, M. Fleming, G. Karlovits, J. Slaughter, and T. North. 2023. "HEC-SSP Statistical Software Package User's Manual Version 2.3." Hydrologic Engineering Center.

Bermudez, M., J. F. Farfan, P. Willems, and L. Cea. 2021. "Assessing the effects of climate change on compound flooding in coastal river areas." *Water Resour. Res.*, 57 (10): n/a. Washington, DC: American Geophysical Union. https://doi.org/10.1029/2020WR029321.

Brunner, G. W. 2020. "HEC-RAS Hydraulic Reference Manual version 6.5." Hydrologic Engineering Center.

Bulcock, H. H., and G. P. W. Jewitt. 2010. "Spatial mapping of leaf area index using hyperspectral remote sensing for hydrological applications with a particular focus on canopy interception." *Hydrol. Earth Syst. Sci.*, 14 (2): 383–392. Copernicus GmbH. https://doi.org/10.5194/hess-14-383-2010.

Campbell, W. H., G. Savant, A. S. Leon, and L. Bian. 2023. "Applying HEC-RAS to Simulate the Complex Tidal Conditions for Estuaries and Bays: A Case Study of the San Francisco Bay." 185–193. American Society of Civil Engineers. https://doi.org/10.1061/9780784484852.018.

Cheung, H. M., and J.-E. Chu. 2023. "Global increase in destructive potential of extratropical transition events in response to greenhouse warming." *Npj Clim. Atmospheric Sci.*, 6 (1): 1–10. Nature Publishing Group. https://doi.org/10.1038/s41612-023-00470-8.

Chow, V. T. 1964. *Handbook of Applied Hydrology: A Compendium of Water-resources Technology*. McGraw-Hill.

Couasnon, A., D. Eilander, S. Muis, T. I. E. Veldkamp, I. D. Haigh, T. Wahl, H. C. Winsemius, and P. J. Ward. 2020. "Measuring compound flood potential from river discharge and storm surge extremes at the global scale." *Nat. Hazards Earth Syst. Sci.*, 20 (2): 489–504. Katlenburg-Lindau: Copernicus GmbH. https://doi.org/10.5194/nhess-20-489-2020.

Episode 21: Tidal Modeling Using HEC-RAS with Gary Brunner. 2022.

Fall, G., D. Kitzmiller, S. Pavlovic, Z. Zhang, N. Patrick, M. St. Laurent, C. Trypaluk, W. Wu, and D. Miller. 2023. "The Office of Water Prediction's Analysis of Record for Calibration, version 1.1: Dataset description and precipitation evaluation." *JAWRA J. Am. Water Resour. Assoc.*, 59 (6): 1246–1272. https://doi.org/10.1111/1752-1688.13143.

"Gathright Dam Lake Moomaw." n.d. Accessed March 31, 2024. https://www.nao.usace.army.mil/Missions/Civil-Works/Gathright-Dam-and-Lake-Moomaw/.

Gori, A., and N. Lin. 2022. "Projecting Compound Flood Hazard Under Climate Change With Physical Models and Joint Probability Methods." *Earths Future*, 10 (12): e2022EF003097. https://doi.org/10.1029/2022EF003097.

Gori, A., N. Lin, and J. Smith. 2020. "Assessing compound flooding from landfalling tropical cyclones on the North Carolina coast." *Water Resour. Res.*, 56 (4): n/a. Washington, DC: American Geophysical Union. https://doi.org/10.1029/2019WR026788.

Hellweger, F., and D. Maidment. 1997. "AGREE-DEM surface reconditioning system."

Hendry, A., I. D. Haigh, R. J. Nicholls, H. Winter, R. Neal, T. Wahl, A. Joly-Laugel, and S. E. Darby. 2019. "Assessing the characteristics and drivers of compound flooding events around the UK coast." *Hydrol. Earth Syst. Sci.*, 23 (7): 3117–3139. Katlenburg-Lindau: Copernicus GmbH. https://doi.org/10.5194/hess-23-3117-2019.

Hydrologic Engineering Center. 2023. "HEC-HMS Technical Reference Manual version 4.11." USACE Hydraulic Engineering Center.

Jalili Pirani, F., and M. R. Najafi. 2023. "Characterizing compound flooding potential and the corresponding driving mechanisms across coastal environments." *Stoch. Environ. Res. Risk Assess.*, 37 (5): 1943–1961. Berlin/Heidelberg: Springer Berlin Heidelberg. https://doi.org/10.1007/s00477-022-02374-0.

Jane, R., L. Cadavid, J. Obeysekera, and T. Wahl. 2020. "Multivariate statistical modelling of the drivers of compound flood events in south Florida." *Nat. Hazards Earth Syst. Sci.*, 20 (10): 2681–2699. Katlenburg-Lindau: Copernicus GmbH. https://doi.org/10.5194/nhess-20-2681-2020.

Kalra, A., B. Thakur, A. Aryal, and R. Gupta. 2023. "A 2D Rain-on-Mesh Model for Simultaneous Hydrologic and Hydraulic Computation." 594–606. American Society of Civil Engineers. https://doi.org/10.1061/9780784484852.057.

Knapp, K. R., M. C. Kruk, D. H. Levinson, H. J. Diamond, and C. J. Neumann. 2010. "The International Best Track Archive for Climate Stewardship (IBTrACS): Unifying Tropical Cyclone Data." *Bull. Am. Meteorol. Soc.*, 91 (3): 363–376. American Meteorological Society. https://doi.org/10.1175/2009BAMS2755.1.

Konrad II, C. E., and L. B. Perry. 2010. "Relationships between tropical cyclones and heavy rainfall in the Carolina region of the USA." *Int. J. Climatol.*, 30 (4): 522–534. https://doi.org/10.1002/joc.1894.

Kumbier, K., R. C. Carvalho, A. T. Vafeidis, and C. D. Woodroffe. 2018. "Investigating compound flooding in an estuary using hydrodynamic modelling: a case study from the Shoalhaven River, Australia." *Nat. Hazards Earth Syst. Sci.*, 18 (2): 463–477. Copernicus GmbH. https://doi.org/10.5194/nhess-18-463-2018.

Lee, S., T. Kang, D. Sun, and J.-J. Park. 2020. "Enhancing an Analysis Method of Compound Flooding in Coastal Areas by Linking Flow Simulation Models of Coasts and Watershed." *Sustainability*, 12 (16): 6572. Multidisciplinary Digital Publishing Institute. https://doi.org/10.3390/su12166572.

Leonard, M., S. Westra, A. Phatak, M. Lambert, B. van den Hurk, K. McInnes, J. Risbey, S. Schuster, D. Jakob, and M. Stafford-Smith. 2014. "A compound event framework for understanding extreme impacts." *WIREs Clim. Change*, 5 (1): 113–128. https://doi.org/10.1002/wcc.252.

Lonfat, M., F. D. Marks, and S. S. Chen. 2004. "Precipitation Distribution in Tropical Cyclones Using the Tropical Rainfall Measuring Mission (TRMM) Microwave Imager: A Global Perspective." *Mon. Weather Rev.*, 132 (7): 1645–1660. American Meteorological Society. https://doi.org/10.1175/1520-0493(2004)132<1645:PDITCU>2.0.CO;2.

Loveland, M., A. Kiaghadi, C. N. Dawson, H. S. Rifai, S. Misra, H. Mosser, and A. Parola. 2021. "Developing a Modeling Framework to Simulate Compound Flooding: When Storm Surge Interacts With Riverine Flow." *Front. Clim.*, 2. Frontiers Media SA.

Maidment, D. R. 1992. *Handbook of hydrology.*

Maidment, D. R. 2002. *Arc Hydro: GIS for water resources*. ESRI, Inc.

Matyas, C. J. 2010. "Associations between the size of hurricane rain fields at landfall and their surrounding environments." *Meteorol. Atmospheric Phys.*, 106 (3–4): 135–148.

Matyas, C. J. 2017. "Comparing the Spatial Patterns of Rainfall and Atmospheric Moisture among Tropical Cyclones Having a Track Similar to Hurricane Irene (2011)." *Atmosphere*, 8 (9): 165-.

"National Inventory of Dams." n.d. Accessed March 31, 2024a. https://nid.sec.usace.army.mil/#/dams/system/VA041001/summary.

"National Inventory of Dams." n.d. Accessed March 31, 2024b. https://nid.sec.usace.army.mil/#/dams/system/VA177002/summary.

National Weather Service. n.d. "The Hurricane History of Central and Eastern Virginia." Accessed March 29, 2024. https://www.weather.gov/media/akq/miscNEWS/hurricanehistory.pdf.

Nederhoff, K., M. van Ormondt, J. Veeramony, A. van Dongeren, J. A. Á. Antolínez, T. Leijnse, and D. Roelvink. 2024. "Accounting for uncertainties in forecasting tropical-cyclone-induced compound flooding." *Geosci. Model Dev.*, 17 (4): 1789–1811. Copernicus GmbH. https://doi.org/10.5194/gmd-17-1789-2024.

O'Connor, J. E., and J. E. Costa. 2004. "Spatial distribution of the largest rainfall-runoff floods from basins between 2.6 and 26,000 km2 in the United States and Puerto Rico." *Water Resour. Res.*, 40 (1): W01107-n/a. American Geophysical Union.

Pabst, A. F. 2000. "Corps Water Management System (CWMS)." *Tech. Pap. U Army Corps Eng. Hydrol. Eng. Cent.*, 20.

Peña, F., J. Obeysekera, R. Jane, F. Nardi, C. Maran, A. Cadogan, F. de Groen, and A. Melesse. 2023. "Investigating compound flooding in a low elevation coastal karst environment using multivariate statistical and 2D hydrodynamic modeling." *Weather Clim. Extrem.*, 39: 100534. Elsevier B.V.

Rahimi, R., H. Tavakol-Davani, C. Graves, A. Gomez, and M. Fazel Valipour. 2020. "Compound Inundation Impacts of Coastal Climate Change: Sea-Level Rise, Groundwater Rise, and Coastal Precipitation." *Water Basel*, 12 (10): 2776-. Basel: MDPI AG. https://doi.org/10.3390/w12102776.

Rajib, A., I. L. Kim, H. E. Golden, C. R. Lane, S. V. Kumar, Z. Yu, and S. Jeyalakshmi. 2020. "Watershed Modeling with Remotely Sensed Big Data: MODIS Leaf Area Index Improves Hydrology and Water Quality Predictions." *Remote Sens.*, 12 (13): 2148. Multidisciplinary Digital Publishing Institute. https://doi.org/10.3390/rs12132148.

Sahu, M. K., H. R. Shwetha, and G. S. Dwarakish. 2023. "State-of-the-art hydrological models and application of the HEC-HMS model: a review." *Model. Earth Syst. Environ.*, 9 (3): 3029–3051. https://doi.org/10.1007/s40808-023-01704-7.

Saleh, F., V. Ramaswamy, Y. Wang, N. Georgas, A. Blumberg, and J. Pullen. 2017. "A multi-scale ensemble-based framework for forecasting compound coastal-riverine flooding: The Hackensack-Passaic watershed and Newark Bay." *Adv. Water Resour.*, 110: 371–386. OXFORD: Elsevier Ltd.

Sebastian, A. 2022. "Chapter 7 - Compound flooding." *Coast. Flood Risk Reduct.*, S. Brody, Y. Lee, and B. B. Kothuis, eds., 77–88. Elsevier.

Serafin, K. A., P. Ruggiero, K. Parker, and D. F. Hill. 2019. "What's streamflow got to do with it? A probabilistic simulation of the competing oceanographic and fluvial processes driving extreme along-river water levels." *Nat. Hazards Earth Syst. Sci.*, 19 (7): 1415–1431. Katlenburg-Lindau: Copernicus GmbH. https://doi.org/10.5194/nhess-19-1415-2019.

Shen, Y., M. M. Morsy, C. Huxley, N. Tahvildari, and J. L. Goodall. 2019. "Flood risk assessment and increased resilience for coastal urban watersheds under the combined impact of storm tide and heavy rainfall." *J. Hydrol.*, 579: 124159. https://doi.org/10.1016/j.jhydrol.2019.124159.

Shen, Y., N. Tahvildari, M. M. Morsy, C. Huxley, T. D. Chen, and J. L. Goodall. 2022. "Dynamic Modeling of Inland Flooding and Storm Surge on Coastal Cities under Climate Change Scenarios: Transportation Infrastructure Impacts in Norfolk, Virginia USA as a Case Study." *Geosciences*, 12 (6): 224. Multidisciplinary Digital Publishing Institute. https://doi.org/10.3390/geosciences12060224.

Shields, G. M., J. R. Olsen, M. Medina, J. Obeysekera, P. Ganguli, C. DeMichele, G. Salvadori, M. R. Najafi, H. Moftakhari, F. Diermanse, and A. AghaKouchak. 2023. "Compound Flooding in a Non-Stationary World: A Primer for Practice." 18–27. American Society of Civil Engineers. https://doi.org/10.1061/9780784485163.003.

Tahvildari, N., M. Abi Aad, A. Sahu, Y. Shen, M. Morsy, P. Murray-Tuite, J. L. Goodall, K. Heaslip, and M. Cetin. 2022. “Quantification of Compound Flooding over Roadway Network during Extreme Events for Planning Emergency Operations.” *Nat. Hazards Rev.*, 23 (2): 04021067. American Society of Civil Engineers. https://doi.org/10.1061/(ASCE)NH.1527-6996.0000524.

Tarboton, D. G. 2005. “Terrain analysis using digital elevation models (TauDEM).” *Utah State Univ. Logan*, 3012: 2018.

Villarini, G., J. A. Smith, M. L. Baeck, T. Marchok, and G. A. Vecchi. 2011. “Characterization of rainfall distribution and flooding associated with U.S. landfalling tropical cyclones: Analyses of Hurricanes Frances, Ivan, and Jeanne (2004): RAINFALL AND FLOODING FROM HURRICANES.” *J. Geophys. Res. Atmospheres*, 116 (D23): n/a-n/a. https://doi.org/10.1029/2011JD016175.

Wahl, T., S. Jain, J. Bender, S. D. Meyers, and M. E. Luther. 2015. “Increasing risk of compound flooding from storm surge and rainfall for major US cities.” *Nat. Clim. Change*, 5 (12): 1093–1097. https://doi.org/10.1038/nclimate2736.

Wiederhold, P. R. 1997. *Water Vapor Measurement: Methods and Instrumentation*. Boca Raton: CRC Press.

Xu, K., C. Wang, and L. Bin. 2023. “Compound flood models in coastal areas: a review of methods and uncertainty analysis.” *Nat. Hazards Dordr.*, 116 (1): 469–496. Dordrecht: Springer Netherlands.

Zhang, Y., W. Li, G. Sun, G. Miao, A. Noormets, R. Emanuel, and J. S. King. 2018. “Understanding coastal wetland hydrology with a new regional-scale, process-based hydrological model.” *Hydrol. Process.*, 32 (20): 3158–3173. New York, NY: Wiley-Blackwell. https://doi.org/10.1002/hyp.13247.

Zheng, C., L. Jia, and T. Zhao. 2023. “A 21-year dataset (2000–2020) of gap-free global daily surface soil moisture at 1-km grid resolution.” *Sci. Data*, 10 (1): 139. Nature Publishing Group. https://doi.org/10.1038/s41597-023-01991-w.

Zinke, P. J. 1967. “Forest interception studies in the United States.” *For. Hydrol.*, 137–161. Pergamon Press Oxford.

Zscheischler, J., S. Westra, B. J. J. M. van den Hurk, S. I. Seneviratne, P. J. Ward, A. Pitman, A. AghaKouchak, D. N. Bresch, M. Leonard, T. Wahl, and X. Zhang. 2018. “Future climate risk from compound events.” *Nat. Clim. Change*, 8 (6): 469–477. London: London: Nature Publishing Group. https://doi.org/10.1038/s41558-018-0156-3.

APPENDIX

Tropical Storm Andrea Hydrographs at Model Outfalls figures 45 – 53. Figures show simulated versus observed flows at the outfalls of the model. Each outfall location by USGS gauge name is listed in the captions below the graph. In some locations precipitation is included in the output. These are only for locations where the basin was calibrated as a whole to observed flows as opposed to a junction in the model.

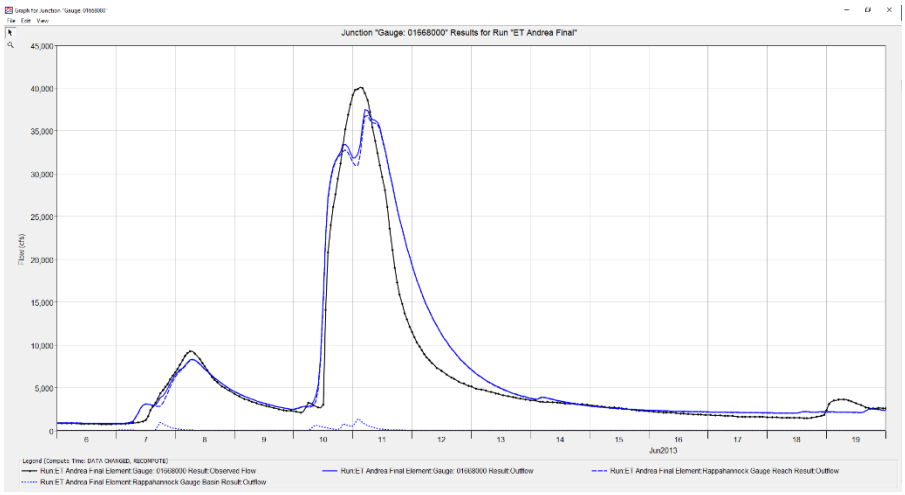

Figure 45. TS Andrea – Rappahannock River near Fredericksburg, VA hydrograph with simulated and observed data.

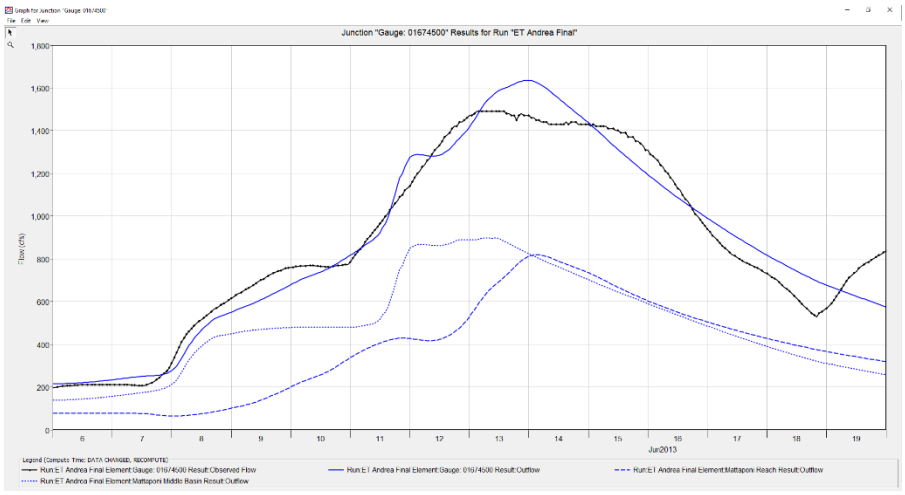

Figure 46. TS Andrea – Mattaponi River near Beulahville, VA hydrograph with simulated and observed data.

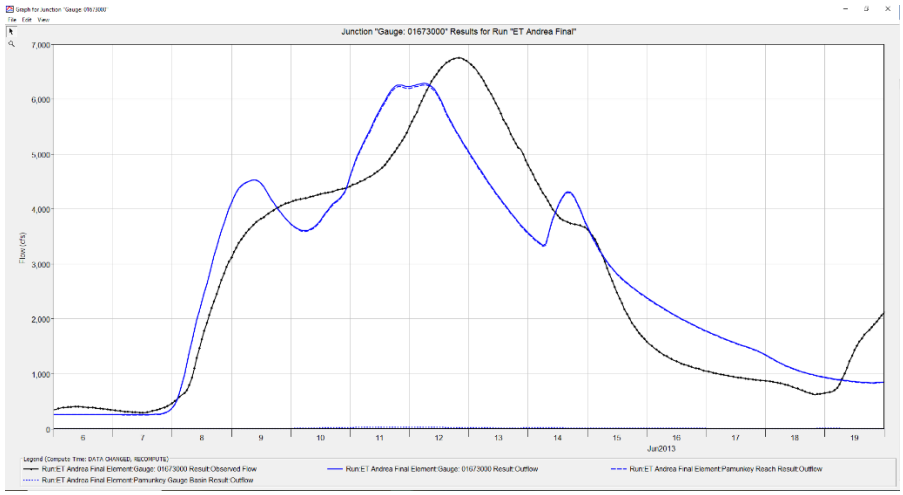

Figure 47. TS Andrea – Pamunkey River near Hanover, VA hydrograph with simulated and observed data.

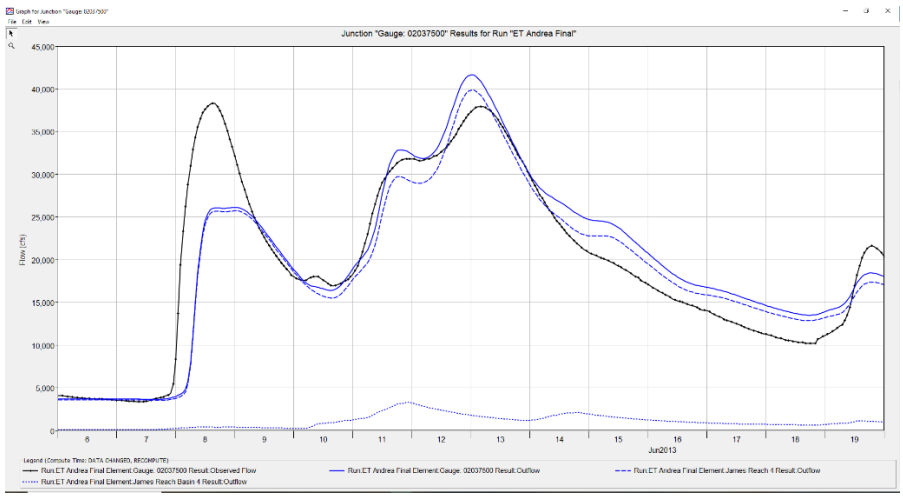

Figure 48. TS Andrea - James River near Richmond, VA hydrograph with simulated and observed data.

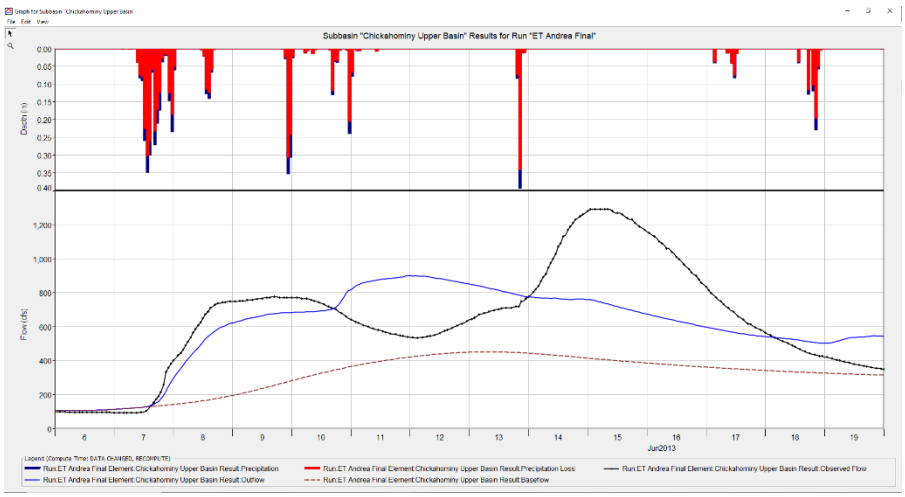

Figure 49. TS Andrea - Chickahominy River at Providence Forge, VA hydrograph with simulated and observed data.

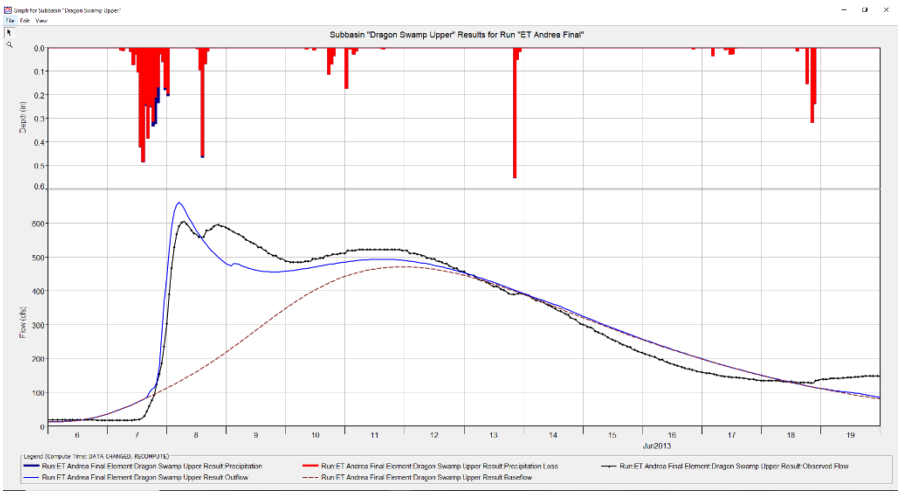

Figure 50. TS Andrea - Dragon Swamp at Mascot, VA hydrograph with simulated and observed data.

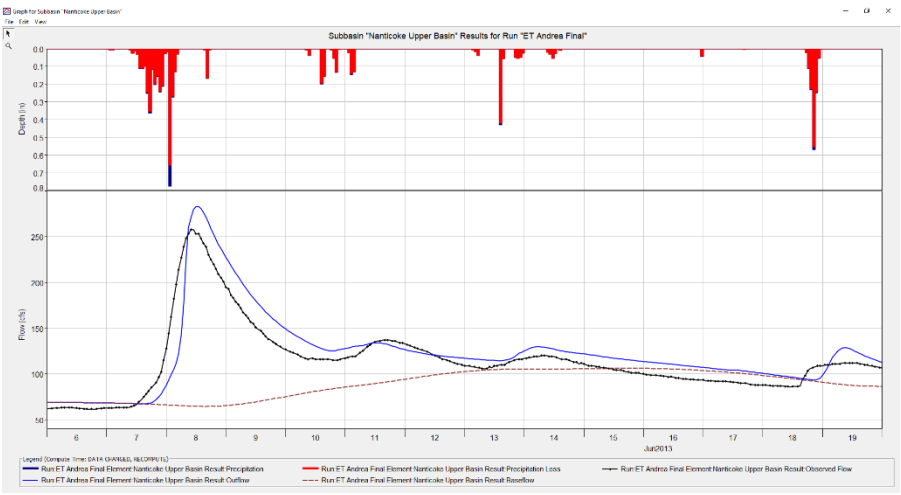

Figure 51. TS Andrea - Nanticoke River near Bridgeville, DE hydrograph with simulated and observed data.

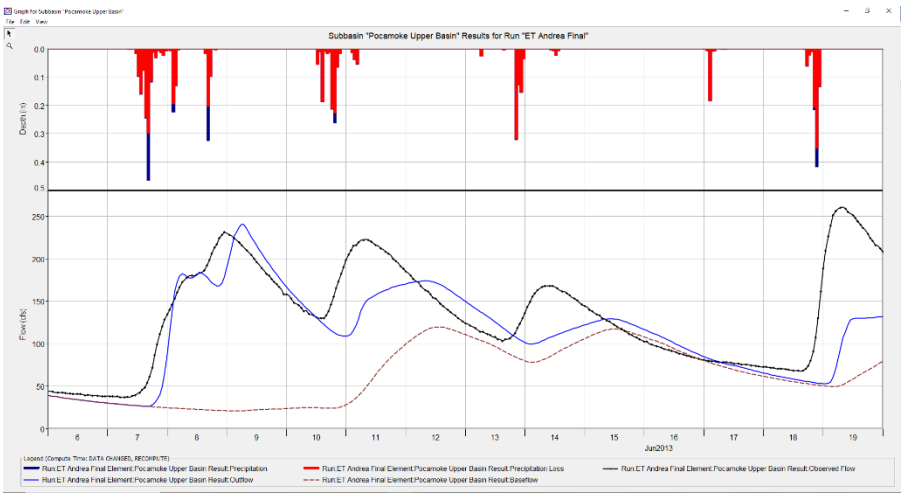

Figure 52. TS Andrea - Pocomoke River near Willards, MD hydrograph with simulated and observed data.

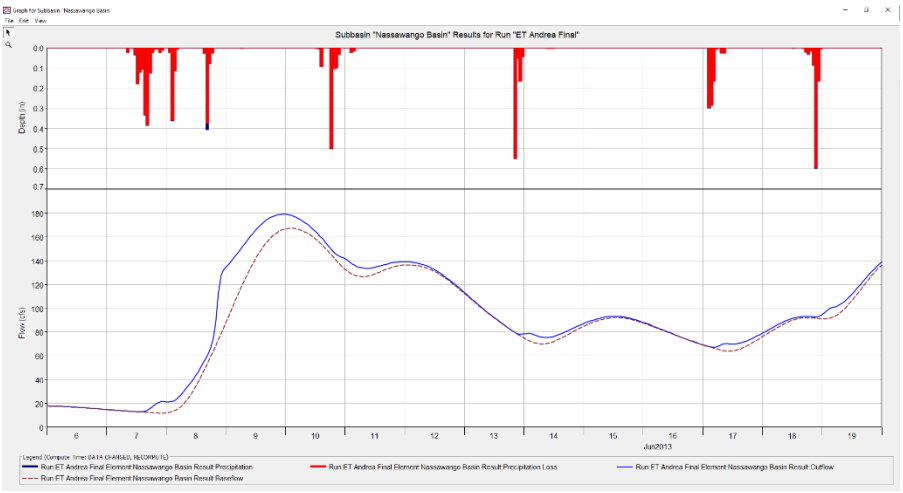

Figure 53. TS Andrea - Nassawango Creek near Snow Hill, MD hydrograph with simulated and observed data.

Tropical Storm Michael Hydrographs at Model Outfall, Figures 54 - 63s. Figures show simulated versus observed flows at the outfalls of the model. Each outfall location by USGS gauge name is listed in the captions below the graph. In some locations precipitation is included in the output. These are only for locations where the basin was calibrated as a whole to observed flows as opposed to a junction in the model.

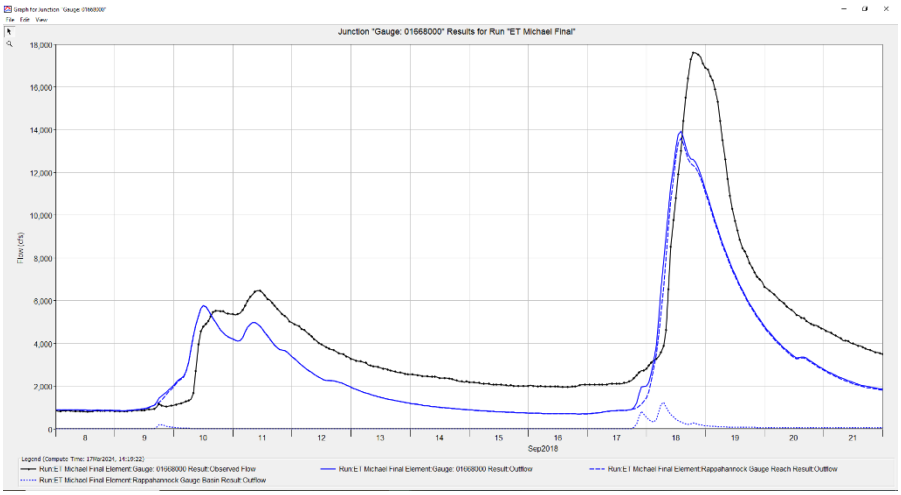

Figure 54. TS Michael - Rappahannock River near Fredericksburg, VA hydrograph with simulated and observed data.

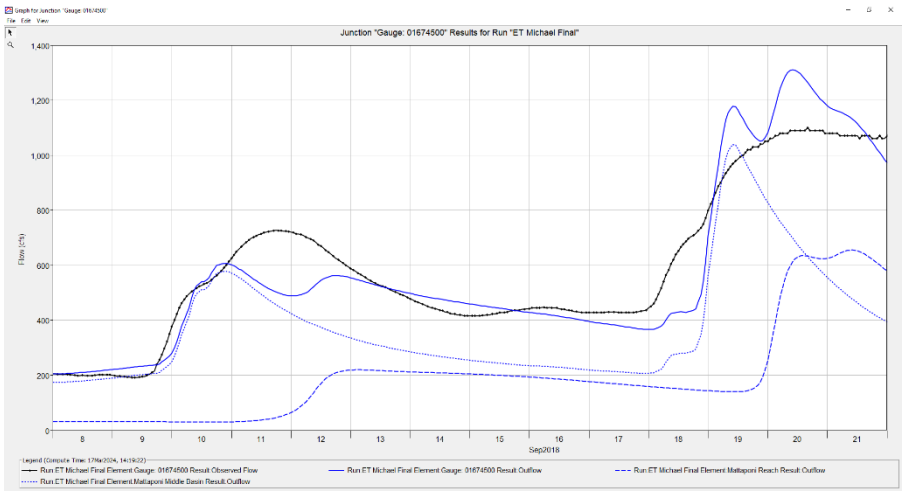

Figure 55. TS Michael -Mattaponi River near Beulahville, VA hydrograph with simulated and observed data.

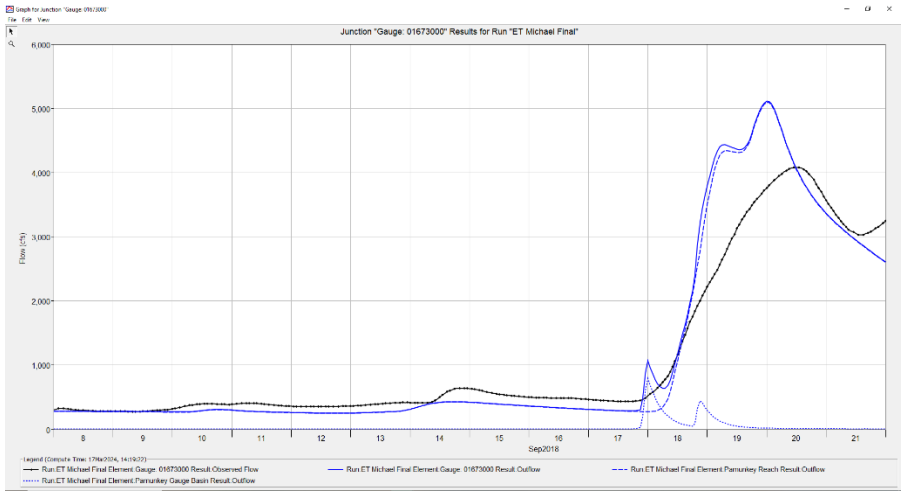

Figure 56. TS Michael - Pamunkey River near Hanover, VA hydrograph with simulated and observed data.

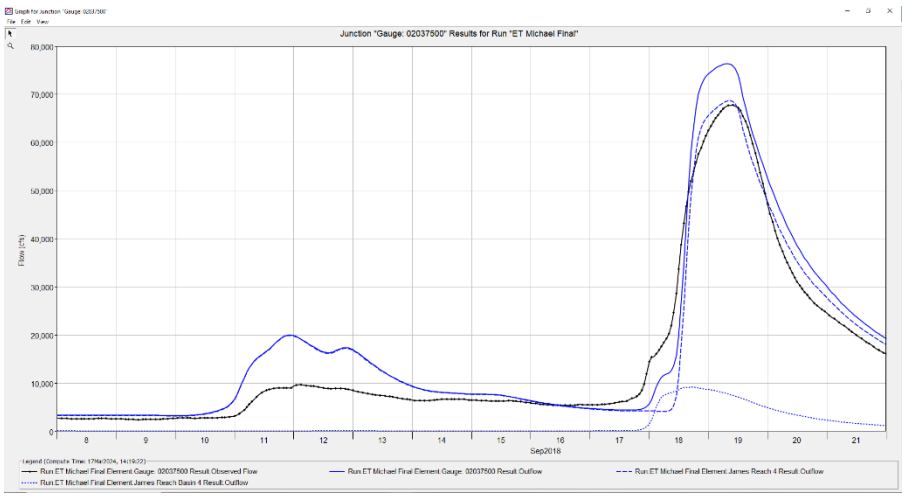

Figure 57. TS Michael - James River near Richmond, VA hydrograph with simulated and observed data.

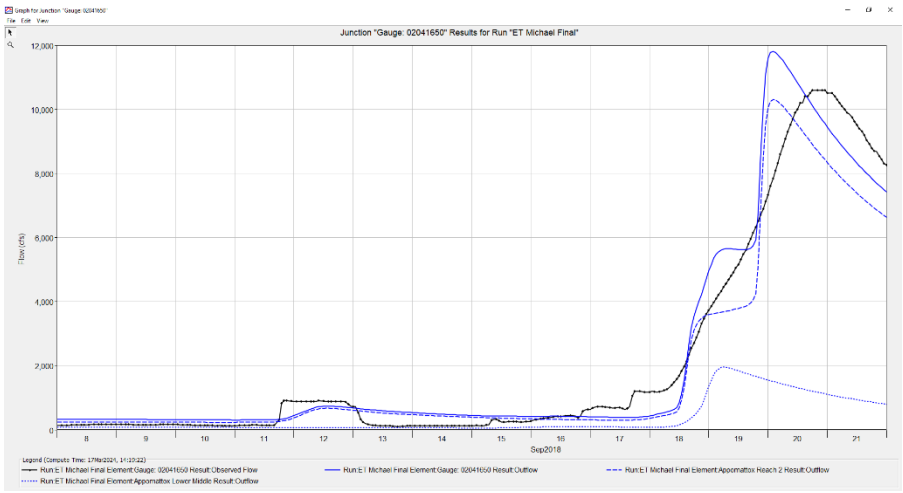

Figure 58. TS Michael - Appomattox River near Mataoca, VA hydrograph with simulated and observed data.

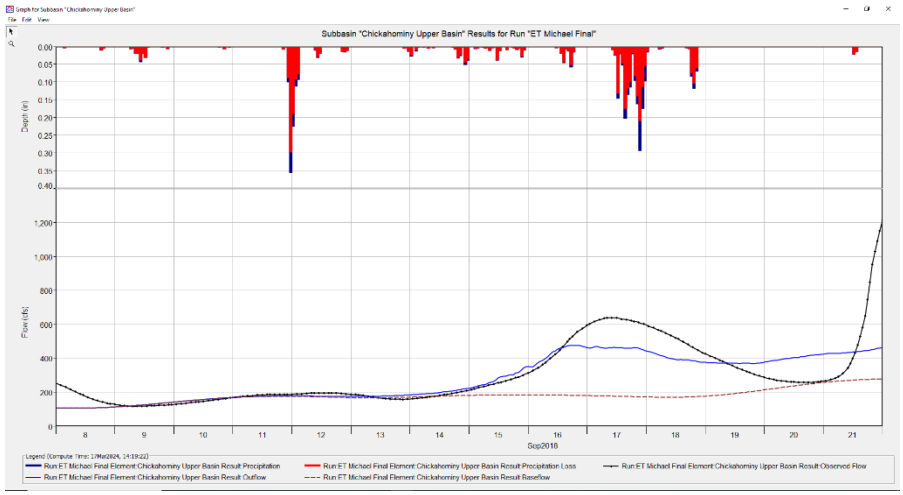

Figure 59. TS Michael -Chickahominy River near Providence Forge, VA hydrograph with simulated and observed data.

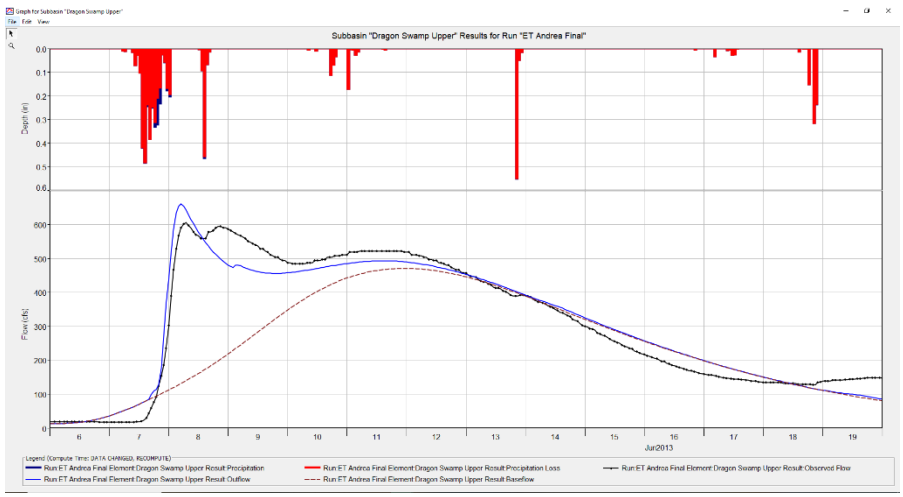

Figure 60. TS Michael - Dragon Swamp River at Mascot, VA hydrograph with simulated and observed data.

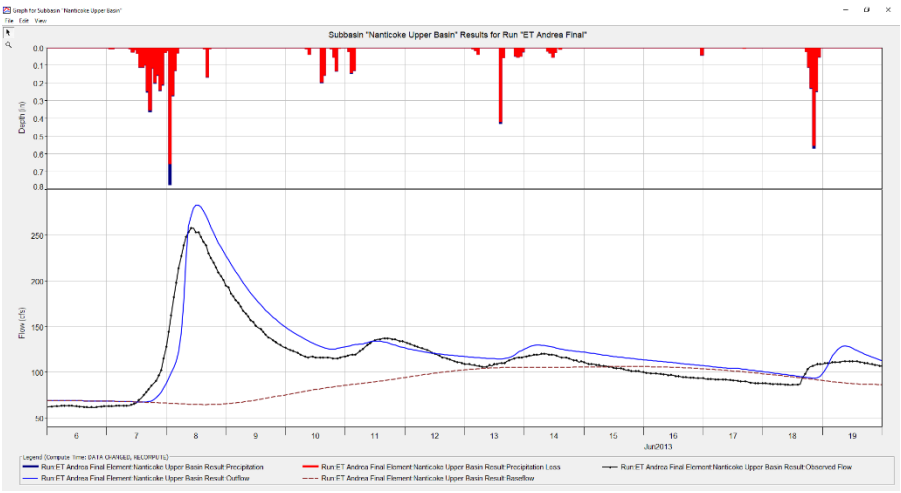

Figure 61. TS Michael - Nanticoke River near Bridgeville, DA hydrograph with simulated and observed data.

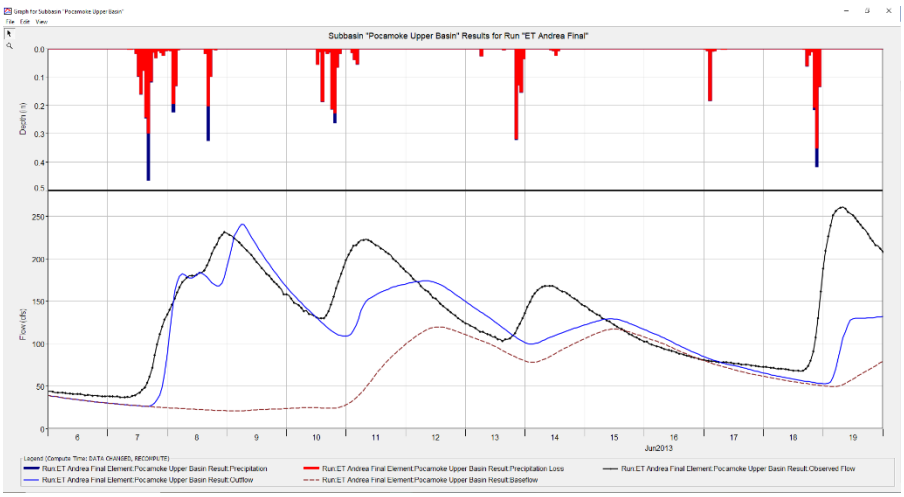

Figure 62. TS Michael - Pocomoke River near Willards, MD hydrograph with simulated and observed data.

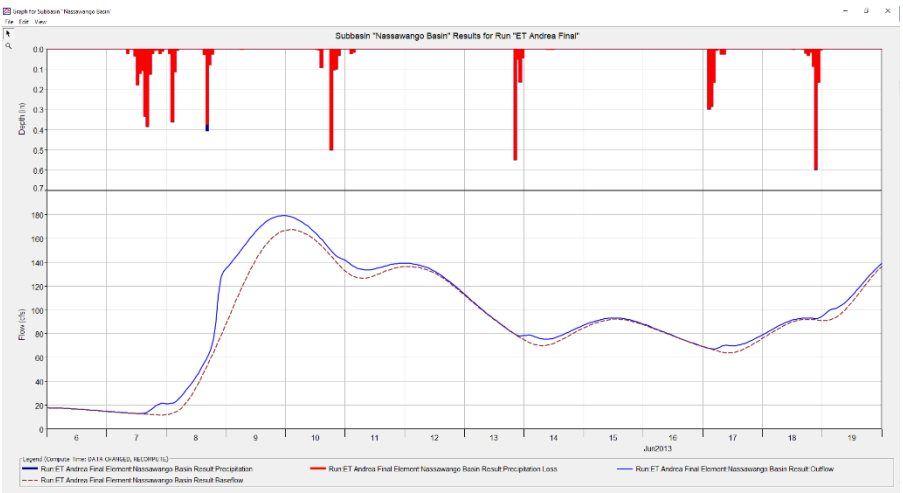

Figure 63. TS Michael - Nassawango Creek near Snow Hill, MD hydrograph with simulated and observed data.

Tropical Storm Zeta Hydrographs at Model Outfalls, Figures 64 - 73s. Figures show simulated versus observed flows at the outfalls of the model. Each outfall location by USGS gauge name is listed in the captions below the graph. In some locations precipitation is included in the output. These are only for locations where the basin was calibrated as a whole to observed flows as opposed to a junction in the model.

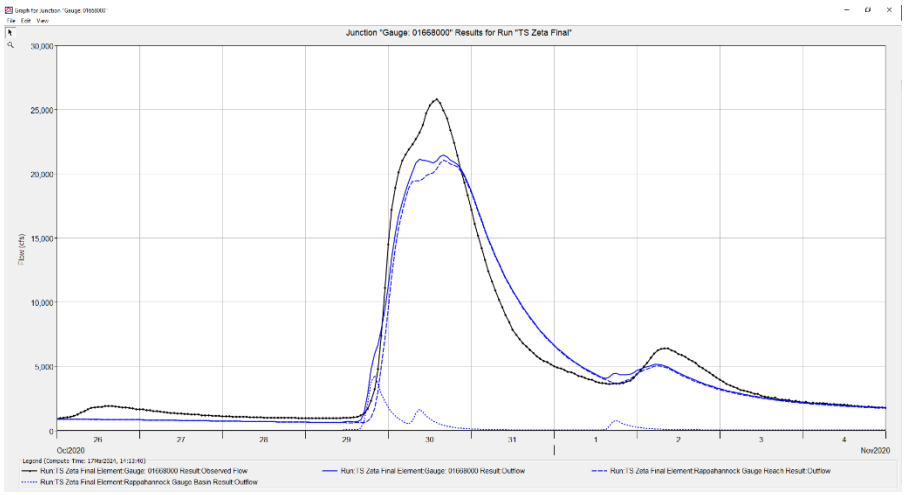

Figure 64. TS Zeta - Rappahannock River near Fredericksburg, VA hydrograph with simulated and observed data.

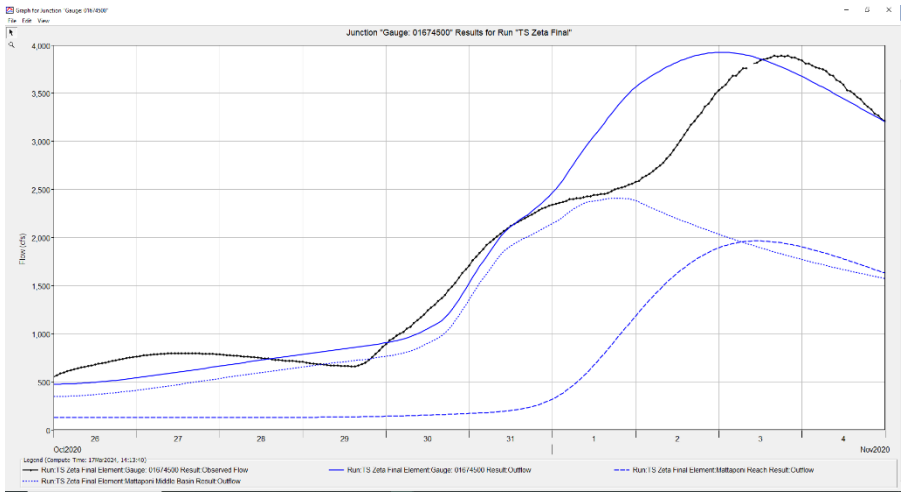

Figure 65. TS Zeta - Mattaponi River near Beulaville, VA hydrograph with simulated and observed data.

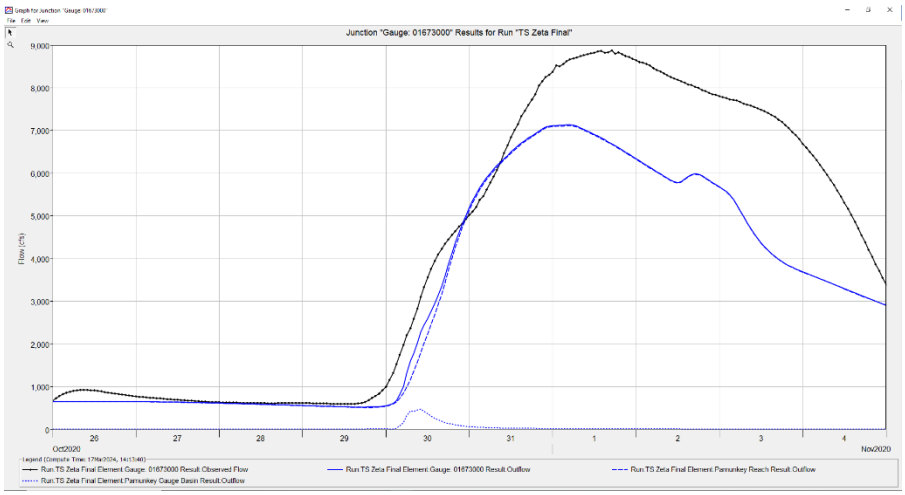

Figure 66. TS Zeta - Pamunkey River near Hanover, VA hydrograph with simulated and observed data.

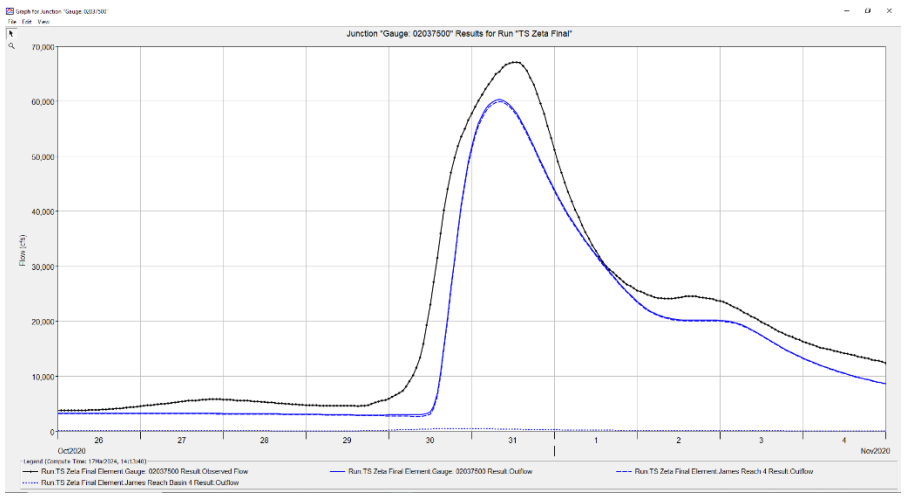

Figure 67. TS Zeta - James River near Richmond, VA hydrograph with simulated and observed data.

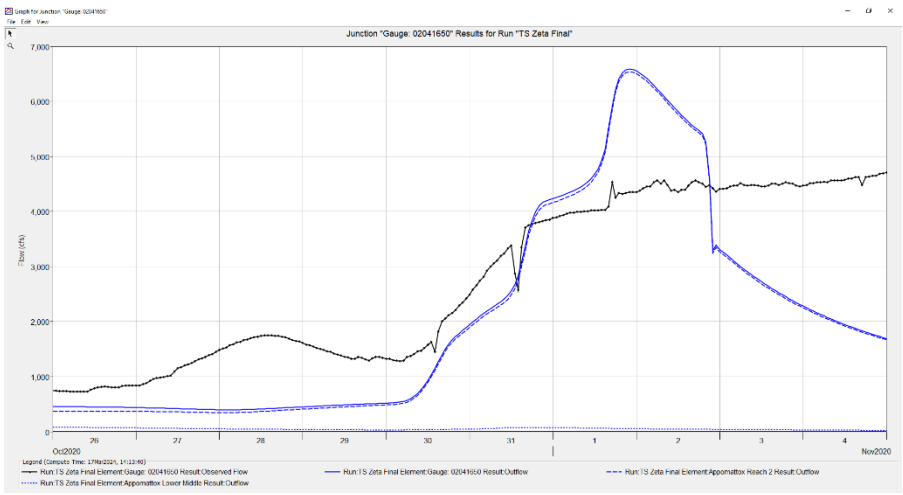

Figure 68. TS Zeta - Appomattox River near Matoaca, VA hydrograph with simulated and observed data.

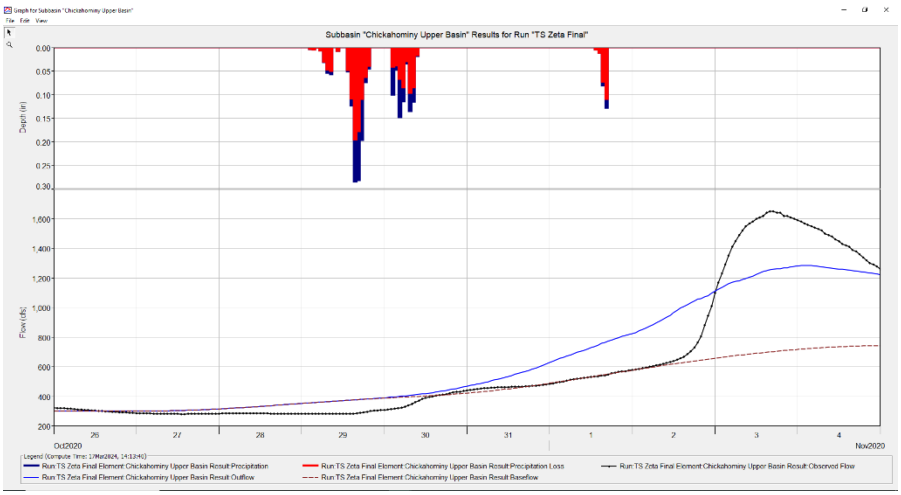

Figure 69. TS Zeta - Chickahominy River near Providence Forge, VA hydrograph with simulated and observed data.

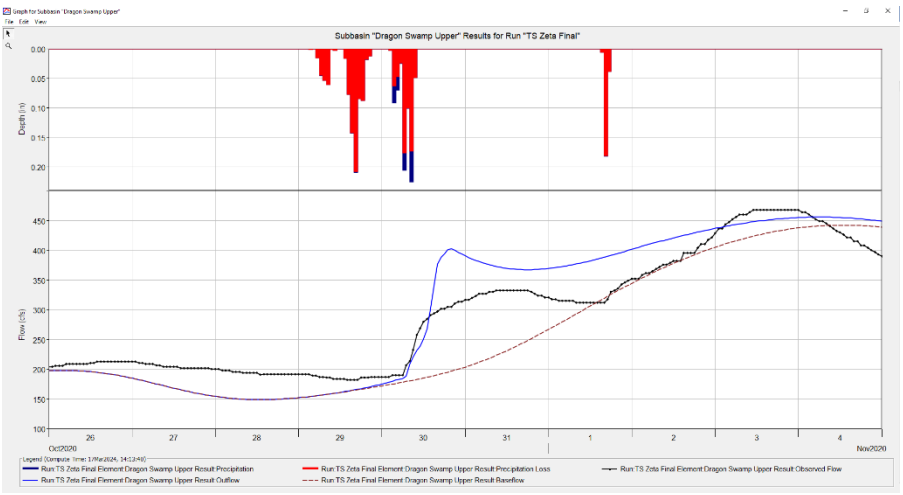

Figure 70. TS Zeta - Dragon Swamp at Mascot, VA hydrograph with simulated and observed data.

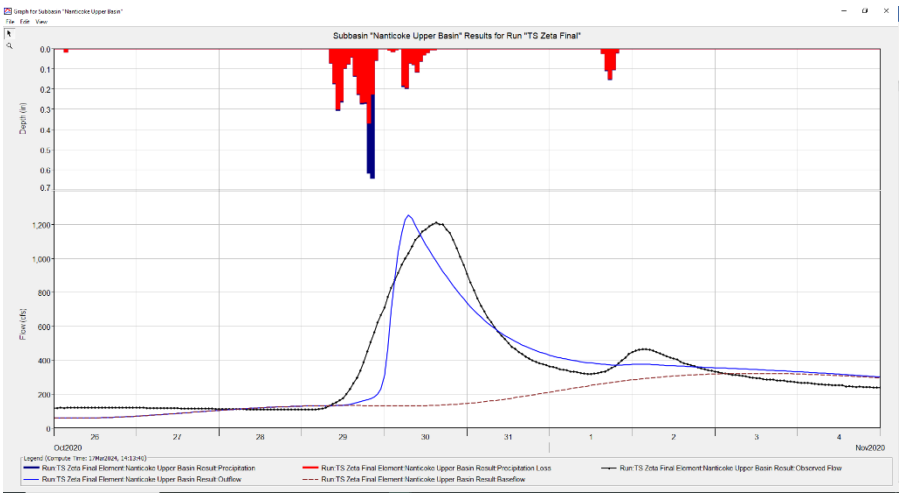

Figure 71. TS Zeta - Nanticoke River near Bridgeville, DA hydrograph with simulated and observed data.

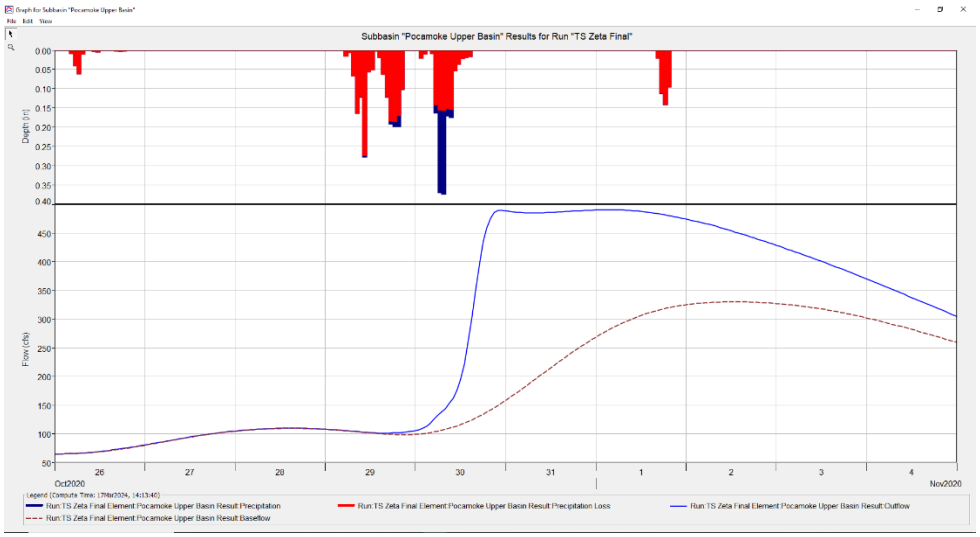

Figure 72. TS Zeta - Pocomoke River near Willards, MD hydrograph with simulated and observed data.

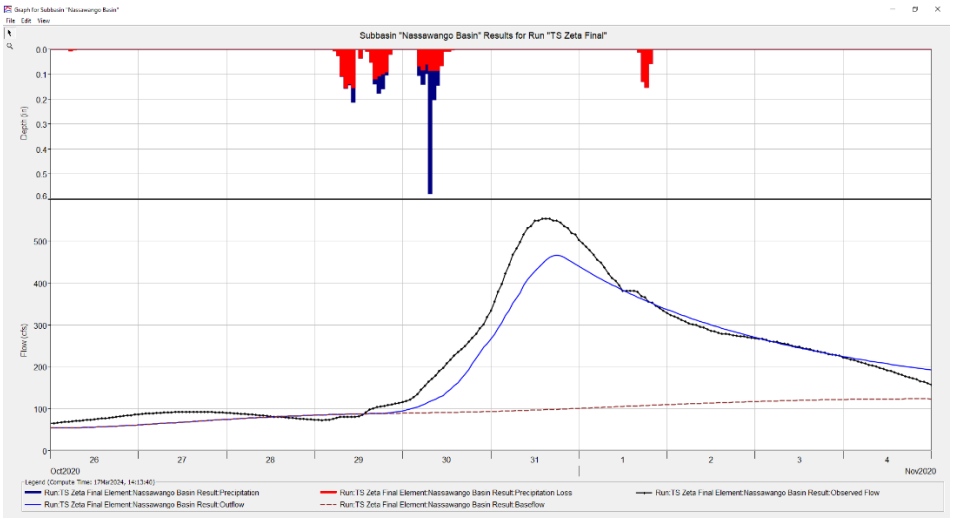

Figure 73. TS Zeta - Nassawango Creek near Snow Hill, MD hydrograph with simulated and observed data.

VITA

Christopher Leonard Frost

Old Dominion University

Department of Civil Engineering

135 Kaufman Hall

Norfolk, VA 23529

Christopher Frost is a professional civil engineer and geospatial information system professional working at the United States Army Corps of Engineers in Albuquerque, New Mexico. He received a Bachelor of Science in Ecology and Evolutionary Biology from the University of Arizona in 2009. He also received a Bachelor of Science in Civil Engineering from the University of Houston in 2016. His professional work has included the analysis and creation of FEMA floodplain models, work on the US Army Corps Water Management System, and analysis of snowmelt and frequency storm runoff in several basins in the Southwest.